

# Scientific Description of LPJ-GUESS version 4.1

2021-10-13

## Table of Contents

<b>1. Biogenic volatile organic compounds (BVOC)</b> .....	<b>4</b>
<i>Introduction</i> .....	4
<i>Calculation of terpenoid production</i> .....	4
<i>Calculation of emissions</i> .....	5
<i>Initialization of standard fractions</i> .....	6
<i>Parameterization of BVOC production and emission</i> .....	6
<i>Temperature corrections</i> .....	7
<i>References</i> .....	8
<i>Appendix A. PFT parameters used for global and European benchmarks</i> .....	10
<i>Appendix B. List of symbols and their abbreviations in the model code</i> .....	12
<b>2. Synchronised hydrology</b> .....	<b>14</b>
<i>Issue</i> .....	14
<i>Solution</i> .....	14
<i>Physical rationale</i> .....	14
<i>Remaining issue</i> .....	14
<b>3. Diurnal canopy-exchange processes</b> .....	<b>15</b>
<i>Assumptions</i> .....	15
<i>Miscellaneous</i> .....	15
Monthly mode.....	15
Sub-daily root respiration .....	15
<b>4. Nitrogen cycle with new SOM scheme</b> .....	<b>16</b>
<i>Introduction</i> .....	16
<i>Ecosystem N fluxes</i> .....	17
N input to ecosystem .....	17
N loss from ecosystem .....	17
<i>Soil organic matter dynamics</i> .....	18
<i>Vegetation N cycling</i> .....	20
Plant N demand and uptake .....	20
Plant growth and C and N allocation.....	22
<i>Additional updates</i> .....	23
$\alpha_a$ .....	23

SLA.....	23
Photosynthesis optimization.....	24
References.....	24
Appendix A. List of symbols and their abbreviations in the model code.....	26
Appendix B. C:N ratios and base decay rates for soil and litter organic matter pools.....	27
Appendix C. PFT parameter changes for BNS .....	27
<b>5. Nitrogen transformations .....</b>	<b>28</b>
<b>6. Land cover and land use .....</b>	<b>32</b>
Land cover representation .....	32
Cropland representation .....	33
Sowing and harvest (C-only and N-limited versions) .....	40
References.....	41
<b>7. C:N ratios of plant tissues .....</b>	<b>42</b>
References.....	42
<b>8. Soil input .....</b>	<b>43</b>
References.....	43
<b>9. Weather generator GWGEN (Global Weather GENERator) .....</b>	<b>44</b>
Implementation .....	44
Adjustments: Accuracy vs Runtime-efficiency.....	45
References.....	46
<b>10. Burnt area model SIMFIRE (SIMple FIREmodel) .....</b>	<b>47</b>
SIMFIRE biomes.....	47
fAPAR .....	49
The Nesterov-Index .....	49
Human population density.....	49
Monthly and daily burned area.....	50
References.....	50
<b>11. The wildfire combustion model BLAZE.....</b>	<b>51</b>
Fire-weather characteristics and potential fire-line intensity.....	51
Fire occurrence - "Ignition" .....	53
Fire-mortality .....	54
Combustion .....	55
References.....	58

<b>12. Updates to soil temperature and hydrology calculations.....</b>	<b>59</b>
<i>Introduction .....</i>	59
<i>Soil layers and their thermal properties.....</i>	59
<i>Soil column and temperature calculations.....</i>	62
Snow.....	62
Boundary conditions, padding layers & bedrock .....	63
<i>Soil water freezing and thawing processes.....</i>	63
<i>Hydrology changes resulting from phase change.....</i>	64
<i>Updates to SOM daily decay rates.....</i>	67
<i>Updated root distributions.....</i>	68
<i>Soil organic carbon and soil physical properties .....</i>	69
<i>References.....</i>	70
<b>13. High-latitude peatlands .....</b>	<b>71</b>
<i>Introduction .....</i>	71
<i>Peat stands and soil layers.....</i>	71
Peatland soil temperature .....	71
Peat hydrology .....	72
Peatland PFTs.....	74
Moss photosynthesis and leaf respiration .....	75
Assimilation stress due to water table fluctuations.....	75
<i>SOM decomposition in peatland stands .....</i>	76
<i>References.....</i>	77
<b>14. Methane dynamics .....</b>	<b>78</b>
<i>Introduction .....</i>	78
<i>Low-latitude peatland stands – hydrology, PFTs and methane fluxes.....</i>	78
<i>Methane fluxes in high-latitude peatland stands .....</i>	79
Methane production.....	79
Gas diffusion .....	80
Plant mediated gas transport.....	81
Methane oxidation.....	82
Methane ebullition .....	82
Total methane flux .....	83
<i>References.....</i>	84

## 1. Biogenic volatile organic compounds (BVOC)

*Guy Schurgers, October/November 2011, updated January 2013 (GS) & July 2016 (Stijn Hantson)*

### Introduction

Emissions of the terpenoids isoprene (C<sub>5</sub>H<sub>8</sub>) and monoterpenes (C<sub>10</sub>H<sub>16</sub>), were incorporated in LPJ-GUESS because of their role in atmospheric chemistry and aerosol formation. Terpenoid production is closely linked to photosynthesis.

### Calculation of terpenoid production

The implementation of terpenoid production in LPJ-GUESS is based on the algorithms in Niinemets et al. (1999, 2002), and is described in Arneth et al. (2007a, isoprene) and Schurgers et al. (2009a, monoterpenes). Production of isoprene and monoterpenes is calculated by assigning a fraction of the electron flux generated for photosynthesis to terpenoid synthesis. Terpenoid production is calculated as

$$I = \varepsilon J \alpha$$

where  $J$  is the rate of photosynthetic electron transport,  $\varepsilon$  is the fraction of this rate that is attributed to terpenoid production, and  $\alpha$  is the yield of terpenoids per unit of electron flux. The latter is calculated as (Niinemets et al., 1999)

$$\alpha = \frac{C_i - \Gamma^*}{6(4.67 C_i + 9.33 \Gamma^*)}$$

where  $C_i$  is the leaf-internal CO<sub>2</sub> concentration without water stress, and  $\Gamma^*$  is the CO<sub>2</sub> compensation point, both obtained from the photosynthesis calculations. Because of the large temperature sensitivity of terpenoid production,  $J$  is recalculated from the photosynthesis scheme (Haxeltine and Prentice, 1996) applying a daytime leaf temperature rather than a daily average air temperature (see below). The fraction  $\varepsilon$  is based on a species-specific standard fraction  $\varepsilon_s$  (see initialization, below), which is adjusted as a function of temperature, seasonality (in case of isoprene) and atmospheric CO<sub>2</sub> concentration:

$$\varepsilon = f(T)f(\sigma)f(\text{CO}_2)\varepsilon_s$$

The temperature function  $f(T)$  provides a correction for the enhanced temperature optimum of terpenoid production compared to photosynthesis, and is calculated with an exponential function (Arneth et al., 2007a):

$$f(T) = e^{\alpha(T-T_s)}$$

where  $T_s$  is a standard temperature (usually 30°C) and  $a$  defines the temperature sensitivity (0.1; Arneth et al., 2007a).

The seasonality for isoprene,  $f(\sigma)$ , is calculated based on a degree-day method in spring (degree-day requirement for isoprene is assumed to be twice as large as the requirement for phenology), and a decrease in autumn based on temperature and daylength (Schurgers et al., in press). This seasonality function is applied for deciduous PFTs only, evergreen PFTs are assumed to exhibit no seasonal changes in terpenoid synthesis.

The atmospheric CO<sub>2</sub> concentration has been shown to affect terpenoid synthesis (e.g. Possell et al., 2005), enhancing emissions at CO<sub>2</sub> concentrations lower than ambient, and reducing emissions at CO<sub>2</sub> concentrations higher than ambient. This has been attributed (Wilkinson et al., 2009) to changes in the distribution of phosphoenol pyruvate (PEP) between cytosol and chloroplast, but the mechanisms behind this have not been fully unraveled yet (Wilkinson et al., 2009). The model uses a rather empirical function, scaling emissions with the ratio of a reference ambient CO<sub>2</sub> concentration (370 ppm) and the actual CO<sub>2</sub> concentration (Arneth et al., 2007a):

$$f(\text{CO}_2) = \frac{p\text{CO}_2(\text{ref})}{p\text{CO}_2(\text{amb})}$$

Because of the similarity in the synthesis pathways of isoprene and monoterpenes, the same CO<sub>2</sub> sensitivity was applied for both, despite the fact that the sensitivity of monoterpenes to CO<sub>2</sub> in the literature is less obvious.

For monoterpenes, multiple compounds can be represented, each of them following the computations above, but with different parameterizations. Nine monoterpene compounds are separated in the code, which are subsequently divided in two main groups for the output, namely “endocyclic monoterpenes” being monoterpenes with an endocyclic double bond (outputted as TM1) and “others” including both acyclic monoterpenes and exocyclic monoterpenes (outputted as TM2). This separation is chosen because of its relevance for atmospheric chemistry models, and is used in e.g. the EC-Earth ESM incorporating LPJ-GUESS (Döscher et al. 2021).

## Calculation of emissions

Produced monoterpenes in plants have the potential to be (partially) stored, hence the often-observed light-independence of monoterpene emissions. However, this storage does not take place in all plants, and can be done in specific storage pools (e.g. resin ducts) or in non-specific storage. For the European PFTs, specific storage is implemented for all coniferous and herbaceous PFTs, because these species have been shown to emit monoterpenes independently of the availability of light. Monoterpene emissions for many broadleaf species have been reported to respond to light in a similar manner as isoprene (e.g. *Quercus ilex*, Staudt and Seufert, 1995; or *Fagus sylvatica*, Schuh et al., 1997), indicating that storage does

not play a role in these species. For the global PFT's, storage was made dependent on the monoterpene species emitted.

Long-term storage is implemented as a single storage pool, which is filled by transferring part of the produced monoterpenes to this pool. Currently, half of the produced monoterpenes is transferred here for all storing PFTs, because this resulted in the best fit with observations of the annual cycle of emissions for *Pinus ponderosa* (Schurgers et al., 2009a). However, if new data become available, this fraction can be assigned to each PFT individually.

Release from this storage pool is implemented with a temperature-dependent time constant  $\tau$ :

$$M_{emis} = \frac{m}{\tau}$$

where  $m$  is the monoterpene storage pool size, and  $M_{emis}$  is the rate of monoterpene emission from storage. The temperature dependence of  $\tau$  is governed by a  $Q_{10}$  relationship:

$$\tau = \frac{\tau_s}{Q_{10}^{\frac{(T-T_s)}{10}}}$$

The parameterization for this function was derived in Schurgers et al. (2009a):  $\tau_s=80$  d at a standard temperature  $T_s=30^\circ\text{C}$ , and the temperature dependence  $Q_{10}=1.9$ .

A short-term (~hours) storage of monoterpenes can occur as well in the mesophyll, but because of the time scales involved in this, it is not considered here.

## Initialization of standard fractions

The standard fractions  $\varepsilon_s$  of the PFTs used in the model are calculated by conversion from the reported leaf-level emission capacities  $I_s$  (expressed in  $\mu\text{g g}^{-1} \text{DW h}^{-1}$ ), which are emissions standardized to  $30^\circ\text{C}$  and  $1000 \mu\text{mol PAR m}^{-2} \text{s}^{-1}$ . By calculating the photosynthesis rate for these standard conditions, the fraction  $\varepsilon_s$  necessary so that an emission of  $I_s$  can be determined.

## Parameterization of BVOC production and emission

Emission capacities for PFTs were determined from recommendations for global modelling (global PFT set) or from leaf-level observations (European PFT set). Current values applied in the benchmark set are described in Arneth et al. (2007b, supplementary material, global PFT set) and Schurgers et al. (2009b, European PFT set). For monoterpenes, the original total emissions are maintained as in Schurgers et al. (2009), but separated into 9 different groups (listed in Table A2) (thereafter merged together in endocyclic (TM1) and other (TM2) groups) This relative abundance of each monoterpene species was derived from Messina al. (2015; table 4) for the global Pfts. For the European PFT's, only endocyclic monoterpenes

and other monoterpenes were separated (applied in the code as  $\alpha$ -pinene and  $\beta$ -pinene, respectively), and relative abundances were derived from Öström *et al.*, in prep. and if not present, the global values were used. All parameters are listed in Appendix A.

For parameterization of new PFTs, literature values for emission capacities (measured at standard conditions and expressed in  $\mu\text{g g}^{-1} \text{h}^{-1}$ ) can be used.

For monoterpene emission capacities that are based on a temperature dependence only, a multiplication with 2 is recommended to correct for the synthesis taking place during daytime only (see Schurgers *et al.*, 2009a).

## Temperature corrections

Because of the sensitivity of terpenoid production to temperature, corrections were implemented to convert the daily average air temperature to a daytime average leaf temperature.

For calculating the average daytime temperature from the daily value, the diurnal cycle is assumed to follow a sine wave with average temperature  $T_{av}$  and temperature amplitude  $T_{amp}$ , with the maximum temperature reached at noon. This sine wave is integrated over daylength  $d$  (in hours) centered around noon:

$$T_{daytime} = \int_{12-d/2}^{12+d/2} T_{av} + \frac{T_{amp}}{2} \sin\left(2\pi \frac{t-6}{24}\right) dt$$

which can be solved analytically to

$$T_{daytime} = T_{av} + \frac{T_{amp}}{2} \frac{\sin(\pi d/24)}{\pi d/24}$$

This daytime air temperature is used in the calculation of leaf temperatures. This calculation is made by computing the energy balance of the canopy, which can be written as

$$S_{net} + L_{net} + H + \lambda E = 0$$

The fluxes of sensible heat and longwave radiation depend on the leaf temperature, and this is used to make the total of all fluxes balance. Net shortwave radiation is computed already for the downward radiation flux following Prentice *et al.* (1993). Latent heat is computed from the actual evapotranspiration multiplied with the vapourization energy  $\lambda$ .

Incoming and outgoing longwave radiation are computed from the air temperature and the leaf temperature, respectively, using Stefan-Boltzmann law:

$$L_{net} = \varepsilon_a \sigma T_a^4 - \varepsilon_l \sigma T_l^4$$

A first order Taylor expansion is used as approximation to express the leaf temperature contribution  $\varepsilon_l \sigma T_l^4$  as a function of  $T_a$ , and atmosphere and leaf emissivities are assumed

equal, which makes the net longwave radiation a linear function of the difference between leaf temperature and air temperature:

$$L_{net} = 4\varepsilon_l \sigma T_a^3 (T_l - T_a)$$

Similarly, the flux of sensible heat can be expressed as a linear function of the temperature difference, using PFT-specific values for the aerodynamic resistance  $r_{b,h}$ :

$$H = (T_l - T_a) \frac{\rho C_p}{r_{b,h}}$$

in which  $\rho$  and  $C_p$  are the density and the specific heat capacity of air, respectively. The temperature difference can then be computed from the energy balance, resulting in

$$S_{net} + \lambda E = - \left( 4\varepsilon_l \sigma T_a^3 + \frac{\rho C_p}{r_{b,h}} \right) (T_l - T_a)$$

or

$$T_l = T_a - \frac{S_{net} + \lambda E}{4\varepsilon_l \sigma T_a^3 + \frac{\rho C_p}{r_{b,h}}}$$

## References

- Arneth A, Niinemets Ü, Pressley S, Bäck J, Hari P, Karl T, Noe S, Prentice IC, Serca D, Hickler T, Wolf A, Smith B, 2007a. Process-based estimates of terrestrial ecosystem isoprene emissions: incorporating the effect of a direct CO<sub>2</sub>-isoprene interaction.
- Arneth A, Miller PA, Scholze M, Hickler T, Schurgers G, Smith B, Prentice IC, 2007b. CO<sub>2</sub> inhibition of global terrestrial isoprene emissions: Potential implications for atmospheric chemistry. *Geophysical Research Letters*, 34, L18813, doi: 10.1029/2007GL030615.
- Döscher, R., Acosta, M., Alessandri, A., Anthoni, P., Arneth, A., et al. 2021. The EC-Earth3 Earth System Model for the Climate Model Intercomparison Project 6, *Geosci. Model Dev. Discuss.* [preprint], <https://doi.org/10.5194/gmd-2020-446>, in review, 2021.
- Haxeltine A, Prentice IC, 1996. BIOME3: An equilibrium terrestrial biosphere model based on ecophysiological constraints, resource availability, and competition amongst plant functional types. *Global Biogeochemical Cycles*, 10, 693-709.
- Niinemetts Ü, Tenhunen JD, Harley PC, Steinbrecher R, 1999. A model of isoprene emission based on energetic requirements for isoprene synthesis and leaf photosynthetic properties for *Liquidambar* and *Quercus*. *Plant, Cell and Environment*, 22, 1319-1335.
- Niinemetts Ü, Seufert G, Steinbrecher R, Tenhunen JD, 2002. A model coupling foliar monoterpene emissions to leaf photosynthetic characteristics in Mediterranean evergreen *Quercus* species. *New Phytologist*, 153, 257-275.
- Messina P, Lathière J, Sindelarova K, Vuichard N, Granier C, Ghattas J, Cozic A, Hauglustaine DA, 2015. Global biogenic volatile organic compound emissions in the orchidee and megan models and

- sensitivity to key parameters, *Atmos. Chem. Phys. Discuss.*, 2015, 33967-34033, 10.5194/acpd-15-33967-2015, 2015.
- Öström E, Roldin P, Schurgers G, Mishurov M, Putian Z, Kivekäs N, Lihavainen H, Ehn M, Boy M, Swietlicki E, *in prep.* The role of highly oxidized multifunctional organic molecules for the growth of new particles over the boreal forest region. Manuscript in preparation for *Atmospheric Chemistry and Physics*.
- Possell M, Hewitt CN, Beerling DJ, 2005. The effects of glacial atmospheric CO<sub>2</sub> concentrations and climate on isoprene emissions by vascular plants. *Global Change Biology*, 11, 60-69. doi: 10.1111/j.1365-2486.2004.00889.x
- Prentice IC, Sykes MT, Cramer W, 1993. A simulation model of the transient effects of climate change on forest landscapes. *Ecological Modelling*, 65, 51-70.
- Schuh G, Heiden AC, Hoffmann T, Kahl J, Rockel P, Rudolph J, Wildt J, 1997. Emissions of volatile organic compounds from sunflower and beech: dependence on temperature and light intensity. *Journal of Atmospheric Chemistry*, 27, 291-318.
- Schurgers G, Arneth A, Holzinger R, Goldstein AH, 2009a. Process-based modelling of biogenic monoterpene emissions combining production and release from storage. *Atmospheric Chemistry and Physics*, 9, 3409-3423. doi: 10.5194/acp-9-3409-2009.
- Schurgers G, Hickler T, Miller PA, Arneth A, 2009b. European emissions of isoprene and monoterpenes from the Last Glacial Maximum to present. *Biogeosciences*, 6, 2779-2797. doi: 10.5194/bg-6-2779-2009
- Schurgers G, Hickler T, Arneth A, in press. Climate-driven changes in species composition affect regional emission capacities of biogenic compounds. *Journal of Geophysical Research-Atmospheres*, doi: 10.1029/2011JD016278
- Staudt M, Seufert G, 1995. Light-dependent emission of monoterpenes by Holm oak (*Quercus ilex* L.). *Naturwissenschaften*, 82, 89-92.
- Wilkinson MJ, Monson RK, Trahan N, Lee S, Brown E, Jackson RB, Polley HW, Fay PA, Fall R, 2009. Leaf isoprene emission rate as a function of atmospheric CO<sub>2</sub> concentration. *Global Change Biology*, 15, 1189-1200. doi: 10.1111/j.1365-2486.2008.01803.x

**Appendix A. PFT parameters used for global and European benchmarks.***Table A1. BVOC-related PFT parameters in the global benchmark setup. Values originate from Arneth et al. (2007b, supplementary material) and Schurgers et al. (2009a).*

PFT	$I_s$ ( $\mu\text{g g}^{-1} \text{h}^{-1}$ )	Isoprene seasonality	$M_s$ ( $\mu\text{g g}^{-1} \text{h}^{-1}$ )	$f_{stor}$ (-)	$g_a$ ( $\text{m s}^{-1}$ )
BNE	8	0	4.8	0.5	0.14
BINE	8	0	4.8	0.5	0.14
BNS	8	1	4.8	0.5	0.14
TeNE	8	0	4.8	0.5	0.14
TeBS	45	1	1.6	0	0.04
IBS	45	1	1.6	0	0.04
TeBE	24	0	1.6	0	0.04
TrBE	24	0	0.8	0	0.04
TrIBE	24	0	0.8	0	0.04
TrBR	45	0	2.4	0	0.04
C3G	16	1	1.6	0.5	0.03
C4G	8	0	2.4	0.5	0.03
C3crop	16	1	1.6	0.5	0.03
C4crop	8	0	2.4	0.5	0.03

*Table A2. Percentage of speciated monoterpene EFs with respect to the PFT bulk monoterpenes, adapted from Messina et al. (2015; table 4).  $\alpha$ -pinene, limonene and 3-carene are grouped in TM1, the rest in TM2.*

	$\alpha$ -pinene	$\beta$ -pinene	limonene	myrcene	sabinene	camphene	3-carene	t- $\beta$ -ocimene	others
BNE	35.4	14.6	8.3	5	5	4.2	17.5	5.4	4.6
BINE	35.4	14.6	8.3	5	5	4.2	17.5	5.4	4.6
BNS	66.2	15	3.7	2.5	3	2.3	4.2	2.8	0.3
TeNE	35.4	14.6	8.3	5	5	4.2	17.5	5.4	4.6
TeBS	32.6	8.7	6.1	2.8	30.4	0.4	2.4	11.3	5.3
IBS	32.6	8.7	6.1	2.8	30.4	0.4	2.4	11.3	5.3
TeBE	46.3	12.2	12.2	5.4	8.3	4.9	1	4.4	5.3
trBrEv	39.5	11	9.2	7.3	7.3	5.5	4.8	9.2	6.2
trBrEv	39.5	11	9.2	7.3	7.3	5.5	4.8	9.2	6.2
TrBrDe	39.5	11	9.2	7.3	7.3	5.5	4.8	9.2	6.2
C3G	23.1	12.3	14.6	6.2	6.5	5.4	6.5	13.8	11.6
C4G	20	8	28	5.7	5	5.3	5.7	12	10.3
C3crop	27.7	15.4	9.2	4.6	6.2	3.1	20	3.1	10.7
C4crop	27.7	15.4	9.2	4.6	6.2	3.1	20	3.1	10.7

Table A3. BVOC-related PFT parameters in the European benchmark setup. Values originate from Schurgers et al. (2009b), where the emission factor are separated from TM1 and TM2 monoterpene groups, based on Öström et al. (in prep) and when not available Messina et al. (2015).

PFT	$I_s$ ( $\mu\text{g g}^{-1} \text{h}^{-1}$ )	Isoprene seasonality	$M_s$ TM1 ( $\mu\text{g g}^{-1} \text{h}^{-1}$ )	$M_s$ TM2 ( $\mu\text{g g}^{-1} \text{h}^{-1}$ )	$f_{stor}$ (-)	$g_a$ ( $\text{m s}^{-1}$ )
Abi_alb	0.05	0	1.1	0.7	0.5	0.14
BES	2.0	0	2.4	1.6	0.5	0.04
Bet_pen	0.2	1	2.1	3.9	0	0.04
Bet_pub	0	1	0.1	0.9	0	0.04
Car_bet	0	1	0.06	0.02	0	0.04
Cor_ave	0	1	0	0	0	0.04
Fag_syl	0	1	3.5	6.5	0	0.04
Fra_exc	0	1	0	0	0	0.04
Jun_oxy	0	0	1.2	0.8	0.5	0.14
MRS	2.0	0	2.4	1.6	0.5	0.04
Pic_abi	0.5	0	3.9	2.1	0.5	0.14
Pin_syl	0	0	3.2	0.8	0.5	0.14
Pin_hal	0	0	6.1	3.9	0.5	0.14
Pop_tre	20.	1	2.4	1.6	0	0.04
Que_coc	0.1	0	6.	4.	0	0.04
Que_ile	0.05	0	9.6	6.4	0	0.04
Que_pub	50.	1	0	0	0	0.04
Que_rob	40.	1	0	0	0	0.04
Til_cor	0	1	0	0	0	0.04
Ulm_gla	0	1	0	0	0	0.04
C3_gr	0	1	0.45	0.55	0.5	0.03
C4_gr	0	1	0.55	0.45	0.5	0.03

**Appendix B. List of symbols and their abbreviations in the model code**

<b>symbol</b>	<b>code abbrev.</b>	<b>description</b>	<b>unit</b>
$C_i$	pi_co2_opt	leaf-internal CO <sub>2</sub> concentration	ppm
$C_p$	cp	specific heat capacity of air	J kg <sup>-1</sup> K <sup>-1</sup>
$H$	-	sensible heat flux	W m <sup>-2</sup>
$I$	iso mon indiv.iso indiv.mon	isoprene /monoterpene production	g C m <sup>-2</sup> d <sup>-1</sup>
$J$	J_opt	electron flux	mol m <sup>-2</sup> h <sup>-1</sup>
$L$	lai	leaf area index	m <sup>2</sup> m <sup>-2</sup>
$L_{net}$	-	net longwave radiation	W m <sup>-2</sup>
$M_{emis}$	-	monoterpene emission from storage	mg C m <sup>-2</sup> d <sup>-1</sup>
$Q_{10}$	q10_mstor	temperature dependence	-
$S_{net}$	rsnet	net shortwave radiation	W m <sup>-2</sup>
$T$	temp	temperature	°C
$T_a$	temp	air temperature	°C
$T_{amp}$	tempamp	temperature amplitude	°C
$T_{av}$	temp	average temperature	°C
$T_{canopy,av}$	temp temp_leaf_daytime	average canopy temperature	°C
$T_{daytime}$	temp temp_leaf_daytime	daytime temperature	°C
$T_s$	Tstand	standard temperature	°C
$a$	a	temperature sensitivity	-
$d$	daylength	daylength	h
$k$	LAMBERTBEER_K	light extinction coefficient	-
$m$	indiv.monstor	monoterpene storage pool	mg C m <sup>-2</sup>
$pCO_2$	co2	atmospheric CO <sub>2</sub> concentration	ppm
$1/r_b$	gc	boundary layer conductance	mm s <sup>-1</sup>
$t$	-	hour of day	h
$z$	-	relative height in the canopy	-
$\Gamma^*$	gammastar	CO <sub>2</sub> compensation point	ppm
$\alpha$	a_Y_opt	photon content of light	-
$\varepsilon$	eps_eff_iso eps_eff_mon	fraction of electron flux allocated to terpenoid production	-
$\varepsilon_l$	emiss_leaf	leaf emissivity	-
$\varepsilon_s$	pft.Y_eps_iso pft.Y_eps_mon	fraction of electron flux allocated to terpenoid production under standardized conditions	-
$\lambda E$	lhloss	latent heat flux	W m <sup>-2</sup>
$\rho$	rhoair	density of air	kg m <sup>-3</sup>

$\sigma$	sigma	Stephan-Boltzmann constant	W m <sup>-2</sup> K <sup>-4</sup>
$\tau$	tcstor	time constant	d
$\tau_s$	tcstor_s	time constant under standardized conditions	d

---

## **2. Synchronised hydrology**

*Michael Mischurow, November 2011*

### **Issue**

In LPJ-GUESS (revision 833 and earlier) there was a disconnect between calculations of water supply and demand, and as a consequence, of water stress condition. Demand was calculated based on the current day's value of precipitation, whereas supply was based on soil water content that wasn't updated with the same precipitation. This likely was due to the fact that the function `interception()` was included into the `canopy_exchange()` call and therefore it wasn't possible to update soil water content between calls to `interception()` and `aet_water_stress()`.

### **Solution**

Interception, while a canopy process, is not related to the `canopy_exchange()` in other ways. Hence, it is possible by exposing `interception()` to the framework to add a soilwater module function that would deal with distribution of the daily rainfall. It seems reasonable to only deal with the top layer moisture (provided top layer is of reasonable depth) and to keep this new function neat and simple. Such new function, named `initial_infiltration()` is now added to the soil water module. There, `rainmelt` (rainfall + snowmelt) is added to the top soil layer up to the water holding capacity (`wcont = 1`), any remaining `rainmelt` is redistributed in the normal fashion in function `soilwater()` called after `canopy_exchange()`.

### **Physical rationale**

Rainfall is typically a much faster process than soil water transport and it is therefore highly unlikely that the rain water available to the canopy won't be available to the roots in the top soil layer. By the same logic water availability in the lower level(s) would be lagging behind the top layer's one and thus water transport shall have bearing on plant development. Slight reduction in runoff and increase in growth can be predicted and were confirmed with reference to benchmarks.

### **Remaining issue**

In `interception()` there is no distinction made with regard to the type of precipitation, so snow is also deemed to incur evaporation costs. This is flagged as an issue for consideration in a future model revision.

### **3. Diurnal canopy-exchange processes**

*Michael Mischurow, July 2012*

Implementation of a diurnal cycle processes in the canopy exchange module covers the following processes (functions): demand, aet\_water\_stress, water\_scalar, npp (and bvoc).

#### **Assumptions**

This part of canopy exchange module is dealing mainly with calculation of the amount of carbon assimilated by the vegetation, depending on the water-stress conditions. The two major assumptions were incorporated in the code:

- Supply remains constant throughout the day, while demand changes are driven by the canopy conductance; the water stress therefore changes throughout the day too.
- $V_{\max}$  is calculated on a daily scale and therefore daily averages are used for this.

An example of diurnal I/O is available in benchmark watch\_diurnal code.

The reasonable duration for the sub-daily periods is probably from about 15 minutes up to 6 hours: at too high a resolution simulations could become computationally expensive; at too low resolution averaging doesn't make much sense.

#### **Miscellaneous**

##### **Monthly mode**

Monthly mode (ifdailypp = 1) contradicts diurnal mode, therefore in case encountered, the model should exit without performing any calculations.

##### **Sub-daily root respiration**

Currently, soil temperature is calculated analytically as a dampened and lagged air temperature. The analytical formulation is based on an annual cycle and produces daily values. Such approach is not suitable to the sub-daily mode, as the soil temperature follows diurnal cycle (additionally dampened and lagged). This is the reason for using daily values of soil root respiration (based on daily soil gtemp). Additionally, while the value of soil temperature is calculated at 25 cm depth, we have information about PFT-specific fine root distribution between the two soil layers. Simple weighted average root depth would always be lower than 25 cm, as long as root fraction in the lower soil layer is different from zero.

## 4. Nitrogen cycle with new SOM scheme

David Wårlind, Ben Smith, Thomas Hickler, April 2013

### Introduction

Nutrients, and then most often nitrogen, are a limiting factor for plant growth. To account for this the N cycle has been implemented in LPJ-GUESS. The main objective of this work has been to get a stable plant interaction with soil available mineral N. To achieve this, three main areas have been developed; i) new structure for soil organic matter, where it is possible to represent the N dynamics in both the inorganic and organic soil system (Comins and McMurtrie 1993; Parton et al. 1993; Friend et al. 1997; Parton et al. 2010); ii) establish a scheme for plant N allocation, demand, uptake, stress etc (Haxeltine and Prentice 1996; Friend et al. 1997; Zaehle and Friend 2010); iii) ecosystem N fluxes (Cleveland et al. 1999; Lamarque et al. 2011, 2013)

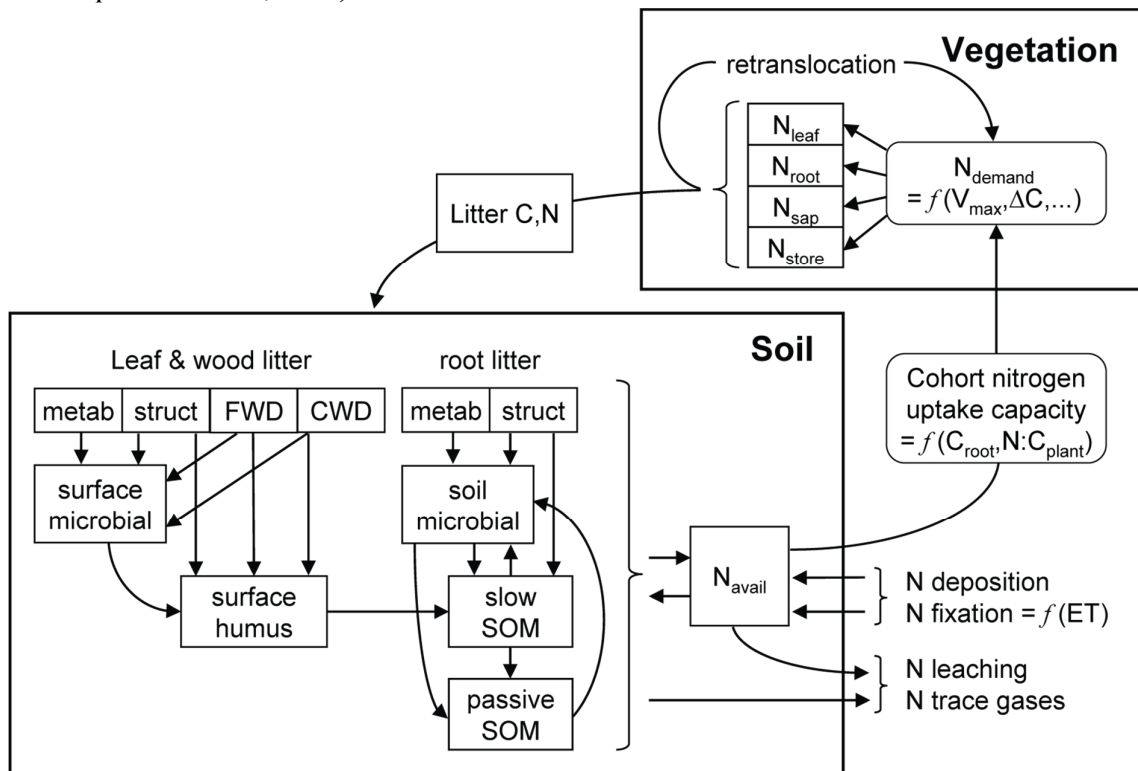


Figure 1. Schematic overview of N cycle in LPJ-GUESS. Abbreviations: FWD=fine woody debris; CWD=coarse woody debris; N<sub>avail</sub>=soil mineral N pool; N<sub>leaf</sub>=leaf N mass; N<sub>root</sub>=fine root N mass; N<sub>sap</sub>=sapwood N mass; N<sub>store</sub>=plant labile N store; N<sub>demand</sub>=daily plant N demand; V<sub>max</sub>=canopy rubisco capacity; ΔC=daily biomass increment; N:C<sub>plant</sub>=aggregate N:C mass ratio for leaves and fine roots; ET=actual evapotranspiration. See text for further details.

## Ecosystem N fluxes

### N input to ecosystem

N enters the ecosystem via N deposition (single bulk value encompassing wet and dry deposition) and biological N fixation (BNF, kgN ha<sup>-1</sup> yr<sup>-1</sup>). N deposition is prescribed as monthly mean values from an external database (Lamarque et al. 2011, 2013), whereas BNF is computed prognostically based on an empirical dependency on ecosystem evapotranspiration (ET) from Cleveland et al. (1999). Among three alternatives proposed by Cleveland et al. (1999) we chose the lower-range “conservative” parameterisation, with 5-year average actual evapotranspiration (AET, mm yr<sup>-1</sup>), prognosed by the model, as the independent variable:

$$BNF = 0.0102 \cdot AET + 0.524$$

BNF is distributed equally throughout the year and added directly to the soil available mineral N pool,  $N_{avail}$  (Fig 1), which is capped at a saturation level of 2 gN m<sup>-2</sup> following Parton et al. (1993). BNF in excess of the saturation level is discarded (assumed not to have occurred). N deposition during periods of snow lie (finite snow pack) is stored in the snow pack and released to the soil in proportion to snow melt.

### N loss from ecosystem

N is lost from the ecosystem via leaching, computed daily as the sum of leached soluble organic N and leached mineral N, and through volatilisation by wildfires. In addition, 1% of daily N mineralisation is assumed to be lost as gaseous emissions from soils (Thomas et al. 2013). Leaching of soluble organic N and C is computed conjointly as a fraction ( $L_O$ ) of the soil microbial SOM N and C pools, dependent on percolation ( $P_{H2O}$ , cm/month) and soil sand fraction ( $T_S$ ), following Parton et al. (1993), using updated parameters from the CENTURY 5 manual:

$$L_O = P_{H2O} / 1.9 \times (0.03 + 0.12 \cdot T_S)$$

For mineral N, the leaching fraction ( $L_M$ ) depends on daily percolation as a fraction of available soil water content ( $W_{TOT}$ , mm):

$$L_M = P_{H2O} / W_{TOT}$$

N lost due to wildfires is released to the atmosphere as NH<sub>3</sub>, NO, NO<sub>2</sub>, N<sub>2</sub>O and N<sub>2</sub>. The relative fractions are taken from Levine (1996).

## Soil organic matter dynamics

C and N dynamics of soils are simulated conjointly by an SOM scheme adopted from the CENTURY model (Parton et al. 1993), with modifications by Comins & McMurtrie (1993) and Kirschbaum & Paul (2002), and updates by Parton et al. (2010). Eleven pools differing in C:N stoichiometry and base decay rate are distinguished (Fig 1). Decomposition, computed daily for each pool, results in heterotrophic respiration (release of CO<sub>2</sub>) and transfer of C and N between pools, satisfying mass balance. Carbon entering the receiver pool drives N mineralisation or immobilisation. N is mineralised (added to the soil mineral N pool,  $N_{avail}$ ) when N transferred from a donor pool exceeds the corresponding increase dictated by the prescribed C:N ratio of a receiver pool (N “supply” exceeds “demand”). Conversely, if the N flux from a donor pool is too small to satisfy the C:N ratio of the receiver pool (demand > supply), N immobilisation occurs, reducing  $N_{avail}$  to satisfy the deficit. If  $N_{avail}$  is insufficient to satisfy the N demand for immobilisation among all pools, decay rates are reduced proportionately so that net immobilisation matches  $N_{avail}$ .

Pool C:N ratios are determined as follows. For the surface microbial pool, the C:N ratio varies between 10 and 20 depending on the bulk N content of current surface litter (determined prognostically by the growth and physiology of the vegetation providing the source of the litter; see below) (Parton et al. 1993; Fig 2). For the soil microbial, surface humus and soil slow pools, C:N ratio varies between upper and lower bounds depending on  $N_{avail}$  (Parton et al. 2010; Fig 2). The soil passive pool has a fixed C:N ratio of 9 (Parton et al. 2010).

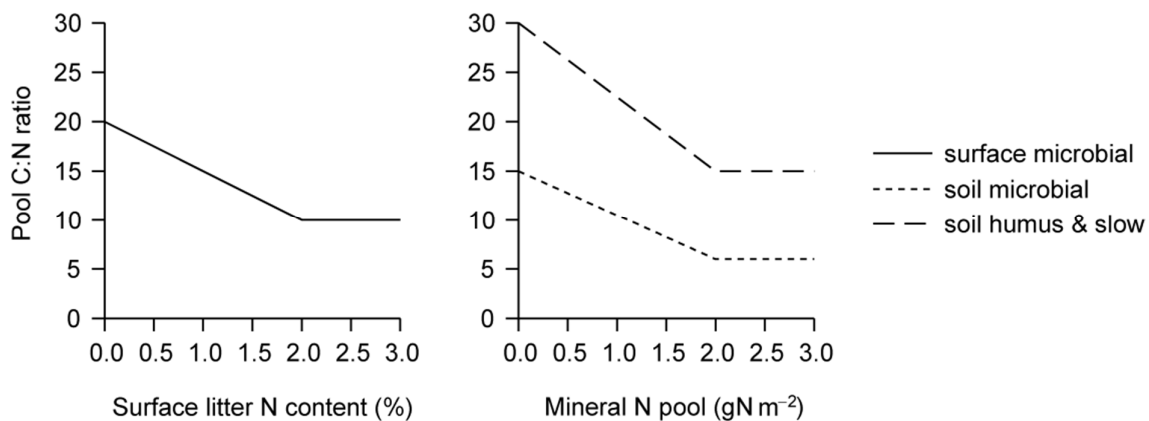


Figure 2. Determination of target C:N ratio of receiver pools in SOM flux transfer scheme (Parton et al. 1993, 2010).

Daily decay rates for each pool (C fraction:  $C_j$ , kgC m<sup>-2</sup>) are determined by a prescribed maximum (base) decay rate ( $k_{j,max}$ ; Parton et al. 2010; Table 1) and dependencies on temperature, soil moisture and soil texture:

$$\frac{dC_j}{dt} = -k_{j,max} f(T_{soil}) f(W) f(S) \cdot C_j$$

where  $f(T_{\text{soil}})$  is a dimensionless scalar in the range 0-1 related to soil temperature ( $T_{\text{soil}}$ , °C) by the relationship (Comins & McMurtrie 1993):

$$f(T_{\text{soil}}) = 0.0326 + 0.00351 \cdot T_{\text{soil}}^{1.652} - (T_{\text{soil}} / 41.748)^{7.19}$$

$f(W)$  is a dimensionless scalar in the range 0-1 related to soil moisture following (Friend et al. 1997):

$$f(W) = \begin{cases} 0.000371\sigma^2 - 0.0748\sigma + 4.13 & ; \sigma \geq 60 \\ \exp[-(\sigma - 60)^2 / 800] & ; \sigma < 60 \end{cases}$$

where  $\sigma$  is a proxy for percentage of water-filled pore spaces in the soil, given by:

$$\sigma = 100 \cdot \theta / \theta_{\text{max}}$$

where  $\theta$  is current soil water content and  $\theta_{\text{max}}$  is soil water saturation capacity as a proportion of soil column depth, calculated from soil texture following Cosby et al. (1984).

$f(S)$  is a dimensionless scalar in the range 0-1 determined from soil fractional silt plus clay content ( $S$ ) following Parton et al. (1993):

$$f(S) = 1 - 0.75 \cdot S$$

Litter resulting from vegetation turnover (mortality or phenology), effected in the model on the last day of a given year, is transferred to the litter SOM pools on the first day of the following year. Leaf and root litter is partitioned into structural (resistant to decomposition) and metabolic (readily decomposable) fractions based on the estimated lignin:N ratio (Parton et al. 1993):

$$F_m = 0.85 - 0.013 \cdot \lambda \cdot cn$$

where  $F_m$  and  $(1-F_m)$  are the metabolic and structural litter fractions, respectively;  $\lambda$  is assumed lignin content as a fraction of total C mass (leaves: 20%; fine roots: 16%), and  $cn$  is the prognostic C:N ratio of the incoming material.

Sapwood and heartwood biomass lost due to mortality or disturbance enters the fine and coarse woody debris litter pools, respectively.

In the ins-file there is a switch, `ifcentury`, to change between the original, `som_dynamics_lpj()`, and `CENTURY`, `som_dynamics_century()`, SOM schemes. If N cycling is enabled then the `CENTURY` SOM scheme needs to be used.

## Vegetation N cycling

### Plant N demand and uptake

Plants obtain N for allocation to their biomass compartments leaves, fine roots and (for woody PFTs) sapwood through root uptake from the soil mineral N pool  $N_{\text{avail}}$ . N uptake takes place daily and is the smaller of current supply, i.e.  $N_{\text{avail}}$ , and demand, subject to a maximum constraint on total uptake.

Vegetation N demand is based on a solution of the carboxylation capacity of rubisco ( $V_{\text{max}}$ ) that maximises net assimilation at the canopy level given current temperature, light interception and intercellular  $[\text{CO}_2]$ , the latter affected by ambient  $[\text{CO}_2]$  but also by the influence of soil moisture and boundary layer humidity on stomatal conductance (Haxeltine & Prentice 1996a,b; Sitch et al. 2003). Following Haxeltine & Prentice (1996a), leaf N content ( $N_{\text{leaf}}$ ,  $\text{gN m}^{-2}$ ) is related to  $V_{\text{max}}$  ( $\text{gC m}^{-2}$ ) by the relationship:

$$N_{\text{leaf}} = 2083 \cdot V_{\text{max}} \exp[-0.693(T - 25)] / L \cdot f(\text{LAI}) + 7.15 \cdot C_{\text{leaf}}$$

where  $T$  is air temperature ( $^{\circ}\text{C}$ ),  $L$  is day length (s),  $C_{\text{leaf}}$  is leaf C mass, accounting for canopy phenology ( $\text{gC m}^{-2}$ ) and  $f(\text{LAI})$  is a modifier dependent on current leaf area index (LAI,  $\text{m}^2 \text{m}^{-2}$ ) that accounts for the empirical finding that leaf N content declines more gradually with canopy depth compared to incoming sunlight (Lloyd et al. 2010; Peltoniemi et al. 2012):

$$f(\text{LAI}) = \exp(0.12 \cdot \text{LAI})$$

Based on the  $N_{\text{leaf}}$  eqn, the target leaf C:N mass ratio may be calculated as  $C_{\text{leaf}}/N_{\text{leaf}}$ . Leaf C:N is, however, constrained to remain within prescribed boundaries  $[CN_{\text{leaf,min}}, CN_{\text{leaf,max}}]$  based on observations (Reich et al. 1992; White et al. 2000). C:N ratios for the further compartments fine roots and (for woody PFTs) sapwood are assumed to vary proportionately with leaf C:N, fine roots maintaining a C:N ratio 1.16 times higher, and sapwood 6.9 times higher than leaves (Friend et al. 1997). Since allocation of the current year's NPP is effected only once per year in LPJ-GUESS, allocation ratios (proportion of biomass increment allocated to each respective compartment) from the previous year are assumed when computing daily demand for allocation to fine roots and sapwood.

Plants maintain a store of labile nitrogen,  $N_{\text{store}}$  ( $\text{kgN m}^{-2}$ ), to buffer fluctuations in the balance between N demand and supply from the soil mineral N pool. Following Zaehle & Friend (2010), the maximum capacity of  $N_{\text{store}}$  is related to current size as:

$$N_{\text{store,max}} = \begin{cases} k \cdot C_{\text{sap}} N_{\text{leaf}} / C_{\text{leaf}} & (\text{woody PFTs}) \\ k \cdot C_{\text{root}} N_{\text{leaf}} / C_{\text{leaf}} & (\text{herbaceous PFTs}) \end{cases}$$

where  $C_{\text{sap}}$ ,  $C_{\text{root}}$ ,  $C_{\text{leaf}}$  and  $N_{\text{leaf}}$  denote sapwood C mass, fine root C mass, leaf C mass and leaf N mass, respectively, on allocation the previous year;  $k$  is set to 0.05 for evergreen

woody, 0.15 for deciduous woody and 0.3 for herbaceous PFTs. The store is replenished by uptake from  $N_{\text{avail}}$ .

Daily N demand for allocation to  $N_{\text{store}}$  is computed as:

$$\max \left[ 0, \frac{NPP_a}{NPP_{y-1}} (N_{\text{store,max}} - N_{\text{turnover}}) - N_{\text{store}} \right]$$

where  $NPP_a$  and  $NPP_{y-1}$  are the current year's accumulated and previous year's NPP, respectively, and  $N_{\text{turnover}}$  is the expected amount of N to be reallocated from turnover of leaves, fine roots and sapwood, based on tissue C:N ratios and biomass from the previous year.

Where the current day's bulk N demand cannot be fulfilled by the present size of  $N_{\text{avail}}$ , total uptake is reduced to  $N_{\text{avail}}$ . Uptake may also be further reduced to a ceiling,  $N_{\text{up,max}}$ , computed following Zaehle & Friend (2010) as:

$$N_{\text{up,max}} = 2N_{\text{up,root}} f(N_{\text{avail}}) f(T_{\text{soil}}) f(NC_{\text{plant}}) C_{\text{root}}$$

Where  $N_{\text{up,root}}$  is a linear scalar of the maximum N uptake per unit fine root biomass,  $C_{\text{root}}$ , assuming a proportional increase in uptake capacity with root exploration volume, assigned the fixed values 2.8 and 5.51 gN kgC<sup>-1</sup> day<sup>-1</sup> for woody PFTs and grasses, respectively (Rothstein et al. 2000; Macduff et al. 2002). Modifiers account for the effects of the current mineral N pool, soil temperature (same as for decay rates) and plant N status on uptake capacity, as follows:

$$f(N_{\text{avail}}) = 0.05 + \frac{N_{\text{avail}}}{N_{\text{avail}} + k_m \theta_{\text{max}} z_{\text{soil}}}$$

representing a combined linear and saturating effect of mineral N concentration on N uptake (Zaehle & Friend 2010), with  $k_m$ , the half-saturation concentration for N uptake, set to 1.48 gN m<sup>-3</sup> for woody PFTs (Rothstein et al. 2000) and 1.19 gN m<sup>-3</sup> for grasses (Macduff et al. 2002);  $z_{\text{soil}}$  is the soil column depth (1.5 m).

$$f(NC_{\text{plant}}) = \max \left( 0, \frac{NC_{\text{plant}} - 1/CN_{\text{leaf,min}}}{2/(CN_{\text{leaf,max}} + CN_{\text{leaf,min}}) - 1/CN_{\text{leaf,min}}} \right)$$

representing a tendency for N uptake to increase as the concentration of relatively mobile N compounds within the plant, characterised by  $NC_{\text{plant}}$  (below) declines.  $CN_{\text{leaf,min}}$  and  $CN_{\text{leaf,max}}$  are the prescribed minimum and maximum bounds for leaf C:N.

$$NC_{\text{plant}} = \frac{N_{\text{leaf}} + N_{\text{root}}}{C_{\text{leaf}} + C_{\text{root}}}$$

Vegetation N demand and uptake are computed each daily time step for each average individual plant (in practice, each age/size class in each replicate patch for woody PFTs, and once for the herbaceous ground layer in each patch). In the event that bulk demand cannot be met by the available N supply, the supply is partitioned among individuals in proportion to their relative uptake strength  $f_{Nup}$  which is related to estimated fine root surface area following:

$$f_{Nup} = X \cdot [k_{Nup} C_{root} \cdot f(NC_{plant}) / X]^{2/3}$$

where  $X$  (indiv  $m^{-2}$ ) is stem (cohort) density (included as a weighting factor for the most abundant cohorts) and  $k_{Nup}$ , set to 1.6 for woody PFTs and 1.9 for grasses, weights N uptake towards PFTs having shallower root distributions, coinciding with an assumed greater concentration of available N in the upper soil layer (Franzluebbers & Stuedemann 2009). It also implies that plants become more efficient at taking up N when their store of relatively mobile N approaches its lower limit, e.g. through physiological up-regulation of root uptake capacity (Raynaud & Leadley 2004); the existence of such a response is also suggested by studies of plant-mycorrhizal associations, which are often more developed in N-depleted habitats (Olsrud et al. 2004).

Where N uptake is insufficient to meet individual demand, individuals attempt to fulfil the deficit using their current labile N store. If demand is still not met after the N store is depleted, rubisco capacity and thereby leaf and whole-plant demand (as well as photosynthesis) are reduced to the maximum level that can be satisfied given the current supply plus storage, effecting N limitation. The N store is replenished, up to its maximum capacity (see above), on the last day of the year by retranslocation of up to 50% of the N mass of shed leaves, fine roots and sapwood on conversion to heartwood (Aerts 1996, Vergutz et al. 2012).

N demand and stress are modelled in a similar way as water demand and stress. First individual N demand and uptake capacity are calculated in `ndemand()`. If uptake capacity cannot meet demand then N stress on rubisco capacity ( $V_{max}$ ) is determined in `vmax_nitrogen_stress()`, all resolved in `canopy_exchange()` just as for water demand and stress.

### Plant growth and C and N allocation

Plant growth takes place on the last day of the simulation year by allocation of annual accrued NPP to the biomass compartments leaves, fine roots and (for woody PFTs) sapwood subject to allometric constraints. The only modification resulting from the incorporation of N cycling in the model to the allocation scheme is the addition of an N stress scalar ( $\nu$ ) in the functional balance constraint that governs the relative allocation of biomass to foliage versus fine roots:

$$C_{leaf} = lr_{max} \cdot \min(\omega, \nu) \cdot C_{root}$$

where  $lr_{\max}$  is a PFT-specific constant (Table 2) and  $\omega$  is a soil moisture stress scalar in the range 0-1, with smaller values reflecting increased soil moisture stress (Sitch et al. 2003). Where  $N$  stress exceeds soil moisture stress, this results in an increased allocation of biomass to fine roots at the expense of foliage:

$$v = \min\left(1, \frac{CN_{\text{leaf,aopt}}}{C_{\text{leaf}} / N_{\text{leaf}}}\right)$$

where  $CN_{\text{leaf,aopt}}$  is the leaf C:N ratio that would have been realised if plant  $N$  demand had been fulfilled by the available supply plus storage every day of the current year;  $C_{\text{leaf}}$  and  $N_{\text{leaf}}$  are realised C and N mass, accounting for N limitation.

## Additional updates

### $\alpha_a$

The incorporation of N limitation naturally results in a reduction in simulated NPP, regionally and globally, relative to the C-only version of the model, which lacks such limitation. To compensate for this nutrient effect on global C balance and fluxes, the quantum efficiency scalar  $\alpha_a$  was recalibrated to a value that resulted in simulated global C fluxes within the approximate range of observation-based estimates. For the C-only simulations of this study, which were performed with the C-N model, but with N limitation switched “off”,  $\alpha_a$  was likewise calibrated to the global fluxes. The resulting settings of this parameter were 0.70 and 0.55 with N limitation enabled and disabled, respectively. It may be postulated that the 15 percentage-point differential between these values corresponds to the global limitation of primary production attributable to N limitation, whereas the residual difference of 30% between realised and potential canopy quantum efficiency, obtained with N limitation enabled, more closely reflects the spectral factors traditionally invoked to explain this parameter.

### SLA

In conjunction with the incorporation of N cycling, an equation linking SLA to the PFT parameter leaf longevity ( $a_{\text{leaf}}$ ), originally adopted from Reich et al. (1997), was replaced with separate parameterisations of the same relationship for needleleaved and broadleaved PFTs, following Reich et al. (1992). The new equation has the form:

$$\text{SLA} = 0.2g(\beta_0 + \beta_1 \log_{10} 12a_{\text{leaf}})$$

$$g(p) = 10^p$$

with SLA in  $\text{m}^2 \text{kgC}^{-1}$  and  $a_{\text{leaf}}$  in yr. The regression coefficients  $\{\beta_0, \beta_1\}$ , fitted to a global dataset by Reich et al. (1992), are set to  $\{2.41, -0.38\}$  and  $\{2.29, -0.40\}$  for needleleaves and broadleaves, respectively.

As a consequence of this update, leaves are simulated to be generally thicker, with lower SLA and consequently reduced PAR per unit invested leaf C. The global data presented in both the 1992 and 1997 Reich et al. papers are, however, more faithfully reproduced, suggesting the presence of a unit conversion error in the original implementation. The resulting reduction in productivity per unit leaf C more strongly penalises species with short-lived leaves, particularly deciduous species and grasses, providing one explanation for an increased dominance by woody PFTs relative to grasses in simulations with the updated model, whether or not N limitations are enabled.

### **Photosynthesis optimization**

Before it has been possible to scale photosynthesis with *fpar* and only calculate it once per PFT, but now each individual has its own N status, precluding this simple optimization approach. Therefore, photosynthesis calculations are now performed separately for each individual (normally representing the average for a PFT cohort) in each patch.

### **References**

- Aerts, R.: Nutrient resorption from senescing leaves of perennials: are there general patterns? *J. Ecol.*, 84, 597-608.
- CENTURY Soil Organic Matter Model Version 5; Century User's Guide and Reference. <http://www.nrel.colostate.edu/projects/century5/reference/index.htm>; accessed Oct.7, 2016.
- Cleveland, C. C., Townsend, A. R., Schimel, D. S., Fisher, H., Howarth, R. W., Hedin, L. O., Perakis, S. S., Latty, E. F., Von Fischer, J. C., Elseroad, A., and Wasson, M. F.: Global patterns of terrestrial biological nitrogen (N<sub>2</sub>) fixation in natural ecosystems, *Global Biogeochem. Cy.*, 13, 623-645, 1999.
- Comins, H. N. and McMurtrie, R. E.: Long-term response of nutrient-limited forests to CO<sub>2</sub> enrichment; equilibrium behaviour of plant-soil models, *Ecol. Appl.*, 3, 666-681, 1993.
- Cosby, B. J., Hornberger, G. M., Clapp, R. B., and Ginn, T. R.: A statistical exploration of the relationships of soil-moisture characteristics of the physical properties of soils, *Water Resour. Res.*, 20, 682-690, 1984.
- Franzleubbers, A. J. and Stuedemann, J. A.: Soil-profile organic carbon and total nitrogen during 12 years of pasture management in the Southern Piedmont, USA, *Agr. Ecosyst. Environ.*, 129, 28-36, 2009.
- Friend, A. D., Stevens, A. K., Knox, R. G., and Cannell, M. G. R. 1997. A process-based, terrestrial biosphere model of ecosystem dynamics (Hybrid v3.0), *Ecol. Model.*, 95, 249-287, 1997.
- Haxeltine, A. and Prentice, I. C.: A general model for the light-use efficiency of primary production, *Funct. Ecol.*, 10, 551-561, 1996a.
- Haxeltine, A. and Prentice, I. C.: BIOME3: An equilibrium terrestrial biosphere model based on ecophysiological constraints, resource availability, and competition among plant functional types, *Global Biogeochem. Cy.*, 10, 693-709, 1996b.
- Kirschbaum, M. U. F. and Paul, K. I.: Modelling C and N dynamics in forest soils with a modified version of the CENTURY model, *Soil Biol. Biochem.*, 34, 341-354, 2002.
- Lamarque, J.-F., Dentener, F., McConnell, J., Ro, C.-U., Shaw, M., Vet, R., Bergmann, D., Cameron-Smith, P., Doherty, R., Faluvegi, G., Ghan, S. J., Josse, B., Lee, Y. H., MacKenzie, I. A., Plummer, D., Shindell,

- D. T., Stevenson, D. S., Strode, S., and Zeng, G.: Multi-model mean nitrogen and sulfur deposition from the Atmospheric Chemistry and Climate Model Intercomparison Project (ACCMIP): evaluation historical and projected changes. *Atmos. Chem. Phys.*, in press.
- Lamarque, J.-F., Kyle, G. P., Meinshausen, M., Riahi, K., Smith, S.J., van Vuuren, D. P., Conley, A. J., and Vitt, F.: Global and regional evolution of short-lived radiatively-active gases and aerosols in the Representative Concentration Pathways, *Climatic Change*, 109, 191-212, 2011.
- Levine, J. S. (1996) *Biomass Burning and Global Change. Remote Sensing, Modeling and Inventory Development, and Biomass Burning in Africa*, J. S. Levine, XXXV–XLIII, MIT Press, Mass.
- Lloyd, J., and Taylor, J. A.: On the temperature dependence of soil respiration, *Funct. Ecol.*, 8, 315-323, 1994.
- Macduff, J. H., Humphreys, M. O., and Thomas, H.: Effects of a stay-green mutation on plant nitrogen relations in *Lolium perenne* during N starvation and after defoliation, *Ann. Bot.-London*, 89, 11-21, 2002.
- Olsrud, M., Melillo, J. M., Christensen, T. R., Michelsen, A., Wallander, H., and Olsson, P. A.: Response of ericoid mycorrhizal colonization and functioning to global change factors, *New Phytol.*, 162, 459-469, 2004.
- Parton, W. J., Hanson, P. J., Swanston, C., Torn, M., Trumbore, S. E., Riley, W., and Kelly, R.: ForCent model development and testing using the Enriched Background Isotope Study experiment, *J. Geophys. Res.*, 115, G04001, DOI: 10.1029/2009JG001193, 2010.
- Parton, W. J., Scurlock, J. M. O., Ojima, D. S., Gilmanov, T. G., Scholes, R. J., Schimel, D. S., Kirchner, T., Menaut, J.-C., Seastedt, T., Garcia Moya, E., Kamnalrut, A., and Kinyamario, J. I. 1993. Observations and modeling of biomass and soil organic matter dynamics for the grassland biome worldwide, *Global Biogeochem. Cy.*, 7, 785-809, 1993.
- Peltoniemi, M. S., Duursma, R. A., and Medlyn, B. E.: Co-optimal distribution of leaf nitrogen and hydraulic conductance in plant canopies, *Tree Physiol.*, 32, 510-519, 2012.
- Raynaud, X., and Leadley, P. W.: Soil characteristics play a key role in modeling nutrient competition in plant communities, *Ecology*, 85, 2200-2214, 2004.
- Reich, P. B., Walters, M. B., and Ellsworth, D. S.: Leaf life-span in relation to leaf, plant and stand characteristics among diverse ecosystems, *Ecol. Monogr.*, 62, 365-392, 1992.
- Reich, P. B., Walters, M. B., and Ellsworth, D. S.: From tropics to tundra: global convergence in plant functioning, *P. Natl. Acad. Sci. USA*, 94, 13730-13734, 1997.
- Rothstein, D. E., Zak, D. R., Pregitzer, K. S., and Curtis, P. S.: Kinetics of nitrogen uptake by *Populus tremuloides* in relation to atmospheric CO<sub>2</sub> and soil nitrogen availability, *Tree Physiol.*, 20, 265-270, 2000.
- Sitch, S., Smith, B., Prentice, I. C., Arneth, A., Bondeau, A., Cramer, W., Kaplan, J., Levis, S., Lucht, W., Sykes, M., Thonicke, K., and Venevsky, S.: Evaluation of ecosystem dynamics, plant geography and terrestrial carbon cycling in the LPJ Dynamic Global Vegetation Model, *Global Change Biol.*, 9, 161-185, 2003.
- Thomas, R. Q., Bonan, G. B., and Goodale, C. L.: Insights into mechanisms governing forest carbon response to nitrogen deposition: a model-data comparison using observed responses to nitrogen addition, *Biogeosciences Discuss.*, 10, 1635-1683, 2013.
- Vergutz, L., Manzoni, S., Porporato, A., Novais, R.F., and Jackson, R.B. 2012. Global resorption efficiencies and concentrations of carbon and nutrients in leaves of terrestrial plants, *Ecol. Monogr.* 82, 205-220.

White, M. A., Thornton, P. E., Running, S., and Nemani, R.: Parameterisation and sensitivity analysis of the BIOME-BGC terrestrial ecosystem model: net primary production controls, *Earth Interact.*, 4, 1-55, 2000.

Zaehle, S. and Friend, A. D.: Carbon and nitrogen cycle dynamics in the O-CN land surface model: 1. Model description, site-scale evaluation, and sensitivity to parameter estimates, *Global Biogeochem. Cy.*, 24, GB1005, DOI: 10.1029/2009GB003521, 2010.

## Appendix A. List of symbols and their abbreviations in the model code

symbol	code abbrev.	description	unit
$BNF$	anfix	total annual nitrogen fixation	kgN ha <sup>-1</sup> yr <sup>-1</sup>
$L_o$	orgleachfrac	leaching from decayed organic carbon/nitrogen	-
$P_{H2O}$	dperc	daily percolation	mm
$T_s$	sand_frac	fraction of soil that is sand	-
$L_m$	minleachfrac	leaching from available nitrogen mineral pool	-
$W_{TOT}$	-	total amount of water in the soil column	mm
$N_{avail}$	nmass_avail	mineral N in soil column	kgN m <sup>-2</sup>
$C_j$	fracremain	daily decay rates for each pool	-
$k_{j,max}$	K_MAX	max exponential decay constants for each SOM pool	-
$\sigma$	wpfs	water filled pore spaces	-
$\theta_{max}$	wsats	saturation capacity	mm
$S$	clay_frac	fraction of soil that is clay	-
$F_m$	fm	metabolic fraction of litter	-
$\lambda$	leaf_lton root_lton	/ compartment litter lignin:N ratio	-
$cn$	-	C:N ratio of litter	kgC kgN <sup>-1</sup>
$N_{leaf}$	leafoptn	optimal leaf N content	kgN m <sup>-2</sup>
$L$	daylength	day length	s
$N_{store,max}$	max_n_storage	maximum long-term N storage capacity	kgN m <sup>-2</sup>
$k$	fnstorage	PFT specific storage constant	-
$N_{store}$	nstore_labile	labile N storage	kgN m <sup>-2</sup>
$N_{turnover}$	retransn_nextyear	expected amount of N to be retranslocated next year	kgN m <sup>-2</sup>
$N_{up,max}$	maxnup	maximum N uptake capacity	kgN m <sup>-2</sup>
$N_{up,root}$	nuptoroot	maximum N uptake capacity per fine root mass	kgN kgC <sup>-1</sup>
$k_m$	km_volume	half-saturation concentration for N uptake	kgN l <sup>-1</sup>
$z_{soil}$	soildepth	soil column depth	m
$CN_{leaf,min}$	cton_leaf_min	minimum C:N ratio of leaf	kgC kgN <sup>-1</sup>

$CN_{leaf,max}$	cton_leaf_max	maximum C:N ratio of leaf	kgC kgN <sup>-1</sup>
$f_{Nup}$	strenght	relative N uptake strength	-
$X$	densindiv	average density of individuals	indiv m <sup>-2</sup>
$k_{Nup}$	nupscoeff	weighting factor for root distribution	-
$lr_{max}$	ltor_max	leaf to root mass ratio under non-stressed conditions	kgC kgC <sup>-1</sup>
$\upsilon$	nscal	N stress scalar	-
$CN_{leaf,aopt}$	cton_leaf_aopt	annually optimal leaf C:N ratio	kgC kgN <sup>-1</sup>
$a_{leaf}$	leaflong	leaf longevity	year

### Appendix B. C:N ratios and base decay rates for soil and litter organic matter pools.

SOM pool	C:N ratio*	Base decay rate, $k_{max}$ (day <sup>-1</sup> )
surface metabolic litter	prognostic	$3.8 \times 10^{-2}$
surface structural litter	prognostic	$9.5 \times 10^{-3}$
fine woody debris	prognostic	$1.1 \times 10^{-2}$
coarse woody debris	prognostic	$2.2 \times 10^{-3}$
surface microbial	10-20	$2.7 \times 10^{-2}$
surface humus	15-30	$4.8 \times 10^{-4}$
soil metabolic litter	prognostic	$7.0 \times 10^{-2}$
soil structural litter	prognostic	$1.9 \times 10^{-2}$
soil microbial	5-15	$4.2 \times 10^{-2}$
slow SOM	15-30	$1.7 \times 10^{-3}$
passive SOM	9	$3.9 \times 10^{-6}$

\* prognostic = depends on growth and physiology of source plant material; see also Fig 2.

### Appendix C. PFT parameter changes for BNS

parameter	new	old
gdd5min_est	350	500
phengdd5ramp	100	200

## 5. Nitrogen transformations

*Stefan Olin, October 2018*

In conjunction with the addition of N cycling to LPJ-GUESS (Smith et al. 2014), all  $N_r$  (reactive N) were subject to transformations between organic N ( $N_{org}$ ) and  $N_r$ . Here, the exchange of mineral N to and from the SOM (Soil Organic Matter) pools is limited to  $NH_4$ , which is the dominating species in the exchange of N between the mineral and organic pools in soils. The N dynamics previously implemented in LPJ-GUESS were limited to a single mineral nitrogen pool. Here, we extend this further and include a more detailed representation of N dynamics adopted from the DyN model scheme (Xu-Ri and Prentice, 2008). The two major N cycling processes in the soil are nitrification and denitrification, and these can be subdivided into the following processes: aerobic autotrophic nitrification, which is the oxidation of ammonia ( $NH_3$ ) to nitrite ( $NO_2$ ) and nitrate ( $NO_3$ ); anaerobic heterotrophic denitrification, the second of the two main microbial processes in the soil N cycle, where  $NO_3$  is reduced to  $NO_2$ , nitric oxide (NO),  $N_2O$  and molecular nitrogen ( $N_2$ ) under insufficient concentration of oxygen ( $O_2$ ), and nitrifier denitrification, by autotrophic bacteria which oxidise  $NH_3$  to  $NO_2$  and reduce  $NO_2$  to NO,  $N_2O$  and  $N_2$ .

Microbial processes in soils occur on short time-scales and spatially in a highly heterogenic pattern (McClain et al., 2003). A number of factors influence the nitrification and denitrification rates where the processes are not fully understood, and where the influence of the major controlling factors is not easily defined; factors can have multiple roles and interact with other factors. Nonetheless, soil NO,  $N_2O$  and  $N_2$  emissions are reported to be controlled by soil characteristics such as drainage (aeration, texture, compaction), temperature, moisture, *pH*, organic matter, available N ( $NH_4$  and  $NO_3$ ), and C:N ratios of soil organic matter.

The N transformation processes described above are facultative aerobic or anaerobic processes (Pilegaard, 2013) but on the assumed scales LPJ-GUESS — larger regions or grid cells with a typical resolution of  $0.5^\circ$  — making the assumption of a uniform soil moisture is unrealistic, since soil moisture distribution is more patchy (Schurgers et al., 2006). This is also true for the internal modelled patch area of 0.1 ha. Thus, in the model, the simulated aerobic (and anaerobic) fraction of the soil is limited to be between 5 and 95%. Adopted from Pilegaard (2013), the fractionation of  $N_r$  follows the moisture content through the water filled pore space ( $\omega$ ):

$$\omega = \frac{\theta}{\phi}$$

where  $\theta$  is the actual water content of the soil ( $m^3/m^3$ ),  $\phi$  is the porosity which is determined from the soil physical properties, described in Olin et al. (2015b).  $\omega$  is then used to calculate the fraction of the soil that is aerobic or anaerobic ( $f_\omega$ ):

$$f_\omega = 0.95 + \frac{0.05 - 0.95}{1 + e^{-30(\omega - 0.5)}}$$

The different  $N_r$  species are fractionated each simulation day into wet (anaerobic,  $N_{x,anaero} =$

$N_x f_\omega$ ) and dry (aerobic,  $N_{x,aero} = N_x (1 - f_\omega)$ ) where  $x$  is either  $NO_2$ ,  $NO_3$  or  $NH_4$ .

### Ammonification

Production of  $NH_3$  from  $NH_4$  is modelled as a function of the anaerobic fraction of  $NH_4$  ( $NH_4 f_\omega$ ),  $pH$  and temperature:

$$NH_3 = f_\omega f_{T,N} e^{2(pH-10)} k_{NH_3,max} NH_4$$

where  $f_{T,N}$  is a temperature modifier that follows an Arrhenius type response, temperatures equal to or below  $-40^\circ C$  result in 0 and above  $25^\circ C$ , the temperature modifier becomes 1, between these temperature limits the following relationship as used:

$$f_{T,N} = e^{308.56 \left( \frac{1}{71.02} - \frac{1}{T_{soil} + 46.02} \right)}$$

and  $k_{NH_3,max}$  the maximum fraction of  $NH_4^+$  that can be emitted which is  $pH$  dependent. If  $pH$  is above 6, then the value of  $k_{NH_3,max}$  is 0.1%, and 0.001% otherwise. With the standard settings in the model,  $pH$  is read in together with soil mineral properties. In case  $pH$  values are not available, a simple relationship with annual precipitation is implemented.

### Nitrification

Nitrification — an aerobic process in which  $NH_4$  is oxidised to  $NO_2$  and  $NO_3$  — is a well studied microbial process in soils. In LPJ-GUESS nitrification is modelled as a transformation of the aerobic part of the  $NH_4$  pool which is oxidized to  $NO_3$ . During nitrification in the model, the production of  $NO_3$  ( $\Delta NO_3$ ) is formulated as follows:

$$\Delta NO_3 = N_{max} f_{T,nit} (1 - f_\omega) NH_4$$

where  $N_{max}$  is the maximum fraction of the ammonia in the dry phase that can be converted per day, in the model set to 10% (Xu-Ri and Prentice, 2008; Li, 2000), the temperature dependence of nitrification ( $f_{T,nit}$ ):

$$f_{T,nit} = \left( \frac{70 - T_{soil}}{70 - 38} \right)^{12} e^{12 \frac{T_{soil} - 38}{70 - 38}}$$

Of the simulated  $NO_3$  production, a proportion is lost as gases,  $f_{nitri,max-gas}$  (in the model set to 40%), which is divided into  $N_2O$  and  $NO_x$  based on the water saturation level ( $\omega$ ) as follows:

$$q_{N_2O:N_2,w} = 1 - \frac{0.5}{1 + e^{-20(\omega - 0.375)}}$$

derived from Pilegaard (2013), the production of  $NO_x$  from nitrification is thus:

$$\Delta NO_x = \Delta NO_3 q_{NO} f_{nitri,max-gas}$$

and for  $N_2O$ :

$$\Delta N_2O = \Delta NO_3 (1 - q_{NO}) f_{nitri,max-gas}$$

Also connected to nitrification, but without any gaseous losses, is the conversion of the  $\text{NO}_2$  that is in the dry phase to  $\text{NO}_3$ , which represent an abiotic oxidisation.

### Denitrification

Denitrification occurs in the wet (anoxic) parts of the soil (Pilegaard, 2013),  $\omega$  in the model, and entails the conversion of  $\text{NO}_3$  to  $\text{NO}_2$ . During this process, gaseous losses of  $\text{N}_2\text{O}$ ,  $\text{NO}_x$  and  $\text{N}_2$  occur:

$$\Delta \text{NO}_2 = f_{T,den} f_{LC} f_N f_{den,max} (1 - f_\omega) \text{NO}_3$$

where  $f_N$  is a concentration modifier of the maximum denitrification rate ( $f_{den,max}$ ):

$$f_N = \frac{(1 - f_\omega)X}{K_N V_w + (1 - f_\omega)X}$$

where  $X$  can be either  $\text{NO}_3$  or  $\text{NO}_2$  and  $K_N$  is the Michaelis-Menten constant for this rate, and is set to  $0.083 \text{ kg N m}^{-3}$  (Shah 1978),  $V_w$  is the volume of water in the soil in  $\text{m}^3$ ; and  $f_{LC}$  the labile carbon ( $C_{labile}$ ) rate modifier.  $C_{labile}$  is not modelled explicitly in LPJ-GUESS, therefore  $C_{labile}$  is considered to be proportional to the heterotrophic respiration  $R_h$  by the proportionality constant  $q_{LC}$ , currently set to 1 in the model.

$$f_{LC} = \frac{(1 - f_\omega)q_{LC}R_h}{K_C V_w + (1 - f_\omega)q_{LC}R_h}$$

and  $f_{T,den}$  the temperature modifier of denitrification processes:

$$f_{T,den} = e^{308.56 \left( \frac{1}{68.02} - \frac{1}{T_{soil} + 46.02} \right)}$$

After this step, the  $\text{NO}_2$  mass is updated with the  $\Delta \text{NO}_2$  calculated followed by calculation of the gaseous N produced by denitrifiers:

$$\Delta N_{gas,den} = f_N f_{\omega,den} f_{LC} f_{den,max} (1 - f_\omega) \text{NO}_2$$

where  $f_{\omega,den}$  is the moisture dependence of N gas production:

$$f_{\omega,den} = e^{13.04\omega - 11.62}, 0 \leq f_{\omega,den} \leq 1$$

taken from Weier et al. (1993). The fractionation of the gas produced by denitrification into  $\text{N}_2$ ,  $\text{NO}_x$  and  $\text{N}_2\text{O}$  is then determined by the temperature and moisture content of the soil. Relationships between the three N species and their dependence on soil water status have been derived from Pilegaard (2013), with no production of  $\text{N}_2$  if the  $\omega$  is below 70%, and thus only  $\text{N}_2\text{O}$  and  $\text{NO}_x$  can be produced, which is determined by the following:

$$q_{\text{N}_2\text{O}:\text{NO}_x} = 3.2\omega - 0.92, 0 \leq q_{\text{N}_2\text{O}:\text{NO}_x} \leq 1$$

yielding:

$$\Delta \text{NO}_{x,den} = \frac{\Delta N_{gas,den}}{1 + q_{\text{N}_2\text{O}:\text{NO}_x}}$$

$$\Delta \text{N}_2\text{O}_{den} = \Delta N_{gas,den} - \Delta \text{NO}_{x,den}$$

When  $\omega$  is equal to or larger than 70%, no  $\text{NO}_x$  is produced. The fractionation between  $\text{N}_2\text{O}$  and  $\text{N}_2$  follows a similar relationship based on  $\omega$ , but there is also a temperature dependence taken from Maag and Vinther (1996):

$$q_{\text{N}_2\text{O}:\text{N}_2,w} = 1 - \frac{1}{1 + e^{-62(\omega - 0.875)}}$$

$$q_{\text{N}_2\text{O}:\text{N}_2,T} = \frac{1}{1 + e^{-\frac{T_{\text{soil}} - 5}{10}}}$$

$$\Delta N_2 O_{\text{den}} = \Delta N_{\text{gas},\text{den}} q_{\text{N}_2\text{O}:\text{N}_2,T} q_{\text{N}_2\text{O}:\text{N}_2,w}$$

$$\Delta N_{2,\text{den}} = \Delta N_{\text{gas},\text{den}} - \Delta N_2 O_{\text{den}}$$

Results from the equations above are then added to the existing pools for later gaseous emissions from the soil.

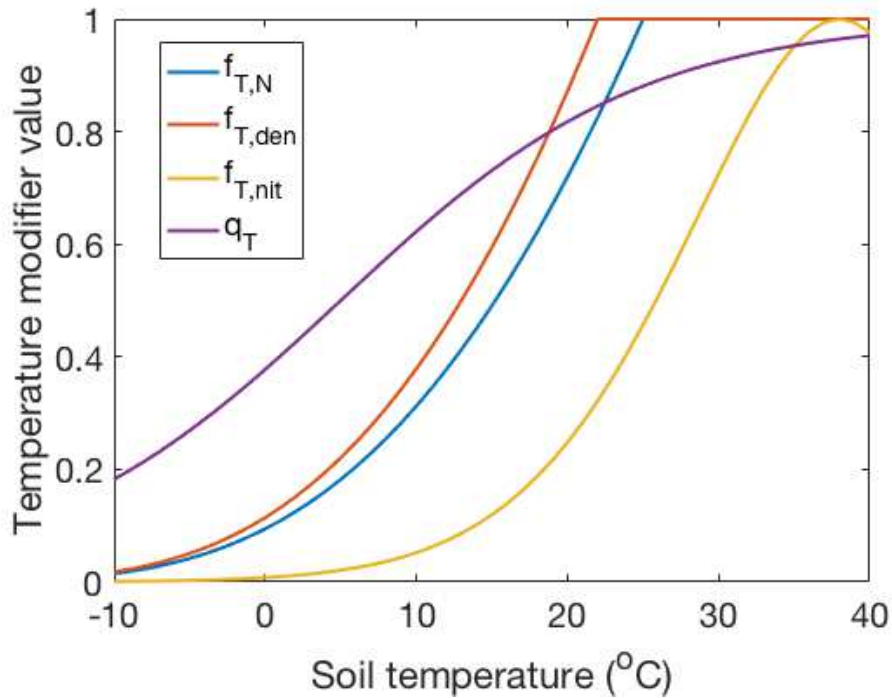


**Figure 1 Temperature modifiers described in this section.**

### **N gas emissions from the soil**

Emissions of the  $\text{N}_r$  gases produced in the soil to the atmosphere are modelled as rate of change in the simulated pools. Emissions of  $\text{N}_x$  ( $x = \text{any of } \text{NH}_3, \text{NO}, \text{N}_2\text{O} \text{ or } \text{N}_2$ ) are modelled as the fraction of dry mass times a temperature function ( $f_{T,N}$ ):

$$E_x = X f_{T,N}$$

## 6. Land cover and land use

*Mats Lindeskog and Stefan Olin, July 2015*

### Land cover representation

Land use and cropland representations are implemented in LPJ-GUESS based on LPJ-mL, (Bondeau et al., 2007), with a number of modifications and extensions (Lindeskog et al., 2013). Supported land cover types in addition to potential natural vegetation (PNV) are cropland, pasture and managed forest (urban and barren land fraction input may be used also, but these have no vegetation implementation). Land cover change is based on net area fraction input data for the land cover types and stand types within a land cover type (e.g. different crops). Optionally, gross land cover transition input (e.g. as provided by the LUH2 gridded land use product) may be used together with the net area fraction input. A number of options for how to treat transferred land (harvest, pooling/creation of new stands etc.) may be selected either in the instruction file or by settings in the code.

At the conversion of forest to cropland, by default 90 % of tree stems are harvested and the rest is transferred to the atmosphere in the same year (burned). Part of the harvested wood (firewood) is transferred to the atmosphere the same year (67 %) and the rest moved to a pool with a 25-year turnover period, representing paper and timber. At cropland abandonment (conversion to natural vegetation), a new stand is created from bare ground, allowing the establishment of natural vegetation with a succession e.g. from grass to deciduous trees and finally evergreen trees. An example of modelled carbon fluxes at cropland expansion and abandonment is shown for a moist tropical site in Africa in Figure 1.

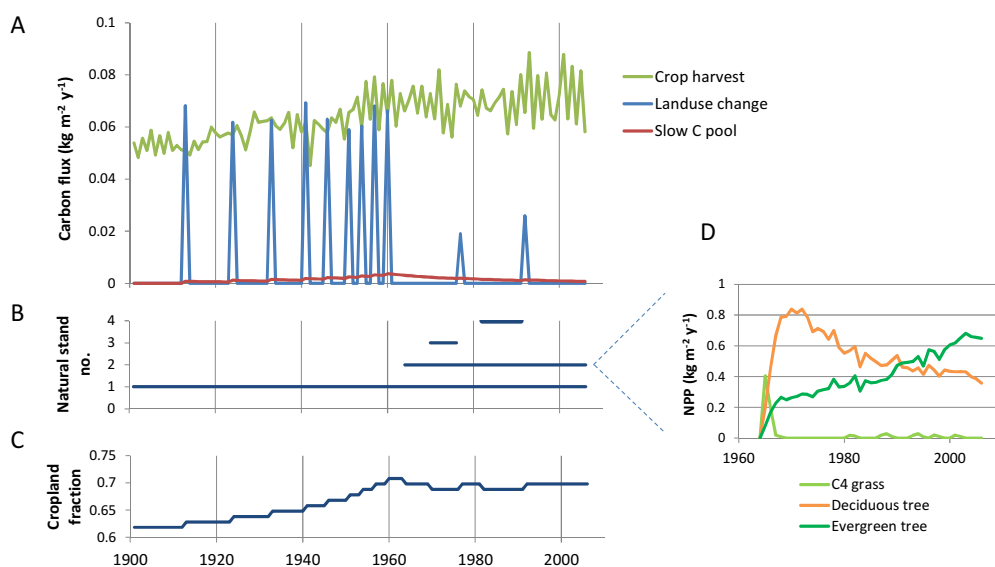


**Figure 1.** Example of land use change modelling at a moist tropical site (9°W, 5.5°N) during the period 1901-2006. **A.** Carbon fluxes to the atmosphere associated with crop harvest and land use change (cropland expansion/deforestation). The “slow C pool” represents the transfer of carbon from the long-lived wood pool harvested at cropland expansion to the atmosphere. **B.** Lifetime of natural vegetation stands. New stands are created at cropland abandonment and destroyed at subsequent cropland expansion. **C.** Cropland area fraction, showing the expansion and reduction of cropland area. **D.** NPP of three PFTs at one of the natural stands created at cropland

**abandonment, representing a typical plant successional sequence where an initial dominance of grass is followed by forest, dominated first by deciduous and later by evergreen trees.**

When converting PNV to managed forest, the forest can either be clearcut or left standing, starting a cycle of simplified continuous cutting based on tree diameters (to be further developed).

Grazing of managed grassland is simulated by removing 50 % of the above-ground carbon. This is roughly in agreement with estimates of a 90 % removal in intensively grazed pastures and a 50 % retention of this carbon in the litter pool as manure.

Fires are excluded by default from pasture, cropland and managed forest.

As for cropland (see below), stand managements for other land cover types may be defined in stand types, or when using rotations, management types, in the instruction file, specifying “planting systems” (limiting PFTs that may establish, specified in the instruction file or by custom rules in the code), “harvest systems” (clearcut, continuous tree cutting), hydrology (irrigated/rain-fed), N fertilisation etc. Limiting establishment of natural PFTs may be specified for all land cover types in the stand type definition.

### **Cropland representation**

Separate crop phenology schemes on a daily time-step are present for simulations with and without N-limitation. Cropland without N-limitation is represented by eleven crop PFTs (temperate cereals, rapeseed, pulses, sugarbeet, maize, soybean, tropical cereals, sunflower, peanut, cassava and rice), simulated separately (without inter-PFT competition) and two grass PFTs (competing C<sub>3</sub> and C<sub>4</sub> grass) as cover crop between harvest and sowing. The same grass PFTs are used to represent pastures. Currently, two crop PFTs are defined for N-limited simulations (wheat and maize).

Irrigated crops are simulated separately. Irrigation water is added if atmospheric demand for transpiration exceeds plant water supply, but irrigated crops can still enter water stress if atmospheric demand exceeds a maximum evapotranspiration rate (5 mm/day).

When N cycling is switched off, there is a simple link between daily crop leaf carbon mass and LAI, while the the sum of heat units (degree days above a crop-specific base temperature, T<sub>b</sub>) accumulated from the time of sowing mainly determines the allocation of photosynthates (Figure 2).

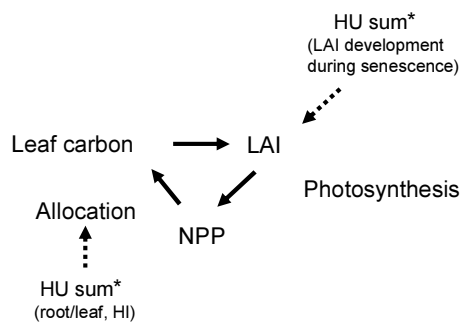


**Figure 2. Non-N-limited crop phenology in LPJ-GUESS. The feedback between leaf area and leaf carbon mass via NPP is denoted by full-line arrows and the heat unit sum control of the carbon allocation and leaf LAI is denoted by dotted arrows. \*HU sum: heat unit sum (dynamic potential HU adapted to local climate); LAI: leaf area index; HI: harvest index, NPP: net primary production.**

Upon sowing, the initial carbon is set to  $10 \text{ g m}^{-2}$ . Carbon allocation to crop roots, leaves and harvestable organs is performed on a daily time-step. The development of the harvest index (HI), i.e. the fraction of above-ground carbon present in the harvestable organs, the root/shoot ratio and the onset of senescence and LAI development during senescence are dependent on accumulated heat units and calculated as in Bondeau et al. (2007). The PHU sum needed for full development of a crop, determining the time at which the crop is harvested, is calculated dynamically, using a 10-year running mean of heat unit sums accumulated from the sowing date to the end of a sampling period (ranging from 190 to 245 days) derived from default sowing and harvest limit dates following Bondeau et al. (2007). The dynamic PHU calculation can be done either for an initial time period only, to calibrate for the local climate, or also for an extended period, to simulate adaptation to a changing climate by selecting suitable crop varieties/genotypes. A lower PHU limit of 900 degree days is used. Maintenance respiration of storage organs is set to zero. The non-N-limited modelled crop yield represents potential optimal yield, limited by climate and  $\text{CO}_2$  only.

#### ***N-limited version, Olin et al. (2015):***

Below the updated version of LPJ-GUESS incorporating C-N interaction also for crops is described; for a more comprehensive description, see Olin et al. (2015). The model allocates daily NPP based on the crop's development phase and allows for an adjustment of the allocation scheme based on the current nutrient and water status of the crop.

#### **Crop development**

Upon sowing, the development of a crop plant in LPJ-GUESS starts with a seedling that has an initial carbon mass in leaves and roots. The N content in the seedling is initiated with the highest N concentration ( $[\text{N}]$ ) (the minimum  $\text{C:N}_{\text{leaf,min}}$  allowed in the model assuming a seed with a high N density).

#### **Development stage**

In most ecosystem and crop models, plant phenological development is modelled based on weather conditions often accumulated over a certain time period such as PHU (see above). Here we define development stage (DS) as a number between 0 and 2 where:  $0 < DS < 1$  is the main vegetative phase, at  $DS=1$  anthesis occurs and  $DS > 1$  represents the grain filling phase. Compared to the original PHU implementation in the model, the use of DS facilitates a more detailed division of the growing period into the different crop phenological stages. Periods when the plant is more susceptible to heat and nitrogen stress can thus be represented in a more precise manner. DS at a given point in time ( $t$ ) is a cumulative function of the maximal development rate  $d_r$  ( $\text{day}^{-1}$ ) which differs between the vegetative phase and the reproductive phase. Following Wang & Engel (1998), DS is also modified using dimensionless scaling factors dependent on temperature ( $f_T$ ), vernalisation days ( $f_{vern}$ ) and photo-period ( $f_{phot}$ ):

$$DS_t = DS_{t-1} + d_r f_T f_{phot} f_{vern}$$

### Daily carbon allocation

For the allocation of the plant's daily assimilates, and their partitioning to the plant organs during the growing-season, we use the established allocation scheme from Penning de Vries et al. (1989). This scheme differs from the one described above for the non N-limited configuration, in that the allocation of C to the different organs is related to the daily NPP and to DS, as opposed to a function that meets a predefined target at the end of the growing season. During the first part of the vegetative phase ( $DS < 0.7$  for winter wheat) most of the assimilates are used for root (R) and leaf (L) growth to maximise the uptake of water and nutrients and the absorption of radiation for photosynthesis, followed by a period when more of the assimilated C is allocated to the stem (St).

After anthesis, the grain-filling period starts, during which most assimilates are allocated to the storage organs. During this period, cereal crops reallocate some of their nutrients from the vegetative organs to the grains.

When a plant experiences water or nutrient deficit during the vegetative phase, it starts to invest a relatively larger fraction of the assimilates into roots to overcome the stress. It is thus important to be able to model the allocation to the roots separately from the other organs. The ratio between the allocation to leaves and stem (L:St), can be treated as constant during stress and thus a relationship between the allocation to R and that to the vegetative parts ( $V=St+L+R$ ) that is also valid under stress can be established. This approach also gives an opportunity for future implementation of dynamic adjustments in the allocation during the vegetative phase, which is lacking in the current allocation model.

Relationships between allocation to L, St, R and grains (Y) from the original allocation model were established and fitted to a logistic growth function.

### Roots

The allocation to R ( $g_R$ ) relative to the vegetative organs ( $g_V$ ) is shown in Fig. 3a:

$$\frac{g_R}{g_V} = 0.52 + \frac{0.47}{1 + e^{7.63(DS - 0.55)}} = f_1$$

### Leaves and stems

Reflecting the shift from L ( $g_L$ ) to St ( $g_{St}$ ) allocation during the initial part of the vegetative phase as outlined above, a relationship between the two organs was derived which is illustrated in Fig. 3a:

$$\frac{g_L}{g_L + g_{St}} = 0.88 + \frac{0.79}{1 + e^{13.99(DS - 0.65)}} = f_2 \cdot$$

### Harvestable organs, grains

Finally a relationship of the allocation to grains ( $g_Y$ ) as the fraction of the whole plant ( $g_Y + g_V$ ) allocation was derived:

$$\frac{g_Y}{g_Y + g_V} = \frac{1}{1 + e^{8.32(DS - 1.15)}} = f_3 \rightarrow g_V = 1 - f_3$$

### Dynamic allocation

These relationships between the allocation to the different organs of the plant can be applied to favour allocation to one organ over others. Combining the equations for  $f_1$ ,  $f_2$  and  $f_3$  yields

$$\begin{aligned} g_R &= f_1(1 - f_3) \\ g_L &= f_2(1 - f_1)(1 - f_3) \\ g_{St} &= (1 - f_2)(1 - f_1)(1 - f_3) \\ g_Y &= f_3 \end{aligned}$$

which is illustrated for winter wheat in Fig. 3b

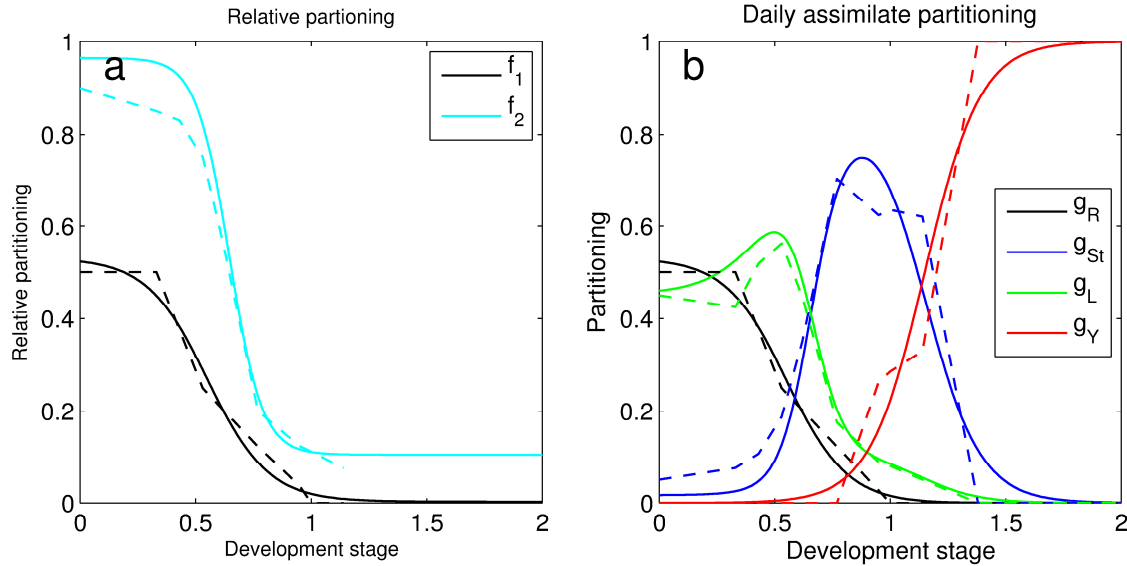


**Figure 3:** (a) The allocation to roots relative to vegetative organs ( $f_1$ ) and the allocation to leaves relative to leaves and stem ( $f_2$ ) for winter wheat. Dashed lines represent the allocation model from Penning de Vries (1989) and solid lines are the fitted equations. (b) The resulting allocation scheme to roots ( $g_R$ ), stem ( $g_{St}$ ), leaves ( $g_L$ ) and grains ( $g_Y$ ) (solid lines) compared to data from Penning de Vries (1989) (dashed lines).

### Carbohydrate retranslocation

Crops store an easily mobilised reserve of carbohydrates in L, St and R (for some crops also tubers). To represent this in the model, a labile C pool is filled with a fraction of the daily assimilates directed to the stem ( $g_{St}$ ), set here to 0.4 for wheat (Penning de Vries 1989). The labile C pool ( $M_{C,labile}$ ) is constrained between 0 and  $0.4M_{C,st}$ . During days when the daily assimilated C is lower than respiration costs (negative NPP), these sugars are used to compensate the loss. Additionally, during the grain-filling period the labile C pool is used to add to the grains and is reduced with a rate of  $0.1 \text{ day}^{-1}$  (Penning de Vries 1989).

### Daily nitrogen allocation

During the vegetative phase in which the leaves and roots are expanding, the plant seeks to maximise photosynthetic gain by having a leaf N content that optimises the carboxylation capacity ( $V_{max}$ ).

### Leaf N content

Nitrogen associated with Rubisco, the key enzyme in photosynthesis, makes up more than 20% of the total N in the leaves of wheat, but N is also important for plant structural tissues. However, the vertical distribution of N in the canopy is not even. Higher [N] is usually found in the upper part of the canopy, where leaves experience the highest levels of irradiance, compared to the more shaded leaves below. The decline in leaf [N] with the increase in cumulative leaf area index (LAI) from top to bottom typically follows an exponential decrease with a N extinction coefficient  $k_N$  that is related to the light extinction coefficient ( $k_L$ ) as follows:

$$k_N = b_0 + b_1 k_L ,$$

where  $b_0$  and  $b_1$  are regression coefficients taken from Yin (2003). From theory on optimal N distribution in a crop canopy, Yin (2000) derived a relationship between the LAI that can be supported given the amount of N that is currently in the leaves ( $LAI_N$ ) and  $k_N$ :

$$LAI_N = \frac{1}{k_N} \ln \left( 1 + k_N \frac{M_{N,L}}{N_b} \right),$$

where  $M_{N,L}$  is the leaf N mass and  $N_b$  is the minimum N requirement for the leaf to function:

$$N_b = \frac{1}{C : N_{L,max} SLA} ,$$

where  $C:N_{L,max}$  reflects the minimum N required for photosynthesis and SLA is the specific leaf area.  $LAI_N$  is then compared to LAI to determine the N status of the canopy, see section on Senescence below.

### Root N content

In LPJ-GUESS, the N requirement of the root follows that of the leaves through the functional balance concept (described above in the N implementation section):

$$\frac{M_{N,L}}{M_{C,L}} \propto \frac{M_{N,R}}{M_{C,R}} ,$$

where  $M_{N,L}$  denotes leaf N mass,  $M_{C,L}$  leaf C mass,  $M_{N,R}$  root N mass and  $M_{C,R}$  root C mass. The theory behind the concept is that the activity of the roots (uptake and transport of water and nutrients) is proportional to that of the leaves (photosynthesis). A high photosynthesis rate in the leaves (high  $[N]_L$ ) implies a corresponding relative  $[N]$  in the roots to supply the demand of the leaves (Zaehle & Friend 2010).

### Plant N uptake

For crops, we have expanded N uptake in the soil N module so that the N available for uptake by the plant ( $M_{N,avail}$ ) is related to the water content of the soil, as proposed by Xu-Ri (2008):

$$M_{N,avail} = \theta \phi M_{N,soil} ,$$

where  $\phi$  is the fraction of projected leaf coverage by the plant (proportional to the fine root area),  $M_{N,soil}$  is the mineral N mass of the soil and  $\theta$  is the mean water content of the soil profile.

### Senescence

Senescence, the killing of cells, can be either genetically programmed and age dependent, or induced by stresses or environmental factors. In the C-only original cropland version of LPJ-

GUESS, leaf senescence is a function of PHU. We develop this further here with a dynamic response of plant senescence to its N status and age (DS).

### Leaf senescence

If the N status of the leaves is suboptimal, the plant tries to maximise the leaf N in the canopy by redirecting some of it from the shaded leaves towards those that are more sunlit. This will eventually turn off the photosynthetic apparatus in the leaves from which all the non-structural N has been retranslocated. Senescence of part of the canopy in the model is induced when the N-determined leaf area index LAI (Yin 2000) is lower than the actual LAI. Senescence of crop leaves is set to take place over 10 days. Implemented here is the proposed reduction of the leaf C mass as in (Yin 2000) but with an inertia of 0.1 day<sup>-1</sup>:

$$m_{C,sen} = 0.1 \frac{LAI - \min(LAI, LAI_N)}{SLA}$$

The leaf C mass is then updated  $M_{C,L}' = M_{C,L} - m_{C,sen}$  and N accordingly using the minimum N content of the leaves,  $C:N_{L,max}$ ,  $M_{N,L}' = M_{N,L} - m_{C,sen} (C:N_{L,max})^{-1}$ . The senesced C and N is then transferred to a pool of dead leaves with a high C:N, currently set to 100 and the residual N is translocated to the labile N pool. In contrast to the labile C pool, N allocated to the labile pool is not determined as a fraction of the total allocation. The amount is constrained by the N translocated from senesced leaves and roots respectively through the functional balance concept. The N that is translocated to the labile N pool due to senescence of the leaf is the leftover after maximising the C:N<sub>L</sub> status:

$$m_{N,sen} = M_{N}' \frac{M_{C,L}'}{C:N_{L,opt}} \quad \text{for } C:N_L < C:N_{L,min}$$

$$0 \quad \text{for } C:N_L \geq C:N_{L,min},$$

where C:N<sub>L,opt</sub> is the C:N below which a decrease has a small or no effect on photosynthesis which is estimated here as 3/4 of the range between C:N<sub>L,max</sub><sup>-1</sup> and C:N<sub>L,min</sub><sup>-1</sup>.

In ageing leaves, observed enzyme efficiency is reduced. After anthesis, degradation of Rubisco is higher than the de novo synthesis. To reflect this in the model, a reduction of the leaf N content at rate of 0.1 day<sup>-1</sup> starts at anthesis (DS>1).

In order to avoid excessive allocation of C to the leaves while the plant experiences leaf N deficit ( $m_{C,sen}>0$ ) during the vegetative phase, a rescaling of the factor that controls the flow of assimilates to the leaves was implemented:

$$f_2' = (f_2)^2, \text{ for } m_{C,sen} > 0.$$

### Root senescence

Root senescence is still a relatively unexplored area. In the absence of full mechanistic understanding, the dynamics of the root in the model are assumed to be coupled to those of the leaves through the functional balance concept (described above).

### Seed development

During flowering and grain filling, a fraction of the assimilates is allocated to the grains, while the N transported to the grains comes primarily from the leaves. This is reflected in the model as a transport of N from the leaves, roots and the labile N pool. In the model the plant tries to meet the demand from the grain:

$$m_{N,Y,dem} = \frac{m_{C,Y}}{C : N_{L,min}},$$

primarily by reducing the labile N pool,  $M_{N,labile}$ .

### Nitrogen retranslocation

If  $m_{N,Y,dem}$  is larger than the labile N pool, the crop plant attempts to meet the unsatisfied N demand from the grains ( $m_{N,Y,dem}' = m_{N,Y,dem} - M_{N,labile}$ ) by N transport from the donor organs (leaves and roots). These donor organs have a resistance to let go of their N,  $r_j$ , to account for the fact that N is needed for maintaining organ processes (e.g. photosynthesis and maintenance respiration):

$$r_j = \left( 1 - \frac{C : N_{j,opt}^{-1} - C : N_j^{-1}}{C : N_{j,opt}^{-1} - C : N_{j,min}^{-1}} \right)^2, r \in [0,1],$$

where  $j$  denotes the organ, L or R. The actual transport of N ( $m_{N,retr}$ ) is calculated by summing the individual organs' relative portion of the total N demand from the grains after the labile pool has been emptied. If the demand on the organ is larger than the available N, it is reduced to its minimum N content ( $C:N_{j,max}$ ):

$$m_{N,j,retr} = \min \left( \frac{M_{C,j}}{C : N_{j,max}}, \frac{m_{N,Y,dem}' (1 - r_j)}{1 - r_L + 1 - r_R} \right).$$

During the initial part of the grain filling period, only leaves contribute to fulfilling the grain N demand. Once more than half of the assimilates goes to the grain ( $DS > 1.15$ ), the model can utilise part of the plant root N as well to fulfil the N requirements of the grains.

### Sowing and harvest (C-only and N-limited versions)

The relative degree of limitation by temperature and precipitation to the sowing dates—or the absence of such limitation in perennially moist areas (where incoming solar radiation generally limits plant production)—is determined based on the local climatology (Waha et al., 2011). To this end, five main seasonality types are distinguished during the simulation by continuously monitoring the latest 20-year climate: TEMP (temperature seasonality); PREC

(precipitation seasonality); TEMPPREC (both temperature and precipitation seasonality, minimum monthly temperature < 10°C), temperature determines sowing date; PRECTEMP (both temperature and precipitation seasonality, minimum monthly temperature >=10°C), precipitation determines sowing date; NONE (neither temperature nor precipitation seasonality), default sowing date used. For irrigated crops at PRECTEMP sites, temperature-dependent sowing is used by default. The temperature limits for temperature-dependent sowing are as in Waha et al. (2011).

Croplands are harvested each year. A PFT-specific fraction of the harvestable organs (the harvest efficiency, default value 0.9 for all crops) constitutes the yield (multiplied by 2.0 for deriving the total dry yield from carbon units, assuming a dry matter carbon content of 50 %) and is assumed to be oxidised within a year. Of the leaf carbon, a further fraction (the residue removal fraction) is removed (and oxidised within one year). This PFT parameter is set to 0.75 for all crops as default.

Different cropland managements are defined in stand types, or when using rotations, management types, in the instruction file with specified values for crop PFT, hydrology (irrigated/rain-fed), N fertilisation, fallow etc.

## References

This is not a complete list of references, in Lindeskog et al. and Olin et al. you will find all references used in this chapter.

- Bondeau, A., Smith, P.C., Zaehle, S., Schaphoff, S., Lucht, W., Cramer, W., Gerten, D., Lotze-Campen, H., Müller, C., Reichstein, M., and Smith, B.: Modelling the role of agriculture for the 20th century global terrestrial carbon balance, *Glob. Change Biol.*, 13, 679-706, 2007.
- Lindeskog M, Arneith A, Bondeau A, Waha K, Seaquist J, Olin S, and Smith B. Implications of accounting for land use in simulations of ecosystem services and carbon cycling in Africa. *Earth Syst. Dynam.*, 4:385-407, 2013.
- Olin, S., Schurgers, G., Lindeskog, M., Wärlind, D., Smith, B., Bodin, P., Holmér, J., & Arneith, A. (2015). Modelling the response of yields and tissue C : N to changes in atmospheric CO<sub>2</sub> and N management in the main wheat regions of western Europe. *Biogeosciences*, 12(8), 2489–2515. <https://doi.org/10.5194/bg-12-2489-2015>
- Waha K, van Bussel LGJ, Müller C, and Bondeau A. Climate-driven simulation of global crop sowing dates, *Global Ecol Biogeogr* 21:247-259, 2012.
- Xu-Ri, and I. C. Prentice. 2008. "Terrestrial Nitrogen Cycle Simulation with a Dynamic Global Vegetation Model." *Global Change Biology* 14 (8): 1745–64. <https://doi.org/10.1111/j.1365-2486.2008.01625.x>.
- Yin, X., Schapendonk, A. H. C. M., Krop, M. J., van Oijen, M., and Bindraban, P. S. (2000). A generic equation for nitrogen-limited leaf area index and its application in crop growth models for predicting leaf senescence. *Annals of Botany*, 85(5):579-585.
- Zaehle, S. and Friend, A. D.: Carbon and nitrogen cycle dynamics in the O-CN land surface model: 1. Model description, site-scale evaluation, and sensitivity to parameter estimates, *Global Biogeochem. Cy.*, 24, GB1005, DOI: 10.1029/2009GB003521, 2010.

## 7. C:N ratios of plant tissues

*Michael Mischurow, November 2015*

As implemented in C-N version of the model (Smith et al. 2014), nitrogen content of plant tissues can vary between minimum and maximum values of C:N. The relationship between the two was calculated based on White et al. (2000) and equals 2.78. As was acknowledged in the paper, these limits might be unreasonably wide, exaggerating biochemical plasticity of the real plants. The same issue was noted in the behaviour of other models with flexible stoichiometry, particularly related to the overestimation of the whole-plant nitrogen-use efficiency (Zaehle et al., 2014).

Meyerholt and Zaehle (2015) showed that fixing of C:N ratio for woody tissues can improve modelling performance. Here we go one step further and fix both woody and root C:N ratios in a very narrow range. The ratio between minimum and maximum C:N values is, therefore, set to be 10/9 rather than 2.78 (i.e., minimum = 0.9 \* maximum). The choice of implementation approach was motivated, in part, by desire to keep changes to the existing framework (with the range of C:N values) to a minimum.

### References

- Meyerholt, J. and Zaehle, S. (2015), The role of stoichiometric flexibility in modelling forest ecosystem responses to nitrogen fertilization. *New Phytol.* doi:10.1111/nph.13547
- Michael A. White, Peter E. Thornton, Steven W. Running, and Ramakrishna R. Nemani, (2000), Parameterization and Sensitivity Analysis of the BIOME-BGC Terrestrial Ecosystem Model: Net Primary Production Controls. *Earth Interact.*, 4, 1–85. doi: 10.1175/1087-3562(2000)004<0003:PASAOT>2.0.CO;2
- Zaehle, S., Medlyn, B. E., De Kauwe, M. G., Walker, A. P., Dietze, M. C., Hickler, T., Luo, Y., Wang, Y.-P., El-Masri, B., Thornton, P., Jain, A., Wang, S., Warlind, D., Weng, E., Parton, W., Iversen, C. M., Gallet-Budynek, A., McCarthy, H., Finzi, A., Hanson, P. J., Prentice, I. C., Oren, R. and Norby, R. J. (2014), Evaluation of 11 terrestrial carbon–nitrogen cycle models against observations from two temperate Free-Air CO<sub>2</sub> Enrichment studies. *New Phytol.* 202: 803–822. doi:10.1111/nph.12697

## 8. Soil input

*Stefan Olin, October 2018*

Soils are characterised by their ability to store and provide water to the plants; a parameterisation of these soil water characteristics based on fractions of grain sizes was introduced in version 4.1. Soil water characteristics used in LPJ-GUESS are derived from data on sand, silt and clay for the top soil layer taken from a map of soil mineral fractions. These fractions were then used as input to empirical relationships (Cosby et al., 1984, Table 3) for the following soil water characteristics: soil water pressure at saturation ( $\Psi_s$ ), volumetric water content at saturation ( $\theta_s$ ) and a shape parameter describing the response of the water retention curve to changes in water content ( $b$ ). These parameters were then used to derive the volumetric water content under specific conditions:

$$\Psi_i = \Psi_s \left( \frac{\theta_i}{\theta_s} \right)^b \Leftrightarrow \theta_i = \theta_s \left( \frac{\Psi_i}{\Psi_s} \right)^{-b}$$

where  $\Psi_i$  is the actual pressure head (m) and  $\theta_i$  is the actual volumetric water content ( $\text{m}^3 \text{m}^{-3}$ ). The percolation coefficient  $K$  (Haxeltine & Prentice 1996a), an empirical parameter used in the model to derive the daily percolated water, was fitted against  $b$  values for four of the soil classes from Haxeltine & Prentice (1996a) (coarse, medium-coarse, medium, fine) and resulted in:

$$K = 5.49 - 0.22b$$

### References

See references in Chapter 4.

## 9. Weather generator GWGEN (Global Weather GENERator)

Lars Nieradzik, November 2019

With the fire model BLAZE demanding additional input it was decided to implement the weather-generator GWGEN. It provides daily data downscaled from monthly sums or averages for

- Precipitation
- Maximum and minimum Temperature
- Cloud-fraction
- 10m horizontal wind

Using a Markov-Chain approach GWGEN provides daily weather parameters cross-correlated to daily precipitation. It also imposes a daily variability. For scientific and technical description of the core algorithms of GWGEN, please refer to the descriptive article by *Sommer and Kaplan 2017*.

### Implementation

GWGEN ingests the following data as monthly input

- Total precipitation [mm]
- Total number of wet days
- Average  $T_{\max}$  [°C]
- Average  $T_{\min}$  [°C]
- Net downward shortwave solar radiation [ $\text{W}/\text{m}^2$ ]
- Average 10m horizontal wind-speed [m/s]

and computes daily values of each of the above (except wetdays, of course). Relative humidity  $\varphi$  is computed using a version of the Arden Buck formula (Buck, 1981) assuming dew-point temperature  $T_{\text{dew}}=T_{\min}$ :

$$\varphi = e^{\frac{18.678 \cdot T_{\min}}{257.14 + T_{\min}} - \frac{(18.678 - T_{\text{mean}}/234.5) \cdot T_{\text{mean}}}{257.14 + T_{\text{mean}}}}$$

Radiation is first transformed into cloud-fraction using the transformation following Prentice et al. 1993 as used in the computation of daylength, insolation and EET.

As GWGEN makes predictions these come with an uncertainty, i.e. the results don't exactly match the ingoing monthly averages and therefore corrections are applied to the daily values for each grid-cell  $i$  (after they have been re-converted into LPJ-GUESS's values insol and relative humidity).

For the temperatures ( $T_{\min}$ ,  $T_{\max}$ ) a bias-shift is applied

$$\tilde{T}_{i,d} = T_{i,d} + \left( \bar{T}_i - \frac{1}{N} \sum_{n=1}^N T_{i,n} \right)$$

where  $\tilde{T}$  is the corrected temperature of day  $d$ ,  $T$  the computed temperature for day  $d$ ,  $\bar{T}$  the monthly mean read as input,  $N$  the number of days in that month, and  $i$  indicates either *maximum* or *minimum* temperature.

For precipitation and wind the values are corrected by a factor  $f$ :

$$f = \frac{\bar{O}}{1/N \sum_{n=1}^N O_n}$$

where  $\bar{O}$  is the monthly mean read as input,  $N$  the number of days in the month, and  $O_n$  the value computed for day  $n$ .

For insolation and relative humidity, the values are corrected with a redistribution that ensures that boundary-values are not exceeded, while the monthly mean is still conserved. These boundary values are  $[0, 1]$  for relative humidity and  $[0, S_{i,max}(doy)]$ , where  $S_{i,max}(doy)$  is the maximum possible solar irradiance for grid-cell  $i$  at the given *day-of-year*.

### Adjustments: Accuracy vs Runtime-efficiency

GWGEN was developed as a stand-alone weather-generator with internal break-off criteria to what can be considered to be a sufficiently accurate result. The implementation in LPJ-GUESS post-adjusts the daily values to fit the monthly values (see previous paragraphs) and, thus, these criteria were redefined, a cost-function was introduced, and a maximum number of iterations was implemented. One critical assumption was made to significantly reduce runtime: The accuracy w.r.t. the correct number of wet-days was made dependent on the input to reflect the fact that the actual number of days is less important the more often it rains in a month.

**Table 1: Required forecast accuracy of GWGEN's wet-days depending on actual number of wet-days**

Number of wet-days	Output accuracy ( $\Delta d_{wet-thresh}$ )
$\leq 5$	$\pm 0$
$\leq 10$	$\pm 1$
$\leq 20$	$\pm 2$
$> 20$	$\pm 3$

The two –modified – direct break-off criteria for finding a sufficiently accurate result are:

$$p_m \leq 0.01 \text{ mm} \wedge |\Delta \overline{T_{min}}| < 2.5^\circ\text{C}$$

and

$$|\Delta d_{wet}| \leq \Delta d_{wet-thresh} \wedge |\Delta p_m| \leq 0.5 \cdot p_m \wedge |\Delta \overline{T_{min}}| < 2.5^\circ\text{C}$$

where  $p_m$  is monthly total precipitation,  $\Delta T_{min}$  difference between actual and computed monthly average minimum daily temperature,  $\Delta d_{wet}$  the number of rainy days this month, and  $\Delta d_{wet-thresh}$  the accuracy acc. to Table 1.

If neither of these criteria is met within the set maximum number of iterations ( $MAXITER=20$ ), the set of values that minimizes the cost-function  $f_{cost}$  is chosen:

$$f_{cost} = \left( 20 \cdot \frac{|\Delta d_{wet}|}{\Delta d_{wet-thresh}} + 1 \right) + |\Delta p_m|$$

## References

- Buck, A. L., New equations for computing vapor pressure and enhancement factor, *J. Appl. Meteorol.*, 20, 1527-1532, 1981
- Prentice IC, Sykes MT, Cramer W, 1993. A simulation model of the transient effects of climate change on forest landscapes. *Ecological Modelling*, 65, 51-70.
- Sommer, P. S. and Kaplan, J. O.: A globally calibrated scheme for generating daily meteorology from monthly statistics: Global-WGEN (GWGEN) v1.0, *Geosci. Model Dev.*, 10, 3771–3791, <https://doi.org/10.5194/gmd-10-3771-2017>, 2017.

## 10. Burnt area model SIMFIRE (SIMple FIREmodel)

Lars Nieradzik, October 2019

SIMFIRE (Knorr et al. 2014) is a simple statistical model that provides annual burned area (BA) via a trained algorithm. The version applied in LPJ-GUESS version 4.1 solves the following burned-area-equation for each grid-cell  $i$ :

$$BA_i = a(i) \cdot \overline{f_{max,i}}^b \cdot N_{max,i}^c \cdot e^{e \cdot \rho_i}$$

with BA: Burned area [fraction of grid-cell];  $\overline{f}$ : Average annual maximum fAPAR (averaged over 3 years); N: Maximum Nesterov-index over the past 365 days;  $\rho$ : human population density; a-e: empirically determined constants as depicted in table 1.

**Table 1 Empirical parameters for the SIMFIRE burned area function**

Parameter	Biome	Index variable	Value
a	No vegetation	SF_NOVEG	0.000
	Crop, Pasture, Forest Mosaic	SF_CROP	0.110
	Needleleaf	SF_NEEDLEAF	0.095
	Broadleaf	SF_BROADLEAF	0.092
	Mixed	SF_MIXED_FOREST	0.127
	Shrubs	SF_SHRUBS	0.470
	Savanna	SF_SAVANNA	0.889
	Tundra	SF_TUNDRA	0.059
	Barren	SF_BARREN	0.113
b			0.905
c			0.860
e			-0.0168

### SIMFIRE biomes

SIMFIRE has its own nine biomes for each gridcell as listed in Table 1. These are determined first by the dominant land-cover as depicted in Fig 1.

**Table 2: Natural and barren fractions as used in Fig 1.**

frac_nat	Sum of NATURAL, PEATLAND, and FOREST fractional landc-cover
frac_barren	Sum of URBAN and BARREN fractional land-cover

```

if (frac_nat > 0.5) {
    biome = biome_index; *
}
else if (frac_barren > 0.5) {
    biome = SF_BARREN;
}
else if (gridcell.lancover.frac[CROPLAND] > 0.5) {
    biome = SF_NO_VEG; **
}
else if (gridcell.lancover.frac[CROPLAND] > 0.3) {
    biome = SF_NO_CROP;
}
else if (gridcell.lancover.frac[CROPLAND] < 0.1 && frac_nat < 0.4) {
    biome = SF_SHRUBS; ***
}
else {
    biome = SF_SAVANNA;
}

```

**Figure 1: Determination of a gridcell's SIMFIRE-biome by land-cover fraction. \*) biome\_index: dominating biome over patches(see fig 2); \*\*) according to Knorr et al. 2014; \*\*\*)determined such to best represent shrubs as in Knorr 2014 Fig B1**

```

if (fpar_total < 0.5 && fabs(lat) < 50.0) {
    biome = SF_BARREN;
}
else if (fpar_total < 0.35 && fabs(lat) >= 50.0) {
    biome = SF_TUNDRA;
}
else if (patch.stand.landcover == CROPLAND) {
    biome = SF_CROP;
}
else if (fpar_shrubs > 0.9 && fabs(lat) < 50.0) {
    biome = SF_SHRUBS;
}
else if (fpar_shrubs > 0.4 && fabs(lat) >= 50.0) {
    biome = SF_TUNDRA;
}
else if (fpar_needleleaf > 0.8) {
    biome = SF_NEEDLELEAF;
}
else if (fpar_broadleaf > 0.8) {
    if (fpar_trop_broadleaf_raingreen > 0.3) {
        biome = SF_SAVANNA;
    }
    else {
        biome = SF_BROADLEAF;
    }
}
else if (fpar_grass > 0.3) {
    biome = SF_SAVANNA;
}
else if (fpar_broadleaf > 0.2 && fpar_needleleaf > 0.2) {
    biome = SF_MIXED_FOREST;
}
else {
    biome = SF_SAVANNA;
}

```

**Figure 2: Determination of a patch's SIMFIRE-biome.**

For predominantly natural gridcells these biomes are determined patchwise by computing the fractions of total fPAR (indiv.fpar\_leafon) under full leaves for these classes as shown in Fig. 2:

- Grasses (fpar\_grass)
- Needle-leaf Trees (fpar\_needleleaf)
- Broad-leaf Trees (fpar\_broadleaf)
- Shrubs (fpar\_shrub)
- and for tropical raingreen trees (fpar\_trop\_broadleaf\_raingreen)

For smoothing reasons the mean of the past three years of the above values is used. Every patch thus gets assigned a SIMFIRE-biome via these selection criteria, where fpar\_total=total fAPAR in patch; lat = latitude. Finally, the whole grid-cell is assigned the biome that occurs in the highest number of patches.

### fAPAR

SIMFIRE uses the running mean of the maximum annual fAPAR over the past three years as a proxy for the amount of vegetation and, thus, fuel growing in a grid-cell  $i$ . Daily fAPAR is computed by averaging over Stands  $s$  and Patches  $p$ :

$$\overline{fAPAR}_i = \sum_s \sum_p (1 - fAPAR_{soil,p,s})$$

with  $fAPAR_{soil,sp}$  being the fraction of fAPAR remaining at soil-level.

### The Nesterov-Index

As a proxy for fuel moisture and general fire-weather the Nesterov-Index is used. It is computed as a running maximum over the past 365 days for each grid-cell and is updated daily as

$$N_t = \begin{cases} 0 & ; precip_t > 3 \text{ mm} \\ N_{t-1} + (T_{t,max} - T_{t,min}) \cdot T_{t,max} & ; T_{t,max} > T_{t,min} + 4 \\ N_{t-1} & ; else \end{cases}$$

where  $N_t$  is the Nesterov-index;  $T$ : temperature [ $^{\circ}\text{C}$ ],  $t$ : current time-step (here: day). The maximum annual Nesterov-index as used in the Burned-Area-Equation (top of chapter) is then

$$N_{max} = \max(N_{t-364,\dots,t})$$

### Human population density

Humans play an important role in the evolution of a fire., especially in its suppression. This is parameterized by the last term in the burned-area-equation in the beginning of this chapter. The human population density is taken from the HYDE 3.1 dataset (Klein Goldewijk et al. 2010). It has been aggregated onto the  $0.5^{\circ}$  grid of LPJ-GUESS. Annual values are linearly

interpolated between two existing values. For years after 2005 a linear extrapolation from the latest changes is applied.

### **Monthly and daily burned area**

A global fire-climatology has been created using the GFED4 (Giglio et al. 2013) Burned Area product from 1997-2012 containing the fraction  $f$  of all BA over the period occurring in every single month for every grid-cell  $i$ . Thus, BA for month  $m$  is computed by

$$BA_{i,m} = BA_i \cdot f_{i,m}$$

Daily burned area is then generated by simply dividing through the number of days of the current month.

### **References**

- Giglio, L., Randerson, J. T., and van der Werf, G. R.: Analysis of daily, monthly, and annual burned area using the fourthgeneration global fire emissions database (GFED4), *J. Geophys. Res.-Biogeo.*, 118, 317–328, doi:10.1002/jgrg.20042, 2013.
- Klein Goldewijk, K. , A. Beusen, M. de Vos and G. van Drecht (2011). The HYDE 3.1 spatially explicit database of human induced land use change over the past 12,000 years, *Global Ecology and Biogeography***20(1)**: 73-86. DOI: [10.1111/j.1466-8238.2010.00587.x](https://doi.org/10.1111/j.1466-8238.2010.00587.x)
- Knorr, W., Kaminski, T., Arneth, A., and Weber, U.: Impact of human population density on fire frequency at the global scale, *Biogeosciences*, 11, 1085-1102, 10.5194/bg-11-1085-2014, 2014

## 11. The wildfire combustion model BLAZE

Lars Nieradzik, October 2019

BLAZE (BLAZe induced biosphere-atmosphere flux Estimator) has been developed to simulate combustion of living and dead biomass given fire-weather conditions while taking into account the fuel-conditions in a grid-cell. In brief, BLAZE will process the following steps on a daily basis on every patch of a grid-cell, which will be described in detail in the subsequent paragraphs.

- Check for non-zero Burned Area in grid-cell provided by SIMFIRE
- Check, whether the patch has already burned this year
- Check, whether the patch contains a minimum amount of fuel (200 g(C)/m<sup>2</sup>) and compute fire-weather characteristics
- Stochastically check for fire-occurrence by using fractional burned area as a fire-probability for the patch
- Test every Individual/Cohort for survival
- Apply combustion-factors to amount of affected biomass, compute the fluxes between the pools and update the pools. This procedure is applied on a per-patch-basis for litter and grass and on a per-individual/cohort-basis for tree-pfts.

### Fire-weather characteristics and potential fire-line intensity

To compute combustion in case of a fire occurring in a grid-cell a couple of parameters are computed that characterize a day's fire-weather conditions.

The McArthur forest fire-danger index (FFDI), put into a mathematical framework by Noble 1980, is an empirical parameter and is computed as follows:

$$FFDI = 2 \cdot \exp[-0.45 + 0.987 \cdot \ln(D + 0.001) - 0.03456 \cdot RH + 0.0338 \cdot T + 0.0234 \cdot U_{10}]$$

with RH being relative humidity [%], T temperature in [°C], U<sub>10</sub> wind speed at 10 m [m/s], and D, the so-called McArthur-drought-factor,

$$D = \frac{0.0191 \cdot (KBDI + 104) \cdot (DSLRL + 1)^{3/2}}{3.52 \cdot (DSLRL + 1)^{3/2} + P - 1}$$

Where DSLR is the number of days since last rainfall, P the daily total of the last day with rainfall [mm/d], and KBDI the Keetch-Byram-Drought-Index (Keetch, 1968), a daily updated running drought index

$$KBDI_{d_0} = \sum_{d=-\infty}^{d_0} dKBDI_d$$

for day  $d_0$ , and with the daily increment

$$dKBDI_d = \begin{cases} \frac{(800 - KBDI_{d-1}) \cdot (0.968 \cdot e^{0.0486 \cdot (T_{max,d}^9/5+32)} - 8.3)}{(1 + 10.88 \cdot e^{-0.0441 \cdot \langle P_a \rangle / 25.4}) \cdot 254} & ; DSLR > 0 \\ \min(0, 5 - P_d) & ; DSLR = 0 \end{cases}$$

with  $\langle P_a \rangle$  being the average annual precipitation [mm/a],  $P_d$  precipitation [mm/d] of current day  $d$ .

Using a formulation called *Byram's Fire Line Intensity* (Pyne, 1996 derived from Byram 1959) the fire-line intensity  $FLI$  is calculated as

$$FLI = H \cdot \omega \cdot \eta_{spread} \text{ [MW/m]},$$

the product of the heat-yield  $H$  of the burning fuel set to 20 MJ/kg (as in Liedloff et al., 2007), the available fuel  $\omega$  [kgC/m<sup>2</sup>] and the fire's rate-of-spread

$$\eta_{spread} = 1/3 \cdot FFDI \cdot \omega \cdot 10^{-5} \text{ [m/s]}.$$

The available fuel load  $\omega$  indicates the amount of fuel that is ready to burn as the fire approaches. In many models (e.g. FLAMES; Liedloff et al., 2007) it is assumed that all fine fuels are ready to burn which may lead to an underestimation of the affected pools in consequence.

**Table 1: FullCAM combustion coefficients for different carbon pools and different values of FLI**

FullCAM combustion coefficients cF(FLI)		Fire Line Intensity $FLI$ [kW/m]			
		$\leq 750$	$\leq 3000$	$\leq 7000$	$> 7000$
cF <sub>1</sub>	Stem to atmosphere	0	0	0.05	0.20
cF <sub>2</sub>	Branches to atmosphere	0	0	0.15	0.20
cF <sub>3</sub>	Bark to atmosphere	0.03	0.13	0.25	0.50
cF <sub>4</sub>	Leaves to atmosphere	0.02	0.05	0.10	0.60
cF <sub>5</sub>	Stem to litter	0	0	0.05	0.20
cF <sub>6</sub>	Branches to litter	0	0.02	0.07	0.20
cF <sub>7</sub>	Bark to litter	0.03	0.13	0.25	0.50
cF <sub>8</sub>	Leaves to litter	0.05	0.10	0.15	0.30
cF <sub>9</sub>	Roots to atmosphere	0	0.02	0.02	0.04
cF <sub>10</sub>	Coarse woody debris to atmosphere	0.50	0.75	0.75	0.80
cF <sub>11</sub>	Bark litter to atmosphere	0.60	0.65	0.85	1.00
cF <sub>12</sub>	Leaf litter to atmosphere	0.60	0.65	0.85	1.00

Here, we use the revised FullCAM combustion completeness factors for  $FLI < 750 \text{ kW/m}$  (Surawski et al., 2012) to compute the potential FLI for a fire every day. In the stochastic case of an ignition (see below) the potential FLI will in return determine the actual combustion completeness from Table 1.

### Tuning-factors

BLAZE is very sensitive to changes in fuel abundance that often occur due to changes in other parts of the model. To be able to re-calibrate BLAZE in conjunction with changes in other parts of LPJ-GUESS, a set of “tuning factors” was introduced to regulate the amount of coarse woody debris available for instant ignition. These factors have been optimised for regions (see Table 2) and evaluated against the GFED4 carbon-emissions (Giglio et al. 2013). While the factors for the boreal and temperate region are solely dependent on latitude, the factors for the general tropics and tropical savannas depend on the SIMFIRE-biome, too. The combustion completeness for  $cF_{11}$  will be multiplied by the respective factor  $K\_LITTER\_x$ .

**Table 2: Tuning factors for coarse woody debris ( $cF_{11}$  in Table 1) to adjust to changes in the model.**

Tuning-factor	Condition	Value
K_LITTER_BOREAL	$ \text{Latitude}  > 50^\circ$	0.38
K_LITTER_TEMPERATE	$30^\circ <  \text{Latitude}  \leq 50^\circ$	0.0025
K_LITTER_TROPICS	$ \text{LATITUDE}  \leq 30^\circ \ \&\& \ \text{simfire\_biome} \neq \text{SAVANNA}$	0.25
K_LITTER_SAVANNA	$ \text{LATITUDE}  \leq 30^\circ \ \&\& \ \text{simfire\_biome} == \text{SAVANNA}$	0.75

### Fire occurrence - “Ignition”

As described in the previous section on SIMFIRE, there is a burned area (BA) value generated by SIMFIRE on every single day. If there is non-zero BA on a given day every patch whose readily available fuel exceeds the threshold for combustion of  $200 \text{ gC/m}^2$  will be tested for ignition using the fractional BA as the probability for a fire to occur on a patch. If so, the whole patch will be affected. Patches are not allowed to burn a second time in the same year.

## Fire-mortality

In case of an occurrence of a fire in a patch, each individual or cohort on a non-grassy patch has a stochastic chance to survive the fire, depending the computed potential fire-line intensity (FLI) and some allometric properties.

### Needleleaf Trees

Two different survival probabilities for needle-leafed trees are applied:

**Boreal:** For trees at latitudes beyond 50°N/S ( $|\text{latitude}| > 50$ ) according to Dalziel et al. 2008:

$$p_{\text{survival}} = e^{-FLI/500}$$

with  $[FLI] = \text{kw/m}$

**Temperate:** All other needle-leafed trees have survival-probabilities following to Kobziar et al. 2006:

$$p_{\text{survival}} = 1 - \left(1 + e^{-(1.0337 + 0.000151 \cdot FLI - 0.221 \cdot dbh + 0.0219 \cdot m_{\text{cwd}})}\right)^{-1}$$

Where  $dbh$  is diameter-at-breast-height [cm];  $m_{\text{cwd}}$  the dry matter mass of coarse woody debris [Mg/ha].

### Broadleaf trees

**Savanna:** The savanna-mortality by Bond 2008 is applied to all broad-leaved trees living in the SIMFIRE biomes shrubland, savannah, and barren.

$$p_{\text{survival}} = 1 - \left(1 + e^{1.5 \cdot (\text{height} - 500 \cdot FLI - 1)}\right)^{-1}$$

With height being the tree-height [m].

**Tropical:** Tropical survival is based on van Nieuwstadt et al. 2005 is depending on  $dbh$  and was calculated for a fire-line intensity of about 3000 kW/m. A dependence on FLI has been added for FLI above and below 3000kW/m as:

$$P_{\text{survival}}(3000) = 1 - (0.82 - 0.035 \cdot dbh^{0.7})$$

$$P_{\text{survival}} = \begin{cases} (1 - \ln(\text{fli}/7000)) \cdot P_{\text{survival}}(3000) & ; \text{fli} > 7000 \text{ kW/m} \\ P_{\text{survival}}(3000) & ; 3000 < \text{fli} \leq 7000 \text{ kW/m} \\ \exp\left(\frac{\text{fli}}{3000} \cdot \ln(P_{\text{survival}}(3000))\right) & ; \text{fli} \leq 3000 \text{ kW/m} \end{cases}$$

**Temperate:** Extra-tropical non-savannah broadleaved trees are considered to be temperate. Their survival probability is calculated following Hickler et al. 2004 using the resilience-value  $res$  to distinguish between seeders and resprouters that is set as

$$res = \begin{cases} 0.04; & \text{sprouter} \\ 0.07; & \text{seeder} \end{cases}$$

Originating from the probability at 3000 kW/m

$$P_{survival}(3000) = 0.95 - \frac{1}{1 + (dbh/res)^{3/2}}$$

The overall survival probability is computed as follows:

$$P_{survival} = \begin{cases} 0.001 & ; fli \geq 7000 \text{ kW/m} \\ P_{survival}(3000) \cdot \left(1 - \frac{fli - 3000}{4000}\right) & ; 3000 \leq fli < 7000 \text{ kW/m} \\ e^{fli/3000 \cdot \ln(P_{survival}(3000))} & ; fli < 3000 \text{ kW/m} \end{cases}$$

With  $fli$  being the fire-line intensity.

## Combustion

After the amount of biomass that is affected in a cohort/individual has been determined by the stochastic mortality in the previous step, the combustion factors from Table 1 are now taken to compute the fluxes between the affected pools. LPJ-GUESS has both grassy and woody components for each grid cell and both are affected by the fire. The fluxes from litter and grasses are computed on a patch basis according to Table 3. For grasses a fixed value of 75% is set, i.e. this amount of grass will be killed.

**Table 3:** Turnover-rates for litter and grass used in BLAZE to compute fluxes between source pool  $i$  and target pool  $j$  ( $i, j$  indicated by numbers in columns 2 and 4).  $fm_{leaf}$  is the metabolic litter fraction depending on the lignin-to-nitrogen ratio as defined in soil-dynamics.

Source Pool $i$		Target Pool $j$		BLAZE flux coefficient $f_{ij}$
<i>Litter pools (both, soil-surface and last year's litter spread over the current year)</i>				
metabolic	1	Atmosphere	1	$cF_{12} \cdot fm_{leaf}$
Structural	2	Atmosphere	1	$cF_{12} \cdot (1 - fm_{leaf})$
Fine woody debris	3	Atmosphere	1	$cF_{11}$
Coarse woody debris	4	Atmosphere	1	$cF_{10}$
<i>Grass</i>				
Grass leaf	5	Atmosphere	1	$\equiv 0.75$

The total amounts turned over from live biomass to litter and atmosphere depend on the actual percentage of trees killed in the fire. As mentioned above this is processed on individual/cohort level. It is further assumed that the turnover of root biomass to litter is of the same ratio as the overall loss of aboveground live biomass in an individual/cohort. Firstly, the relative fluxes from live wood into the target pools are computed as in Table 4. Table 5 depicts the actual turnover-rates between the affected pools.

**Table 4: Separation of relative fluxes for live woody biomass to target pools**

Source Pool	Target Pool	BLAZE flux coefficient for live biomass
Live wood	Atmosphere	$f_{lw2atm} = (1 - f_{br} - f_{ba}) \cdot cF_1 + f_{br} \cdot cF_2 + f_{ba} \cdot cF_3$
	Surface Structural Lit	$f_{lw2str} = (1 - f_{lw2atm}) \cdot f_{ba}$
	Fine woody debris	$f_{lw2fwd} = (1 - f_{lw2atm}) \cdot f_{br}$
	Coarse woody debris	$f_{lw2cwd} = (1 - f_{lw2atm}) \cdot (1 - f_{br} - f_{ba})$

The same separations are applied to both Carbon (cmass) and Nitrogen (nmass) pools. The total fluxes between pool  $i$  and pool  $j$  in a patch can now be summarized as follows using the indices from Tables 3 and 5:

$$F_{carbon_{i,j}} = f_{i,j} \cdot cmass_i$$

and

$$F_{nitrogen_{i,j}} = f_{i,j} \cdot nmass_i.$$

An analogous way is chosen to remove already built up NPP from a patch by using the same turnover-rates as in Tables 3 and 5, with  $j$  being the target pool:

$$F_{npp,j} = \left( \frac{\sum_i f_{i,j}}{\sum_{i,k} f_{i,k}} \right) \cdot npp$$

And, finally, the cmass\_debt-pool will be affected by removing all of it from autotrophic respiration and adding it to NPP instead.

**Table 5: Turn-over rates for fluxes from the live woody biomass pools, with  $f_w = 0.94$  the fraction of stem of total wood,  $f_{br} = 0.05$  branch fraction, and  $f_{ba} = 0.01$  bark fraction; \*) using live biomass-fluxes from Table 3,  $f_{kill}$  is the fraction of trees killed, and  $f_{m_{root}}$  is the metabolic litter fraction depending on the lignin-to-nitrogen ratio as defined in soil-dynamics.**

Source Pool $i$		Target Pool $j$		BLAZE flux coefficient $f_{ij}$
<i>Live woody biomass</i>				
Leaf	6	Atmosphere	1	$cF_4 \cdot f_{kill}$
		Surface Metabolic Lit	2	$cF_8 \cdot f_{m_{leaf}} \cdot f_{kill}$
		Surface Structural Lit	3	$cF_8 \cdot (1 - f_{m_{leaf}}) \cdot f_{kill}$
Sapwood*	7	Atmosphere	1	$f_{lw2atm} \cdot f_{kill}$
		Surface Structural Lit	3	$f_{lw2str} \cdot f_{kill}$
		Fine woody debris	4	$(f_{lw2fwd} + f_{lw2scwd}) \cdot f_{kill}$
Heartwood*	8	Atmosphere	1	$f_{lw2atm} \cdot f_{kill}$
		Structural Lit	3	$f_{lw2str} \cdot f_{kill}$
		Coarse woody debris	5	$(f_{lw2fwd} + f_{lw2scwd}) \cdot f_{kill}$
<i>Roots</i>				
Roots	9	Soil Metabolic Litter	6	$f_{m_{root}} \cdot f_{kill}$
		Soil Structural Litter	7	$(1 - f_{m_{root}}) \cdot f_{kill}$

## References

- Bond, WJ, What Limits Trees in C4 Grasslands and Savannas?, *Annu. Rev. Ecol. Evol. Syst.* 2008. 39, doi:10.1146/annurev.ecolsys.39.110707.173411
- Dalziel, BD, Tree Mortality Following Boreal Forest Fires Reveals Scale-Dependant Interactions Between Community Structure and Fire Intensity, *Ecos.*, 12, 2009<https://doi.org/10.1007/s10021-009-9272-2>
- Giglio, L., Randerson, J. T., and van der Werf, G. R., (2013), Analysis of daily, monthly, and annual burned area using the fourth-generation global fire emissions database (GFED4)*J. Geophys. Res. Biogeosci.*, 118, 317– 328, doi:[10.1002/jgrg.20042](https://doi.org/10.1002/jgrg.20042).
- Hickler, T, Using a generalized vegetation model to simulate vegetation dynamics in northeastern USA, *Ecology*, 85, 2004, doi: 10.1890/02-0344
- Keetch, JJ, A Drought Index for Forest Fire Control, Res. Pap. SE-38. Asheville, NC: U.S. Department of Agriculture, 1968
- Kobziar, L, Tree mortality patterns following prescribed fires in a mixed conifer forest, *Can. J. For. Res.*, 36, 2006, doi:10.1139/X06-183
- Liedloff, A, Predicting a tree change in Australia's tropical savannas: Combining different types of models to understand complex ecosystem behaviour, *Ecological Modelling* 221, 2010, doi:10.1016/j.ecolmodel.2010.07.022
- Noble, IR, McArthur's fire-danger expressed as equations, *Austr. J. Ecol.* 5, 1980, doi:10.1111/j.1442-9993.1980.tb01243.x
- Surawski, N, A. Sullivan, S. Roxburgh, G.Cook, Review of FullCAM forest forest fire event parameters with recommendations supported by a literature review, CSIRO Ecosystem Sciences report EP2806132, 2012
- van Nieuwstadt, MGL, Drought, fire and tree survival in a Borneo rain forest, East Kalimantan, Indonesia,*J.o. Ecology*, Vol.93, 1, 2005, <https://doi.org/10.1111/j.1365-2745.2004.00954.x>

## **12. Updates to soil temperature and hydrology calculations**

*Paul Miller, Adrian Gustafson, September 2020*

### **Introduction**

Compared with the versions of the model (Smith et al. 2014) up to and including version 4, versions 4.1 and above include updated and differentiated representations of processes operating in upland (i.e. mineral soil) and peatland ecosystems of the tundra and taiga biomes, as well as PFTs characteristic of these ecosystems, including evergreen and deciduous shrubs, forbs, graminoids and bryophytes. The model includes improved soil temperature calculations, a description of soil freezing processes (affecting water available to plants), and, on the fraction of each gridcell deemed to be a peatland, a peatland hydrology, peatland-specific PFTs, and CH<sub>4</sub> emissions. These developments and process descriptions were adopted from updates to the LPJ DGVM made by Wania et al. (2009a, 2009b, 2010), and are described more briefly in McGuire et al. (2012).

### **Soil layers and their thermal properties**

Calculations of soil temperature in versions of the model before version 4.1 are inaccurate for soils underlain by permafrost and in cold regions experiencing soil water phase change. Soil temperatures are now calculated and updated daily for each of fifteen, 10 cm layers in the 1.5 m-deep active soil column (i.e. those layers of greatest importance for vegetation and biological processes), overlain by up to 5 snow layers to a maximum depth corresponding to 10,000 mm water equivalent (see below), and underlain by 5 additional padding layers to a depth of 48m. See Figure 12.1 for an overview of the overall layer structure.

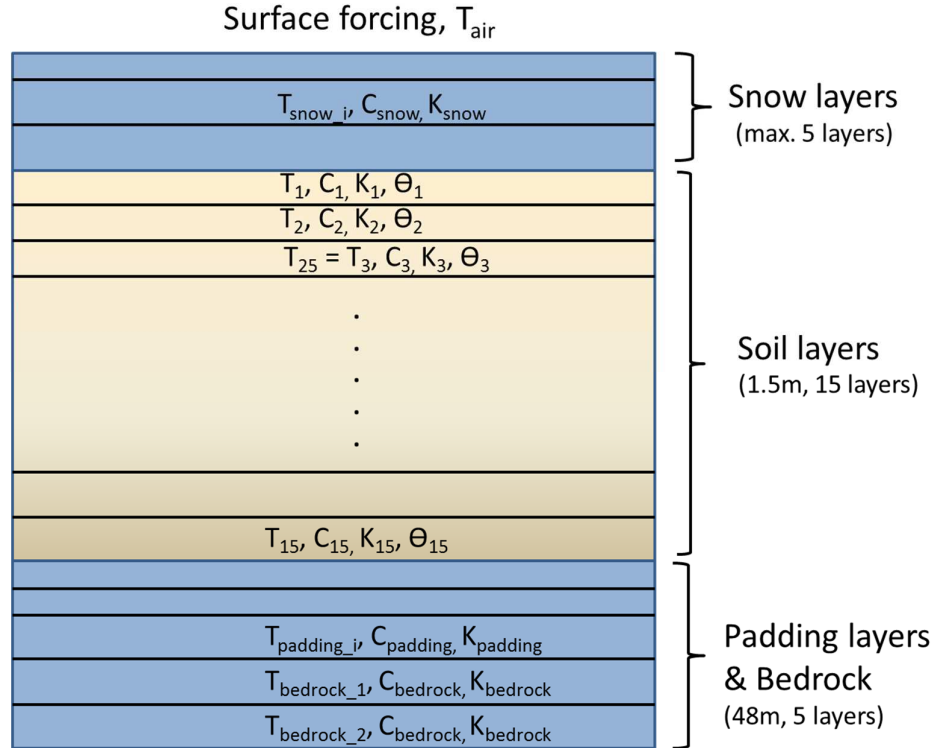


**Figure 12.1.** Soil layer structure in upland/mineral soils (not to scale). Up to 5 snow layers overlie 15 active soil layers, underneath which 5 padding layers extend to a total depth of 49.5 m.

Each day, LPJ-GUESS numerically solves the heat diffusion equation

$$\frac{\partial T}{\partial t} = \frac{\partial}{\partial x} \left( D(z, t) \frac{\partial T}{\partial z} \right)$$

where  $T(z, t)$  is the soil temperature at depth  $z$  (m) at time  $t$ , and  $D(z, t)$  ( $\text{m}^2 \text{s}^{-1}$ ) is the thermal diffusivity at depth  $z$ , defined as

$$D(z, t) = \frac{K(z, t)}{C(z, t)}$$

where  $K(z, t)$  is the thermal conductivity ( $\text{W m}^{-1} \text{K}^{-1}$ ), and  $C(z, t)$  ( $\text{J m}^{-3} \text{K}^{-1}$ ) is the heat capacity of the soil layer, each at a depth  $z$  and time  $t$ .

Optionally, the model solves the more general equation:

$$C(z, t) \frac{\partial T}{\partial t} = \frac{\partial}{\partial x} \left( K(z, t) \frac{\partial T}{\partial z} \right)$$

which reduces to the equation above when  $C(z, t)$  is constant.

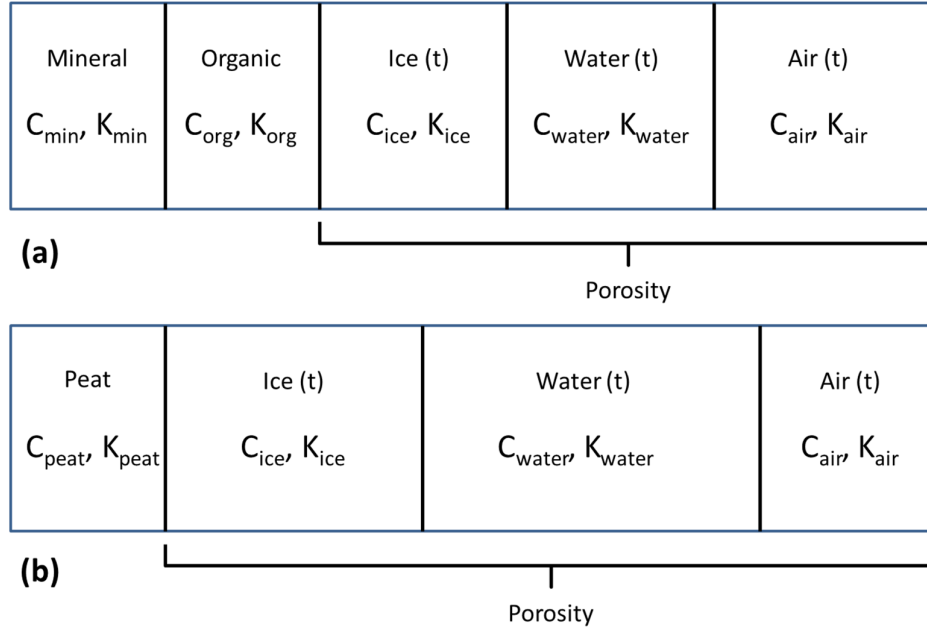


**Figure 12.2.** Composition and thermal properties of upland (a) and peatland (b) soil layers.

As shown in Figure 12.2(a), the mineral soil layers comprise fixed (in time) volumetric fractions of mineral ( $F_{min}$ ) and organic ( $F_{org}$ ) content, as well as dynamic volumetric fractions of water ( $F_{water}$ ), ice ( $F_{ice}$ ) and air ( $F_{air}$ ). Both  $F_{min}$  and  $F_{org}$ , as well as the porosity,  $por$ , are calculated based on soil texture or soil code (both read from input files - see Section 5 above) specifying the percentage of sand, silt and clay, and organic content, such that

$$F_{min} + F_{org} + por = 1$$

Both the soil heat capacity and the thermal conductivity are updated daily for each snow, active soil and padding layer. For active soil layers in upland areas,  $C(z, t)$  is calculated as the weighted average of the heat capacities of the individual components of the soil layer (e.g.  $C_{water}$ ,  $C_{ice}$  etc.), using the volumetric fractions as the weights:

$$F_{min} \cdot C_{min} + F_{org} \cdot C_{org} + F_{water} \cdot C_{water} + F_{ice} \cdot C_{ice} + F_{air} \cdot C_{air} = C(z, t)$$

where we have dropped the subscripts for  $F_{water}$ ,  $F_{ice}$ , and  $F_{air}$ , each of which vary with depth and time.

Table 12.1 gives the heat capacities and thermal conductivities of the soil layer components.

Soil layer component	Heat capacity ( $10^6 \text{ J m}^{-3} \text{ K}^{-1}$ )	Thermal conductivity ( $\text{W m}^{-1} \text{ K}^{-1}$ )
Mineral	2.38	2.0
Organic	2.5	0.25
Peat	0.58	0.06

Water	4.18	0.57
Ice	1.94	2.2
Air	0.0012	0.025
Bedrock	2.1	8.6

**Table 12.1.** Heat capacities and thermal conductivities of the soil layer components. Values taken from Bonan (2002), Wania et al. (2009a, 2009b), Granberg et al. (2008), and Chadburn et al. (2015).

Calculation of  $K(z,t)$  follows Wania et al. (2012a) and Granberg et al. (2008), using geometric means, as follows:

Defining  $F_{total}$  as

$$F_{min} + F_{org} + F_{water} + F_{ice} = F_{total}$$

and

$$lK_* = \frac{F_*}{F_{total}} \ln(K_*)$$

for each (\*) component (mineral, organic, water and ice), we define  $K(z,t)$  as:

$$K(z,t) = F_{air} \cdot K_{air} + (1 - F_{air}) \cdot e^{(lK_{ice} + lK_{water} + lK_{org} + lK_{min})}$$

## Soil column and temperature calculations

Besides the 15 active soil layers described above, the soil column is completed by overlying snow layers and underlying padding layers (Figure 12.1).

### Snow

Snow layers insulate the underlying active soil layers, and store both water and nitrogen for release each spring. LPJ-GUESS models the snow pack using up to 5 homogeneous layers of variable thickness. At the start of the period of snow accumulation, one snow layer is used until the snow thickness reaches 100mm. Thereafter, new layers of thickness 50mm are created each time the snow depth exceeds thresholds of 100mm, 150mm, 200mm and 250mm. The thinner 50mm layers are always placed at the top of the snow pack, nearest the overlying air. Above a depth of 250mm, the thickness of the bottom snow layer in contact with the uppermost active soil layer is allowed to grow.

The depth of the snow pack is determined by its density,  $\rho_{snow}$ . There are options to use a fixed density of 250 kg m<sup>-3</sup> as in Ekici et al. (2015) or, following Wania et al. (2009a), a variable density that remains at 275 kg m<sup>-3</sup> until the final period (25%) of the snow season, during which the density increases linearly to a value more representative of older, more compact snow:  $\rho_{snow\_compact} = 500$  kg m<sup>-3</sup>.

The heat capacity,  $C_{snow}$ , and thermal conductivity,  $K_{snow}$ , of snow are defined as (Wania et al. (2009a)):

$$C_{snow} = 0.01 \cdot \rho_{ice} \cdot (185 + 689 \cdot T_K)$$

where  $\rho_{ice} = 917 \text{ kg m}^{-3}$ , and  $T_K$  is the air temperature in Kelvin.

Defining  $\rho_{snow\_scaled} = \rho_{snow}/1000$ , we define

$$K_{snow} = 0.138 - 1.01 \rho_{snow\_scaled} + 3.233 \rho_{snow\_scaled}^2$$

giving values that vary between 0.1 for fresh snow and 0.44  $\text{W m}^{-1} \text{K}^{-1}$  for older snow with a higher density.

Snow melt ( $S_{melt}$ ,  $\text{mm day}^{-1}$ ) occurs when air temperature exceeds  $0^\circ\text{C}$ :

$$S_{melt} = (1.5 + 0.007 \cdot P) \cdot T_C$$

Here,  $T_C$  is the air temperature in degrees Celsius, and  $P$  is the daily precipitation ( $\text{mm day}^{-1}$ ). Snow melt enters the top of the soil in the hydrology scheme (see below).

### Boundary conditions, padding layers & bedrock

Since LPJ-GUESS does not consider the full energy balance at the surface, the upper boundary condition driving the temporal evolution in the snow, soil and padding layer temperatures is the surface air temperature (Figure 12.1). At the bottom of the soil column, we assume a zero-gradient condition, namely

$$\frac{\partial T}{\partial z} \rightarrow 0 \text{ as } z \rightarrow \infty.$$

Since a depth of 1.5m is insufficient to achieve this condition (Lawrence & Slater, 2008), the soil column has an additional 5 padding layers below the bottommost active soil layer with thicknesses 0.3, 1.0, 3.2, 10.4 and 33.1m, to give a total padding layer depth of 48m (default values). The padding layers are thermally active, but hydrologically inactive, i.e. there is no water infiltration from the upper soil layers and the maximum rooting depth is 1.5 m. The thermal properties of the three padding layers nearest the active soil layers are updated daily and assumed to be equal to the bottommost active soil layer. The two deepest padding layers have the thermal properties of bedrock (Table 12.1, Chadburn et al. 2015).

The soil temperatures are calculated daily with a user-defined timestep ( $\leq 1$  day) using the Crank-Nicolson finite difference scheme – see Wania et al. (2009a) for full details.

### Soil water freezing and thawing processes

Since soil temperature varies with time and depth,  $T(z,t)$ , the fractional (volumetric) water and ice contents,  $F_{ice}$  and  $F_{water}$ , must also vary with the same spatial (10 cm) and temporal (1 day) resolution along the soil column. LPJ-GUESS adopts the simple approach to phase change described in more detail by Wania et al. (2009a), based on the following assumptions:

- Whenever water is freezing (ice is melting) in a layer, latent heat release (consumption) keeps the temperature at a constant value of 0°C until the water is completely frozen (the ice has completely melted).
- Rainfall or snow melt both update  $F_{water}$  (see below), but they do not introduce additional heat from the atmosphere to the soil.
- Freezing is only permitted when temperature is falling. This is a numerical stability condition.
- Thawing is only permitted when temperature are rising. This is a numerical stability condition.

In contrast to Wania et al., however, LPJ-GUESS accounts for freezing and thawing of water below the wilting point. When water in a layer is freezing, it is assumed that water below the wilting point is frozen first and that liquid water above the wilting point can only freeze once all the water below the wilting point has frozen. Only then does this result in a potential reduction in plant water uptake. Similarly, water stored as ice above the wilting point can only melt after all the ice below the wilting point has melted.

The model calculates the daily thaw depth as the depth ( $z_{thaw}$ ) of the first layer below the surface where  $T(z_{thaw}) > 0^\circ\text{C}$ .

## Hydrology changes resulting from phase change

The introduction of phase change necessitates some minor adjustments to the standard hydrology for upland soils introduced and described by Gerten et al. (2004).

In the Gerten et al. scheme, phase change was not considered, and there were two active soil layers, consisting of a 0.5 m thick surface layer overlying a 1 m thick deep layer. However, though the fractional (volumetric) water and ice contents,  $F_{ice}$  and  $F_{water}$ , respectively, can now vary along the active soil column's 15, 10 cm layers, we use the same basic algorithm, updated to account for phase change, increased vertical resolution and water conservation.

Let us label the soil layers from 1 to 15 (Figure 12.1), where layer 1 is the top soil layer in contact with air or snow, and layer 15 the bottommost layer in contact with the padding layers. In what follows, we refer to layers 1 to 5 as the surface layers, and layers 6 to 15 as the deep layers, in keeping with Gerten et al. (2004).

The (volumetric) wilting point ( $wp_i$ ), the (volumetric) field capacity ( $fc_i$ ) and the (volumetric) water holding capacity ( $whc_i = fc_i - wp_i$ ) have the same values for each soil layer,  $i$  (1 to 15), determined by the soil code or texture. All layers have the same thickness,  $Dz_i = Dz = 100\text{mm}$ .

We define the available water holding capacity for layer  $i$  ( $awc_i$ ) as

$$awc_i = Dz_i \cdot whc_i$$

which is the maximum amount of water (mm) layer  $i$  can hold ( $< 100\text{mm}$ ).

We define the available (liquid) water in layer  $i$  ( $aw_i$ ) as

$$aw_i = Dz_i \cdot (F_{water,i} - wp_i)$$

which is the actual liquid water contained in layer  $i$ , such that  $aw_i < awc_i$ . Note that this definition does not include ice in layer  $i$ ,  $F_{ice,i}$ .

The dimensionless ratio of these quantities,  $wcont_i$ :

$$wcont_i = \frac{aw_i}{awc_i}$$

is an indicator of the water available to plants in the layer, such that  $0 \leq wcont_i \leq 1$ . The  $wcont$  ratio is used by Gerten et al. (2004), but for the (0.5 m) surface and (1.0 m) deep layers only.

We now define the potential for water uptake,  $pot_i$ , for soil layer  $i$  as follows:

$$pot_i = Dz_i \cdot (fc_i - F_{water,i} - F_{ice,i})$$

which is the upper limit to additional water (mm) that a soil layer can hold.

We can recover the Gerten et al.  $wcont$  definitions by first defining:

$$wcont_{a,b} = \frac{\sum_a^b aw_i}{\sum_a^b awc_i}$$

and defining  $wcont_{surf} = wcont_{1,5}$ ,  $wcont_{deep} = wcont_{6,15}$  and (for the evaporation layer);  $wcont_{evap} = wcont_{1,2}$ . Similarly, the potential for uptake in the surface ( $pot_{surf}$ ) and deep ( $pot_{deep}$ ) layers is given by the sum of  $pot_i$  over layers 1 to 5, and 6 to 15, respectively, and the total available water the surface ( $aw_{surf}$ ) and deep ( $aw_{deep}$ ) layers is given by the sum of  $aw_i$  over layers 1 to 5, and 6 to 15, respectively.

Using the above definitions, we can now summarize the updates to the hydrology algorithm.

### Evaporation

Evaporation (mm) occurs from the non-vegetated (i.e.  $1 - FPC_{total}$ ) fraction,  $fevap$ , of the uppermost two 10 cm layers,  $i = 1, 2$ , following

$$evap = fevap * EET * PT * wcont_{evap} * wcont_{evap}$$

where  $EET$  is the daily equilibrium evapotranspiration (mm), and  $PT = 1.32$  is the Priestley-Taylor constant. Water conservation is achieved by demanding that  $evap \leq (aw_1 + aw_2)$ . Water evaporated is removed from layers 1 and 2 in proportion to their available water content as a fraction of the total available water in the evaporation layers, i.e.  $aw_i / (aw_1 + aw_2)$ , which acts to equalize the available water in these layers.

*Input from rainfall and snowmelt - initial infiltration*

As described in Section 2 above, an initial infiltration of rainfall and snowmelt,  $rain\_melt$ , into the five surface layers is applied in the model's `initial_infiltration()` function. There are two conditions:

$rain\_melt \leq pot_{surf}$ : distribute  $rain\_melt$  over layers 1 to 5 in proportion to  $pot_i$ . This acts to equalize the available water in these layers. In this case no additional water enters the soil in the hydrology routine.

$rain\_melt > pot_{surf}$ : distribute  $pot_{surf}$  (mm) over layers 1 to 5 in proportion to  $pot_i$ . This equalizes the liquid water + ice fractions in these layers. The remaining water,  $rain\_melt - pot_{surf}$ , enters the soil in the hydrology routine.

*Input from rainfall and snowmelt – hydrology routine*

In the hydrology routine, water input from rainfall and snowmelt ( $rain\_melt$ , mm) that has not initially infiltrated now enters the five surface layers. There are two conditions:

$rain\_melt \leq pot_{surf}$ : distribute  $rain\_melt$  over layers 1 to 5 in proportion to  $pot_i$ . This acts to equalize the available water in these layers.

$rain\_melt > pot_{surf}$ : distribute  $pot_{surf}$  (mm) over layers 1 to 5 in proportion to  $pot_i$ . This equalizes the liquid water + ice fractions in these layers. The remaining water,  $rain\_melt - pot_{surf}$ , enters surface runoff,  $runoff_{surf}$ .

*Percolation*

Percolation from the surface layers to the deep layers, and from the deep layers to base flow, is allowed if  $rain\_melt > 0.1\text{ mm}$ .

Percolation of liquid water from the surface layers to the deep layers,  $P_{surf\_deep}$  (mm) is calculated as

$$P_{surf\_deep} = \min(aw_{surf}, K_1 * e^{K_2 * wcont_{surf}})$$

where  $K_1$  and  $K_2$  are soil texture-dependent percolation coefficients (Eqn. 31, Haxeltine & Prentice, 1996). Percolated water is removed from each of the five surface layers in proportion to their available water content,  $aw_i/aw_{surf}$ , and fills the deeper soil layers as follows:

$P_{surf\_deep} \leq pot_{deep}$ : distribute over layers 6 to 15 in proportion to  $pot_i$ . This acts to equalize the available water in these layers.

$P_{surf\_deep} > pot_{deep}$ : distribute  $pot_{deep}$  (mm) over layers 6 to 15 in proportion to  $pot_i$ . This equalizes the liquid water + ice fractions in these layers. The remaining water,  $P_{surf\_deep} - pot_{deep}$ , enters drainage runoff,  $runoff_{drain}$ .

Finally, percolation of liquid water from the deep layers -  $P_{deep\_surf}$  (mm) - is lost to the soil column as base flow runoff and calculated as follows

$$P_{deep\_base} = \min(aw_{deep}, 0.5 * K_1 * e^{K_2 * w_{cont\_deep}})$$

Percolated water is removed from each of the ten deep layers in proportion to their available water content,  $aw_i/aw_{deep}$ .

Total daily runoff (mm),  $runoff_{total}$ , is then calculated as

$$runoff_{total} = runoff_{surf} + runoff_{drain} + P_{deep\_base}$$

## Updates to SOM daily decay rates

As described in Section 4 above, the daily decay rates for each pool (C fraction:  $C_j$ , kgC m<sup>-2</sup>) in the CENTURY-based SOM scheme depend on soil temperature and moisture:

$$\frac{dC_j}{dt} = -k_{j,max} \cdot f(T_{soil}) \cdot f(W) \cdot f(S) \cdot C_j$$

where  $f(T_{soil})$  is a dimensionless scalar in the range 0-1 related to soil temperature ( $T_{soil}$ , °C) and  $f(W)$  is a dimensionless scalar in the range 0-1 related to soil moisture.

The updates to soil temperature and moisture described above influence daily decay rates through  $f(T_{soil})$  and  $f(W)$ .  $T_{soil}$  is updated daily as the temperature calculated for the third 10 cm soil layer – see Figure 12.1 above. Similarly,  $f(W)$  is determined by the amount of unfrozen (available) soil water in the surface layers.

Observations suggest that daily decay rates below 0°C are small but non-negligible, and decrease rapidly as the temperature decreases (Schaefer & Jafarov, 2006).  $f(T_{soil})$  is now adjusted to reflect this fact, such that:

$$f(T_{soil}) = 0.0326 + 0.00351 \cdot T_{soil}^{1.652} - (T_{soil} / 41.748)^{7.19}$$

for  $T_{soil} \geq 0^\circ\text{C}$  (i.e. unchanged), and

$$f(T_{soil}) = 0.0326 \cdot Q10_{subzero}^{T_{soil}/10}$$

for  $T_{soil} < 0^\circ\text{C}$ , where  $Q10_{subzero} = 200.5$ , a value calculated as the average of 164 and 237 based on incubation of frozen soil samples (Mikan et al., 2002). Figure 12.3 shows the resulting temperature profile.

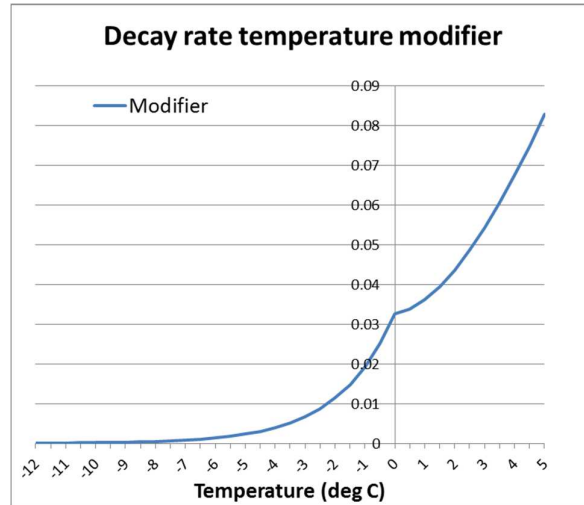


Figure 12.3. Decay rate modifier based on temperature ( $^{\circ}\text{C}$ ),  $f(T_{\text{soil}})$ , adjusted to account for decay below  $0^{\circ}\text{C}$ .

### Updated root distributions

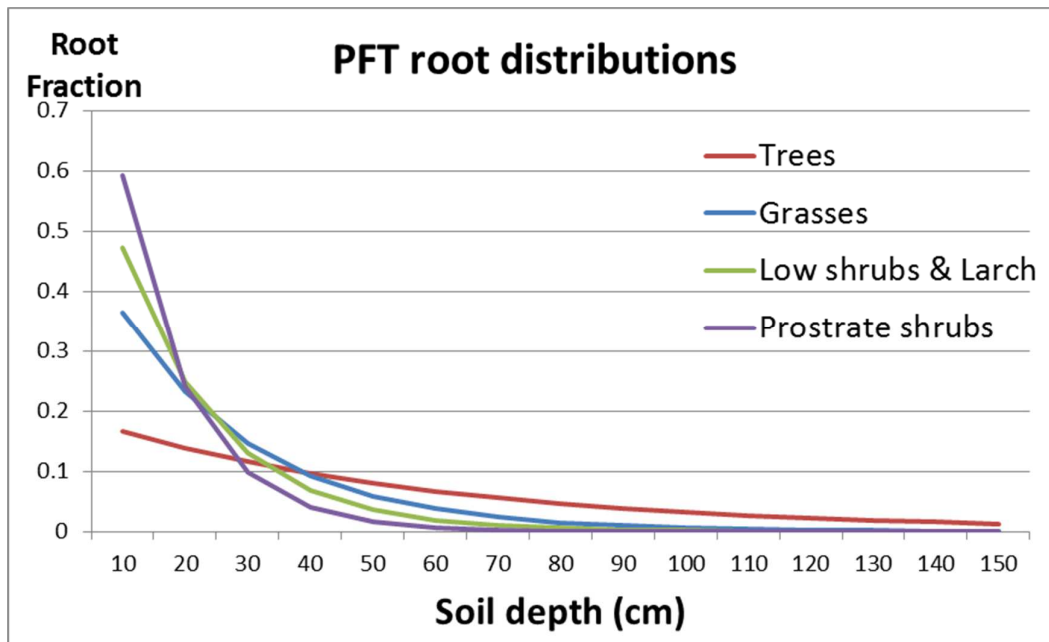


Figure 12.4. PFT-specific root fractions for each 10 cm soil layer, parameterized following Jackson et al. (1996).

The model gives the option to specify how root distributions for each PFT are calculated. The root fractions in soil layer  $i$ ,  $root_i$ , (1 to 15) can either be fixed and specified in the PFT descriptions in the instruction (.ins) files as a one-dimensional array with 15 entries, or they can be calculated following the parameterization described by Jackson et al. (1996) in their review of global root properties. Use the instruction file entry `rootdistribution "jackson"` or `rootdistribution "fixed"` to switch between these two options.

Jackson et al. (1996) parameterize the cumulative fraction  $Y$  (0-1) of roots to depth  $d$  (cm) using a single biome-specific parameter,  $\beta$ , as follows:

$$Y = 1 - \beta^d$$

Lower values of  $\beta$  result in a greater proportion of roots near the surface. Conversely, higher values of  $\beta$  result in a greater proportion of roots at depth.

Table 12.2 shows the values used for each PFT or PFT class, and Figure 12.4 shows the resulting exponential root decrease with depth.

PFT or PFT class	$B$	Fraction of roots in top 50cm
Trees (except Larch (BNS))	0.9820	0.60
Larch (BNS)	0.9380	0.96
Grasses	0.9555	0.90
Low shrubs (< 50cm)	0.9380	0.96
Prostrate dwarf shrubs (< 20cm)	0.9140	0.99

**Table 12.2.** Values of  $\beta$  used to parameterize the root fractions for each PFT or PFT class, and the resulting fractions in the surface layers.

## Soil organic carbon and soil physical properties

Soil thermal and hydrological properties depend strongly on the amount of organic matter,  $F_{org}$ , (Figure 12.2). Inspired by Lawrence & Slater (2008), the instruction file entry `iforganicsoilproperties` can be used to initialize vertically heterogeneous soil thermal and hydrological properties in each layer  $i$ , 1 to 15, as a function of an initial, integrated carbon pool in the column,  $C_{init}$  (kg C m<sup>-2</sup>), specified as input to the model.

We assume that  $C_{init}$  is distributed in the soil column ( $Y_{org}(i)$ ) following Jobbagy & Jackson (2000):

$$Y_{org} = 1 - \beta_{org}^d$$

Where  $\beta_{org} = 0.976$ , and with the restriction that values in each layer cannot exceed values corresponding to a maximum soil carbon density of 130 kg C m<sup>-3</sup> typical of peat soils. Using  $Y_{org}(i)$  to calculate the soil carbon density in each layer,  $C_{dens}(i)$ , the organic fraction in layer  $i$  ( $org_i$ ) is then calculated as  $C_{dens}(i)/130$ .

We use  $org_i$  to scale the porosity in each layer,  $por_i$ , between the value for mineral/upland soils in the cell (determined by soil texture) and organic soils (0.8):

$$por_i = (1 - org_i) \cdot por_{mineral} + org_i \cdot por_{organic}$$

Similarly, the volumetric organic and mineral fractions are updated as

$$F_{org}(i) = org_i \cdot (1 - por_{organic})$$

and

$$F_{min}(i) = (1 - org_i) \cdot (1 - por_{mineral})$$

These influence the soil thermal properties (Figure 12.2) such as heat capacity and thermal conductivity.

Hydrological behaviour is updated using the average organic fraction for the surface and deep layers,  $org_{surf}$  and  $org_{deep}$ , respectively. Percolation coefficients ( $K_1$  and  $K_2$ ), the wilting point and the water holding capacity are then updated in each layer using  $org_i$ ,  $org_{surf}$  or  $org_{deep}$  to linearly scale between values for mineral/upland soils in the cell (determined by soil texture) and organic soils.

Cells with high  $C_{init}$  will have 10 cm layers near the surface that resemble organic soils (e.g. with a high porosity and low thermal conductivity) and deeper 10 cm layers that resemble mineral, upland soils.

## References

See references in Chapter 14.

## 13. High-latitude peatlands

*Paul Miller, June 2021*

### Introduction

In this chapter we describe the physical and biogeochemical process representations characterizing peatland ecosystems of the tundra and taiga biomes, as well as the PFTs characteristic of these ecosystems.

These developments and process descriptions were adopted from updates to the LPJ DGVM made by Wania et al. (2009a, 2009b, 2010), and are described more briefly in McGuire et al. (2012).

### Peat stands and soil layers

A Stand object and associated Patch objects represent the ecosystems on the fraction of each Gridcell deemed to be a peatland. Differences to upland/mineral soils arise from the physical composition of the peat layers, from peatland-specific hydrological processes, peatland-specific PFTs, SOM decomposition and CH<sub>4</sub> emissions, described below.

### Peatland soil temperature

For peatland patches we use the same process representations as described in Ch. 12 to calculate soil temperature in each soil layer, each day. Layers (100 mm thick by default) are composed of fixed fractions of peat, and variable fractions of water, ice and air (Figure 12.2(b)), with thermal properties given in Table 12.1.

The peat layer profile is shown in Fig. 13.1. The uppermost three layers comprise the *acrotelm*, within which the water table can vary (see below), overlying 12 *catotelm* layers that are assumed to be permanently saturated (Wania et al. 2009a, 2009b). The porosity of acrotelm layers is 0.98 (*por\_acro*), but the catotelm layers are assumed to be composed of older, more compact peat, with an assumed porosity (*por\_caro*) of 0.92.

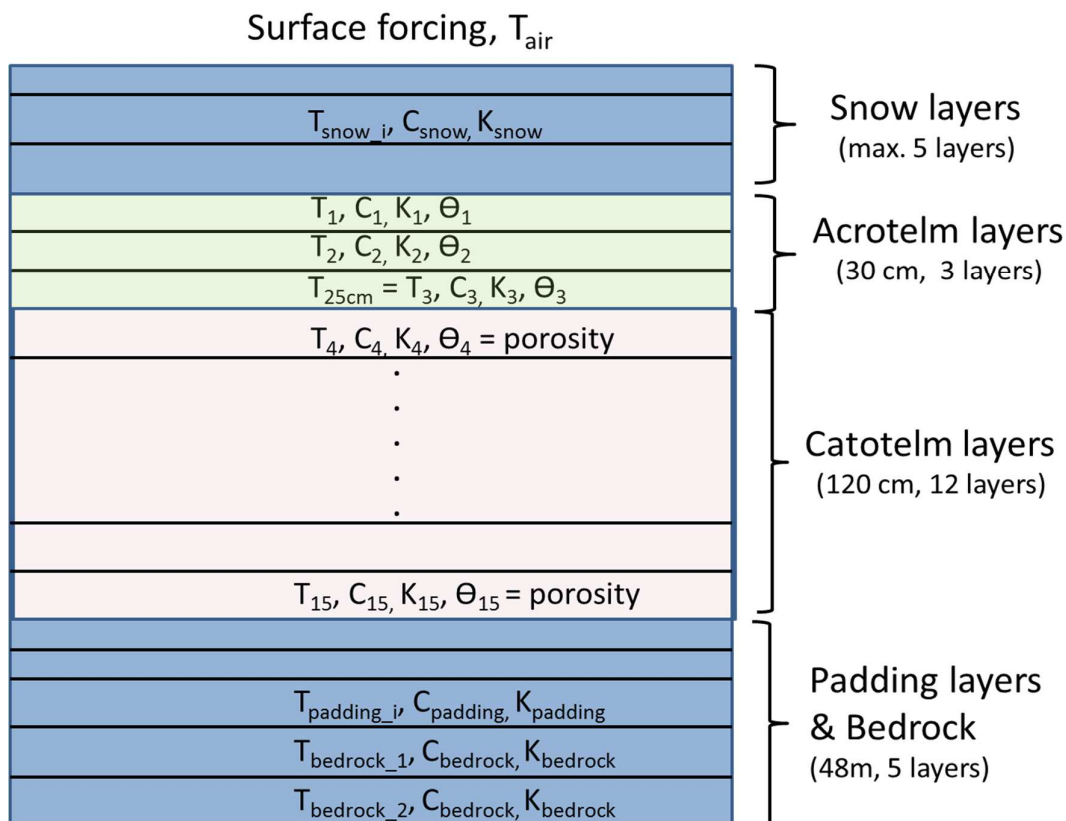


**Figure 13.1.** Soil layer structure in peatland soils (not to scale). Up to 5 snow layers overlie 15 active soil layers, underneath which 5 padding layers extend to a total depth of 49.5 m. The uppermost three layers comprise the acrotelm, within which the water table can vary, overlying 12 catotelm layers that are assumed to be permanently saturated.

### Peat hydrology

The hydrology of the acrotelm layers (upper 300 mm) of peat patches follows the description of Wania et al. (2019a, 2009b), first described in Granberg et al. (1999). The 12 catotelm layers are assumed to be permanently saturated, with no inflow or outflow, and water is added to these layers each day to enforce this if required, for example if water is taken up from these layers by PFTs with root access to the catotelm (only shrubs in the current configuration). Phase changes are treated as described in Ch. 12 above, but are strongly influenced by the porosity and SOM content of peat layers (Fig 12.2 (b)), with the result that summer soil temperatures are generally lower, and active layer depths shallower, in peat stands than they are in stands with mineral soils in the same gridcell.

The peat hydrology routine updates soil water content in the three acrotelm layers, and calculates the water table depth ( $wtd$ ), where  $0 \leq wtd \leq 300$  mm, i.e.  $wtd$  is positive below the surface, and no standing water is allowed.

The first step is to update the total volume of water ( $V$ ) in the acrotelm each day, with the daily change calculated as follows:

$$\Delta V = run_{on/off} + rain\_melt - evap - aet_{acro} - runoff_{acro}$$

where  $rain\_melt$  is the daily input to the patch as rainfall and/or snowmelt (mm),  $evap$  is the evaporation from the bare peat soil fraction,  $aet_{acro}$  is the transpiration (mm) from the acrotelm, calculated based on the peatland PFT root distributions in the acrotelm layers, and  $runoff_{acro}$  (mm) is the runoff from the acrotelm. An optional, additional site-specific  $run_{on/off}$  allows the user to add ( $run_{on/off} > 0$  mm) or to remove ( $run_{on/off} < 0$  mm) water from the acrotelm to mimic local site conditions, but is zero by default for global or regional applications. Its value can be set in the `global.ins` or `arctic.ins` file.

In contrast to Wania et al., we do not combine transpiration and evaporation. Evaporation is allowed if  $wtd \leq 200$  mm and if the snow depth  $< 10$  mm. If these conditions are satisfied, daily evaporation (mm) occurs from the non-vegetated (i.e.  $1 - FPC_{total}$ ) fraction,  $fevap$ , of the acrotelm layers following:

$$evap = fevap * EET * PT * \frac{0.99}{1.02 + \exp(-1 * \frac{(-wtd + 98.7)}{22.6})}$$

where  $EET$  is the daily equilibrium evapotranspiration (mm), and  $PT = 1.32$  is the Priestley-Taylor constant. (Assuming  $fevap = 1$ ,  $evap$  then ranges from  $0.96 * EET * PT$  when  $wtd = 0$  mm (i.e. at the surface), to  $0.011 * EET * PT$  when  $wtd$  falls to 200 mm.)

Daily runoff (mm) from the acrotelm follows Wania et al. (2009a, eqn.(24))

$$runoff_{acro} = \exp(-0.01 * wtd)$$

but is limited to days when the uppermost acrotelm layer (top 10 cm of peat) has  $F_{ice} < 0.7$  (Granberg et al. 1999).

*Updates to the water table depth (wtd)*

The second step is to calculate the water table depth as a function of the total volume of water ( $V$ ) in the acrotelm, following Wania et al (2009a), with a full motivation given by Granberg et al. (1999) who assume the soil water characteristics are linear in the top (“suction”) interval 0-100 mm and constant below this depth to the lower limit of the acrotelm, i.e. 100-300 mm. We do not allow standing water, so  $wtd$  is first calculated as:

$$wtd = \sqrt{\frac{3(\text{por}_{acro} * 300 - V)}{2 * a\_z}}$$

which is used if for  $100 \geq wtd \geq 0$  (i.e. for a water table near the surface), but replaced by

$$wtd = 1.5 * (\text{por}_{acro} * 300 - V) / (\text{por}_{acro} - f_{surfmin})$$

if  $wtd > 100$ , where  $a\_z = (\text{por}_{acro} - f_{surfmin}) / 100$  (is the gradient in the top, 100 mm suction interval) and  $f_{surfmin} = 0.25$  is the minimum fractional water content at the surface in  $\text{mm}^3/\text{mm}^3$ .

To calculate the actual fractional water content ( $F_{water}$ ) in each 100 mm sublayer in the acrotelm (needed for temperature calculations), wtd is first used to calculate the soil water profile,  $\theta(z)$ , in each 10 mm layer from the peat surface to the water table depth following the quadratic profile given by Granberg et al. (1999, eqn 1). First we define the surface water content,  $\theta_{surf}$  as follows,

$$\theta_{surf} = \max(f_{surfmin}, por_{acro} - wtd * a_z)$$

which ensures that  $\theta_{surf} \geq f_{surfmin}$  with equality if  $wtd \geq 100$  mm.

For  $z \leq wtd$  we use

$$\theta(z) = \min(por_{acro}, \theta_{surf} + (por_{acro} - \theta_{surf}) * (\frac{z}{wtd})^2)$$

to calculate the the soil water profile, which results in a quadratic dependence from  $\theta_{surf}$  at the surface to  $por_{acro}$  at wtd.

For  $300 \geq z > wtd$   $\theta(z) = por_{acro}$ , i.e. full saturation.

Once the soil water profile  $\theta(z)$  in each 10 mm layer is known,  $F_{water}$  in each of the three 100 mm acrotelm sublayers is calculated by taking the average of the ten 10 mm layers it contains.

### Peatland PFTs

Table 13.1 lists the new properties of the PFTs that can exist on peatland stands. Peatland PFTs inherit most properties from their parent groups, e.g. “grass” or “low shrub”. We mostly follow the descriptions of Sphagnum mosses and C3 graminoids from Wania et al (2009b) appropriate for regional and global applications, building on work for mosses by Yurova et al. (2007). We also include low evergreen and deciduous shrubs (pLSE and pLSS, respectively) and a generic herbaceous cushion lichen moss PFT (pCLM), both of which are parameterized to prefer dry peatlands with low water table positions over an extended time (see below).

PFT	Maximum WTD for inundation (WTD <sub>inun</sub> , mm)	Inundation duration (inund_days, days)	Has aerenchyma?	$\beta$	WTD Upper (WTD <sub>U</sub> , mm)	WTD Lower (WTD <sub>L</sub> , mm)	WTD photosynthesis stress scalar at WTD Lower
pLSE, pLSS	250	5	No	0.96	N/A	N/A	N/A
Sphagnum moss	50	15	No	0	0	280	0.3
C3	N/A	N/A	Yes	0.9	10	100	0.0

<b>graminoids</b>							
<b>pCLM</b>	200	10	No	0.9	N/A	N/A	N/A

**Table 13.1.** Peatland PFTs and important parameter values used in their definition. Columns are described in the text.

### Moss photosynthesis and leaf respiration

Mosses are assumed to have access to dissolved CO<sub>2</sub> from pore water in the acrotelm, so the CO<sub>2</sub> concentration used in the calculation of photosynthesis is calculated as a weighted mean of the atmospheric CO<sub>2</sub> concentration ( $CO2_{atm}$ ) and CO<sub>2</sub> in the dissolved pore water with the previous year's average water table position ( $0 \geq awtp \geq -300$ ) as the weighting factor. If the water table in a grid cell is high, mosses can access all of the acrotelm CO<sub>2</sub>, but as the water table drops the CO<sub>2</sub> concentrations available to mosses decline to match the atmospheric CO<sub>2</sub> concentration when  $awtp = -300$  mm.

Smolders et al (2001) give an average CO<sub>2</sub> concentration of 70 sites as 934  $\mu\text{mol L}^{-1}$  so we calculate the moss CO<sub>2</sub> availability as follows

$$CO2_{moss} = \min(934, 934 + (934 - CO2_{atm}) * \frac{awtp}{300})$$

Following Yurova et al. (2007), the scaling factor (BC) used to calculate the carboxylation capacity of rubisco ( $V_{max}$ ) and the daily leaf respiration is set to  $BC = 0.03$  for mosses, a value that can be compared to the leaf respiration fraction of maximum rubisco for C<sub>3</sub> plants and C<sub>4</sub> plants of  $BC = 0.015$  and  $0.02$ , respectively.

#### *LAI limits*

When the water table is near the surface, peatland PFTs are not shaded by trees or shrubs and are very productive as a result. An upper LAI limit of  $2 \text{ m}^2 \text{ m}^{-2}$  is imposed on moss and graminoid PFTs by increasing shade mortality when the limit is exceeded. Leaf and root carbon is reduced consistent with that individual's allometric constraints and added to litter pools.

### Assimilation stress due to water table fluctuations

Each day, after  $wtd$  has been updated, gross daily photosynthesis ( $\text{gC/m}^2/\text{day}$ ) and leaf respiration ( $\text{gC/m}^2/\text{day}$ ) are reduced in proportion to a stress factor  $[0, 1]$  if they become desiccated as the water table falls (applies only to mosses and graminoids), or subjected to inundation stress. Stress factors of 1 result in no stress, and values of 0 imply complete cessation of photosynthetic activity on that day. See Wania et al. (2009b – sections 2.1 and 2.2) for further details and motivation, but note that in contrast to Wania et al we apply these stresses daily.

#### *Desiccation stress*

Though there is substantial specific variability, sphagnum moss productivity decreases when its water content decreases. As in Wania et al., we use water table position as a surrogate for

moss water content. Similarly, graminoid productivity has been shown to drop when water table position decreases. We parameterize the fall in daily productivity for wtd values between the  $WTD_U$  and  $WTD_L$  limits set in Table 13.1 using a simple linear relationship between the desiccation stress factor [0, 1] and wtd as follows:

$$Dessication_{stress} = 1 - (wtd - WTD_U) * (1 - stress_{scalar}) / (WTD_L - WTD_U)$$

where  $stress_{scalar}$  is the daily stress factor at wtd values below  $WTD_L$ . Above  $WTD_U$ ,  $Dessication_{stress} = 1$ , i.e. no stress factor is applied. Thus, mosses are never fully desiccated since  $stress_{scalar} = 0.3$  but experience stress as soon as the water table falls below the peat surface. In contrast, graminoid assimilation is fully restricted ( $stress_{scalar} = 0.0$ ) when the water table drops below  $WTD_L = 100\text{mm}$ . We assume that  $Dessication_{stress} = 1$  for pLSE, pLSS and pCLM.

### *Inundation stress*

An inundation stress factor is applied to limit assimilation when there are anoxic conditions in the rooting zone. Unless specially adapted to these conditions (as is the case for C3 graminoids with aerenchyma allowing them to transport oxygen to the rooting zone and methane to the atmosphere – see Sec 14), plant can die in a matter of days (Wania et al. and references therein). To each peatland PFT we assign (Table 13.1) both a maximum wtd threshold ( $WTD_{imm}$ ) and the number of days ( $inund\_days$ ) the PFT can tolerate inundated conditions before assimilation is completely restricted.

Inundation stress is then calculated as follows:

$$Inundation_{stress} = 1 - \min\left(1, \frac{inund_{count}}{inund\_days}\right)$$

Where  $inund_{count}$  is the number of days for which  $wtd < WTD_{imm}$  i.e. when the water table is nearer the peat surface than the level tolerated by the PFT in question. Note that we restrict  $inund_{count}$  to the range  $[0, inund\_days+3]$  to allow plants to recover and again begin to assimilate carbon shortly after the water table drops below their  $WTD_{imm}$  limit. As the values in Table 13.1 indicate, even short periods with wet conditions affect short shrubs and the pCLM PFTs, which in practice restricts these PFTs to conditions typical of drier hummocks. In contrast, C3 graminoids are completely unaffected by inundation, and thrive in wetter or saturated conditions typical of peatland hollows. Mosses are an intermediate case, tolerating all but the wettest conditions.

## **SOM decomposition in peatland stands**

SOM decomposition is treated slightly differently in peatland soils. As for mineral soils, daily decay rates for each CENTURY pool (C fraction:  $C_j$ ,  $\text{kg C m}^{-2}$ ) are determined by a prescribed maximum (base) decay rate ( $k_{j,max}$ ; Parton et al. 2010; Table 1) and dependencies on temperature, soil moisture and soil texture:

$$\frac{dC_j}{dt} = -k_{j,max} \cdot f(T_{soil}) \cdot f(W) \cdot f(S) \cdot C_j$$

where  $f(T_{\text{soil}})$  is a dimensionless scalar in the range [0, 1] related to soil temperature ( $T_{\text{soil}}$ , °C) as described in Sec 4 above with the modifications for sub-zero temperatures described in Sec 12.

In contrast to mineral soils, peat soils are assumed to have negligible soil fractional silt plus clay content, ( $S$ ), so  $f(S) = 1$  when  $S = 0$ , following Parton et al. (1993):

$$f(S) = 1 - 0.75 \cdot S$$

The biggest departure from mineral soil SOM decomposition relates to  $f(W)$ , the dimensionless scalar in the range [0, 1] related to soil moisture. Decomposition rates are slow in the wet and sometimes saturated conditions in the acrotelm, and especially so in the permanently saturated, anaerobic conditions in the catotelm (Frolking et al. 2001, 2010). Wania et al. (2009b) cite Segers (1998) to motivate  $f(W) = 0.37-0.71$ , which is especially relevant for acrotelm conditions. We use  $f(W) = R_{\text{moist}} = 0.4$  for carbon in the acrotelm here – see below. To account for the extremely slow decomposition in the catotelm, we adopt an approach inspired by Wania et al. (2009b), who associated the intermediate carbon pool in LPJ-WHy DGVM with the acrotelm, and the slow carbon pool with the catotelm, and transferred carbon from the acrotelm to the catotelm once the soil carbon build up corresponded to a fully developed acrotelm, i.e. a 30 cm deep peat layer with a carbon density of 25 kg C m<sup>-3</sup>. This translates to a soil carbon amount across all pools of 7.5 kg C m<sup>-2</sup>. However, we do not transfer carbon between the CENTURY pools in LPJ-GUESS (avoiding difficulties with N transfer). Instead we reduce  $f(W)$  from values typical of the acrotelm ( $f(W) = R_{\text{moist}} = 0.4$ ) once the total soil carbon pool ( $\text{soilC}$ ) exceeds the same 7.5 kg C m<sup>-2</sup> threshold, towards decomposition moisture scalars for anaerobic conditions  $f(W) = R_{\text{moist\_anaerobic}} = 0.025$  given by Frolking et al. (2001, 2010) and Ise et al. (2008), i.e. an order of magnitude smaller than acrotelm values. Thus:

$$f(W) = \begin{cases} R_{\text{moist}} & ; \text{soilC} \leq 7.5 \text{ kgC m}^{-2} \\ \frac{(7.5 * R_{\text{moist}} + (\text{soilC} - 7.5) * R_{\text{moist\_anaerobic}})}{\text{soilC}} & ; \text{soilC} > 7.5 \text{ kgC m}^{-2} \end{cases}$$

A final assumption is that the passive SOM and slow SOM CENTURY pools (Appendix B) are always in the catotelm, and for those we always use  $f(W) = R_{\text{moist\_anaerobic}} = 0.025$ .

## References

See references in Chapter 14.

## 14. Methane dynamics

*Paul Miller, June 2021*

### Introduction

In this chapter we describe methane biogeochemistry, including production, oxidation, transport pathways and fluxes. Developments and process descriptions for methane dynamics in high-latitude peatland stands were adopted from LPJ-WHyMe (Wania et al. 2010), building on the development of LPJ-WHy (Wania et al. 2009a, 2009b) described above.

### Low-latitude peatland stands – hydrology, PFTs and methane fluxes

The LPJ-WHy(Me) parameterizations are only valid for the carbon-rich peatlands found at high-latitudes. Peatland/wetland stands in gridcells with a latitude south of 40°N are treated more simply.

Soil properties are assumed to be identical to the mineral soils in natural stands in the same gridcell. However, we keep their soil water content at field capacity by adding water each day as necessary, subtracting the input from runoff where possible. SOM decomposition is affected by assuming that the water-filled pore space is 100% and setting  $\theta = \theta_{\max}$  in the calculation of  $f(W)$ , the decomposition water scalar (0-1) (Section 4 above), where  $\theta$  is the current soil water content and  $\theta_{\max}$  is soil water saturation capacity as a proportion of soil column depth. This gives  $f(W) = 0.36$ , approximately.

Only two PFTs are allowed to establish on peatland/wetland stands south of 40N, namely C<sub>3</sub> and C<sub>4</sub> grasses, which are parameterized identically to the C<sub>3</sub> and C<sub>4</sub> grass PFTs on natural stands apart from set bioclimatic limits of  $t_{\min\_surv} = 5$  °C and  $t_{\min\_surv} = 5$  °C to ensure that they do not establish on high-latitude peatland stands. Furthermore, since these PFTs are not shaded by trees they are very productive, so an upper LAI limit of 4 m<sup>2</sup> m<sup>-2</sup> is imposed by increasing shade mortality when the limit is exceeded. Leaf and root carbon is reduced consistent with that individual's allometric constraints and added to litter pools.

Methane fluxes ( $F_{CH_4}$ , gCH<sub>4</sub>-C m<sup>-2</sup> day<sup>-1</sup>) are calculated using a simple parameterization introduced by Spahni et al. (2011). In non-peatland stands, decomposition results in heterotrophic respiration ( $R_h$ , release of CO<sub>2</sub>) and transfer of C and N between pools, satisfying mass balance. In low-latitude peatland stands we assume that a set fraction of the carbon respired is instead released as carbon in methane, i.e.

$$F_{CH_4} = r_{CH_4toCO_2inund} * R_h$$

Where  $r_{CH_4toCO_2inund} = 0.027$  is very close to the carbon conversion ratio value introduced by Spahni et al. (2011) to account for (low-latitude wetland) processes not yet treated in the

model such as methane oxidation and transport. It can be used as a tuning parameter to match global wetland emissions (approx. 180 TgCH<sub>4</sub> year<sup>-1</sup>), but values of 0.03 +/- 0.02 are consistent with data from field studies compiled by Christensen et al. (1996). Once  $F_{CH_4}$  has been calculated,  $R_h$ , the release of CO<sub>2</sub>, is reduced by 2.7% to conserve carbon.

### Methane fluxes in high-latitude peatland stands

The LPJ-WHyMe process descriptions for methane production, oxidation and transport described by Wania et al. (2010) are valid for the carbon-rich peatlands found at high-latitudes and are followed closely here. We do not reproduce all equations used, but rather refer to the equation numbers in Wania et al. (2010) where appropriate.

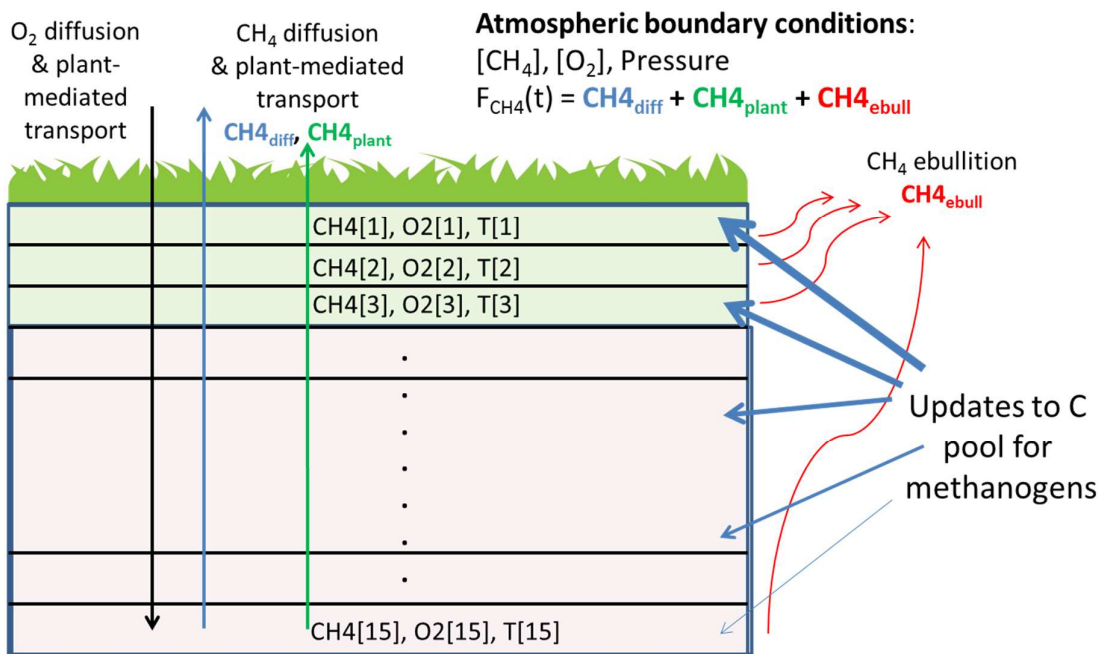


**Figure 14.1:** Schematic representation of the methane model. The potential carbon pool for methanogens is allocated to each layer in proportion to root density, producing methane in each layer. Both oxygen and methane are diffused between the atmosphere and soil, with an additional transport pathway via aerenchyma when C3 graminoid PFTs are present. Methane in each layer is oxidised in the presence of oxygen. Bubble formation (ebullition) occurs once gaseous methane exceeds defined thresholds.

### Methane production

In high-latitude peatland stands we assume that a set fraction of the carbon respired is made available as a potential carbon pool for methanogens (Fig 14.1), but we assume that this pool is distributed vertically in the soil column in proportion to the degree of anoxia ( $1 - F_{air}(z)$ ), and a vertical root distribution derived from fen and bog peat core data:

$$rootfrac(z) = C_{root} * e^{(z/\lambda_{root})}$$

Where  $C_{root} = 0.025$  and  $\lambda_{root} = 25.17$  cm are normalization constants. This distribution ensures that the majority of roots (60% approx.) are found in the acrotelm. The value of the root fraction in the bottom soil layer is chosen such that the root distribution sums to 1 across the 15 soil layers.

The daily production of methane in each layer is then given by

$$CH4_{prod} = (1 - F_{air}(z)) * rootfrac(z) * r_{CH4toCO2peat} * R_h \quad (\text{Eq. 14.1})$$

Where  $r_{CH4toCO2peat} = 0.085$  is a tuning parameter for the methane to carbon dioxide production ratio. Note that we set  $CH4_{prod} = 0$  when  $F_{water} < 0.1$ , ensuring that there is no methane production in dry and/or frozen soils.

### Gas diffusion

The diffusion of oxygen and methane between the soil and the atmosphere depends on the atmospheric concentrations of these gases, the air pressure, and the concentration of oxygen and methane in each layer. Numerical calculations of the diffusion process use the same Crank-Nicholson routine used for soil temperature calculations and daily updates to the molecular diffusivity of these gases ( $D_{CH4}$ ,  $D_{O2}$ ) in each layer. We follow Eqns. (8-12) to calculate  $D_{CH4}$  and  $D_{O2}$  in Wania et al. (2010) exactly, assuming polynomial dependence on layer temperature,  $T(z)$ , and strong dependence on both  $F_{air}(z)$  and layer porosity.

The boundary conditions at interface between the top soil layer and the atmosphere are determined using the gas flux,  $J_{gas}$ , at the interface to update the concentration of dissolved gas in the top soil layer. Following Wania et al. (2010), Eqn. (4):

$$J_{gas} = -\varphi_{gas} * (C_{surf} - C_{equil}) \quad (\text{Eqn. 14.2})$$

where  $C_{surf}$  is the concentration of the gas in the top soil layer, and  $C_{equil}$  is the concentration of dissolved gas in equilibrium with the atmospheric concentration (partial pressure) of that gas. The so-called piston velocity,  $\varphi_{gas}$ , is updated daily for each gas ( $\varphi_{O2}$ ,  $\varphi_{CH4}$ ) using the polynomial dependence (of Schmidt numbers) on layer temperature,  $T(z)$ , following Wania et al. (2010), Eqns. (5-7).

$C_{equil}$  (mol L<sup>-1</sup>) is calculated using Henry's Law

$$C_{equil} = P_{partial} / K_{Hinv}$$

where  $P_{partial}$  is the partial pressure of the gas in question (e.g.  $1.7 * 10^{-6}$  atm for methane, 0.209 atm for oxygen), and  $K_{Hinv}$  is the Henry coefficient for that gas, given by Wania et al. Eqn. (8) and Table 2.

Each day,  $J_{gas}$  above is used to update the dissolved gas content in the top soil layer before diffusion is calculated, resulting in fluxes of oxygen and methane into and out of the soil, respectively, though it is possible for methane to diffuse into the soil in small amounts if the concentrations at the surface are suitable (e.g. if the dissolved methane content in the top soil layer is very low). The resulting, daily flux of methane from diffusion,  $CH4_{diff}$  ( $gCH_4-C m^{-2} day^{-1}$ ), is one of three components of the total methane flux (Figure 14.1).

### Plant mediated gas transport

Both oxygen and methane can also be transported between the soil and the atmosphere through vascular plants that have adapted to survive in inundated conditions by developing aerenchyma, which are tissues that can transport oxygen to roots in anaerobic layers, but that can also transport methane to the atmosphere, potentially bypassing aerobic conditions near the soil-air interface. We assume that the flood-tolerant  $C_3$  graminoid is the only PFT with aerenchyma, so plant-mediated transport of oxygen and methane can only occur when  $C_3$  graminoids occur in a patch.

The gas flux calculated through vascular plants is assumed to be proportional to the cross-sectional area of tillers in each soil layer, where the term tiller refers to all the secondary shoots produced by grasses (Poaceae or Gramineae). Each tiller stem is segmented with its own two-part leaf. The total biomass of tillers,  $m_{tiller}$  ( $kgC m^{-2}$ ) in a patch is determined by the carbon content of the flood-tolerant  $C_3$  graminoid leaves, taking into account phenological state ( $phen$ , 0-1), i.e.  $m_{tiller} = phen * C_{leaf}^{graminoid}$ . The density of tillers ( $n_{tiller}$ , tillers  $m^{-2}$ ) is then determined by dividing  $m_{tiller}$  by an observed average of tiller masses, 0.22  $gC/tiller$ .

The cross-sectional area of an individual tiller is given by  $\pi (r_{tiller})^2$ , where  $r_{tiller} = 2.9$  mm is an observed average of tiller radii. Finally, the tiller area in each soil layer at depth  $z$  is given by

$$A_{tiller}(z) = 0.5 * n_{tiller} * rootfrac(z) * \pi r_{tiller}^2$$

, where the factor of 0.5 is to account for the tiller porosity.

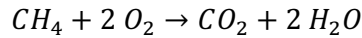
Plant-mediated transport from the atmosphere to each layer separately is calculated each day for oxygen and methane following Eqn. (14.2) above, assuming a rescaling of the gas diffusivity for that layer by  $A_{tiller}(z)$ .

The daily plant mediated flux of methane,  $CH4_{plant}$  ( $gCH_4-C m^{-2} day^{-1}$ ) (Figure 14.1), is calculated by summing the plant-mediated methane fluxes from each layer.

### Methane oxidation

A fraction,  $f_{oxid}$ , of the oxygen transported to a soil layer by diffusion or mediated by plants (see above) is immediately used by roots themselves, or by other soil microorganisms. As in Wania et al. (2010), we assume that  $f_{oxid} = 0.5$ .

The remaining oxygen is used to oxidise available dissolved methane while maintaining stoichiometric balance:



i.e. two moles of oxygen are needed to oxidise one mole of methane. The carbon in the oxidised methane is added to a  $CO_2$  store to ensure carbon balance.

### Methane ebullition

Citing Yamamoto et al. (1976), Wania et al. (2010, Eqn. 15) give the maximum solubility of methane at a given temperature ( $T(z)$ ),  $S_B$ , as

$$S_B = 0.05708 - 0.001545 * T + 0.00002069 * T^2$$

with units of ml  $CH_4$  ml<sup>-1</sup>  $H_2O$ . The maximum number of moles of methane that can be dissolved ( $CH4_{diss\_max}$ ) is calculated for each soil layer using the layer temperature and the total (atmospheric plus hydrostatic) pressure felt by gas in that layer in combination with the ideal gas law (Wania et al. 2010, Eqn. 16). After conversion to a maximum allowable dissolved mass of methane per layer, this limit is used to separate the methane in each layer into its dissolved and gaseous components,  $CH4_{diss}$  and  $CH4_{gas}$ , respectively.

Ebullition, i.e. bubble formation, is assumed in a layer if volumetric gas content ( $CH4_{gas\_vgc}$ , m<sup>3</sup> m<sup>-3</sup>) exceeds  $0.15 * bubble\_CH4\_frac$ , where  $bubble\_CH4\_frac = 0.57$  is a typical methane fraction of gas bubbles observed in the field. If bubble formation occurs, the total methane in a layer is reduced to  $0.145 * bubble\_CH4\_frac$ , and the excess methane for that layer is emitted immediately to the atmosphere. Note that we set  $CH4_{gas\_vgc} = 0$  when  $F_{water} < 0.1$  or  $T(z) < 0^\circ C$ , ensuring that there is no methane ebullition in extremely cold and/or frozen soils.

The daily ebullition flux of methane,  $CH4_{ebull}$  (g $CH_4$ -C m<sup>-2</sup> day<sup>-1</sup>) (Figure 14.1), is calculated by summing the ebullition fluxes from each layer.

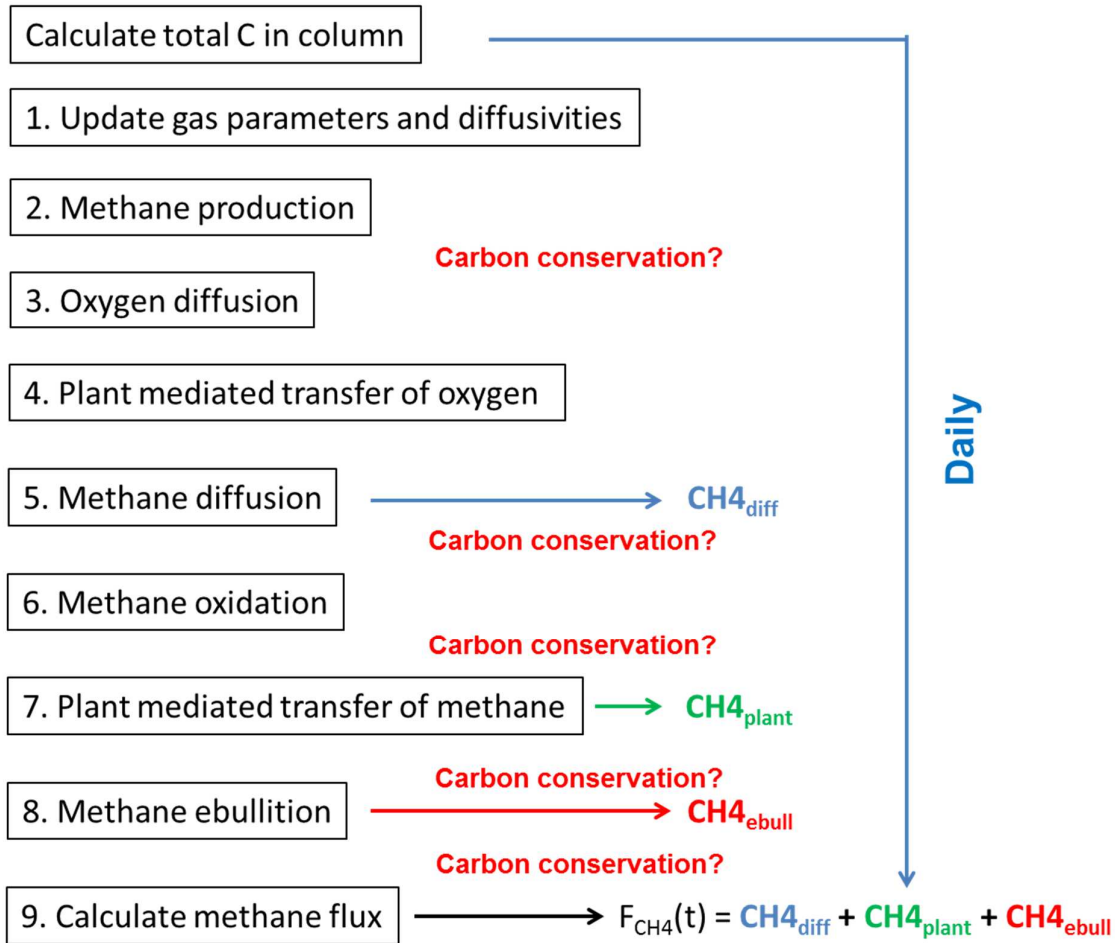


Figure 14.2. Methane dynamics algorithm in LPJ-GUESS, showing the process descriptions considered and their order.

### Total methane flux

Figure 14.2 above shows the steps used to calculate the daily flux of methane ( $F_{CH4}$ ,  $gCH_4-C m^{-2} day^{-1}$ ) from high-latitude peatland patches:

$$F_{CH4} = CH4_{diff} + CH4_{plant} + CH4_{ebull}$$

Checks for carbon conservation are applied after each step that can potentially influence carbon content in soil layers in the form of carbon dioxide and methane. Since the daily production of methane in each layer,  $CH4_{prod}$ , is determined by daily heterotrophic respiration ( $R_h$  in Eqn. 14.1 above), we subtract  $F_{CH4}$  from  $R_h$  before saving the daily heterotrophic respiration. We assume that all carbon dioxide produced, e.g. through heterotrophic respiration or methane oxidation, is immediately released to the atmosphere.

## References

- Aerts, R., Verhoeven, J.T.A., & Whigham, D.F. (1999) Plant-mediated controls on nutrient cycling in temperate fens and bogs, *Ecology*, 80 (7), 2170-2181.
- Best et al. (2011) *Geosci. Model Dev.*, 4, 677-699. [www.geosci-model-dev.net/4/677/2011/](http://www.geosci-model-dev.net/4/677/2011/) doi:10.5194/gmd-4-677-2011
- Bonan, G.B. 2002 *Ecological Climatology*, Cambridge University Press
- Chadburn, S., Burke, E., Essery, R., Boike, J., Langer, M., Heikenfeld, M., Cox, P., and Friedlingstein, P.: An improved representation of physical permafrost dynamics in the JULES land - surface model, *Geosci.Model Dev.*, 8, 1493 - 1508, <https://doi.org/10.5194/gmd-8-1493-2015>, 201
- Christensen, T., Prentice, I., Kaplan, J., Haxeltine, A., and Sitch, S. (1996) Methane flux from northern wetlands and tundra - An ecosystem source modelling approach, *Tellus B*, 48, 652–661.
- Clein, J. S., and J. P. Schimel, Microbial activity of tundra and taiga soils at sub-zero temperatures, *Soil Biol. Biochem.*, 27(9), 1231-1234, 1995.
- Cronk, J. K. and Fennessy, M. S.: *Wetland Plants: Biology and Ecology*, CRC Press LLC, 2001.
- Ekici, A., Chadburn, S., Chaudhary, N., Hajdu, L. H., Marmy, A., Peng, S., Boike, J., Burke, E., Friend, A. D., Hauck, C., Krinner, G., Langer, M., Miller, P. A., and Beer, C.: Site-level model intercomparison of high latitude and high altitude soil thermal dynamics in tundra and barren landscapes, *The Cryosphere*, 9, 1343-1361, <https://doi.org/10.5194/tc-9-1343-2015>, 2015.
- Frolking, S., Roulet, N. T., Moore, T. R., Richard, P. J. H., Lavoie, M., and Muller, S. D.: Modeling northern peatland decomposition and peat accumulation, *Ecosystems*, 4, 479-498, 2001.
- Frolking, S., Roulet, N. T., Tuittila, E., Bubier, J. L., Quillet, A., Talbot, J., and Richard, P. J. H.: A new model of Holocene peatland net primary production, decomposition, water balance, and peat accumulation, *Earth Syst. Dynam.*, 1, 1-21, <https://doi.org/10.5194/esd-1-1-2010>, 2010.
- Fukusako, S. (1990) Thermophysical properties of ice, snow, and sea ice. *Int. J. Thermophys.*, 11(2): 353-372. doi:10.1007/BF01133567
- Gerten, D., Schaphoff, S., Haberlandt, W., Lucht, W. & Sitch, S. 2004. Terrestrial vegetation and water balance—hydrological evaluation of a dynamic global vegetation model. *Journal of Hydrology* 286: 249-270.
- Granberg, et al. 1999 A simple model for simulation of water content, soil frost, and soil temperatures in boreal mixed mires. *Water Resour. Res.*, 35(12), 3771-3782.
- Hillel D., (1982) *Introduction to soil physics*. Academic Press, San Diego, CA, USA.
- Ise, T., Dunn, A.L, Wofsy, S.C. & Moorcroft, P.R.: High sensitivity of peat decomposition to climate change through water-table feedback. *Nature Geoscience* volume 1, pages 763-766 (2008)
- Jackson, R.B., Canadell, J., Ehleringer, J.R., Mooney, H.A., Sala O.E. & Schulze, E.D. 1996. A global analysis of root distributions for terrestrial biomes. *Oecologia*, Volume 108: 389–411

Jaehne, B., Heinz, G., and Dietrich, W.: Measurement of the diffusion coefficients of sparingly soluble gases in water, *J. Geophys. Res.*, 92, 10767-10776, 1987.

Koven, C.D, Ringeval, B., Friedlingstein, P., Ciais, P., Cadule, P., Khvorostyanov, D., Krinner, G., and Tarnocai C. (2011) Permafrost carbon-climate feedbacks accelerate global warming, *PNAS*, vol. 108 no. 36, 14769-14774.

Lawrence, D. M., and A. G. Slater, 2008: Incorporating organic soil into a global climate model. *Climate Dynamics*, 30, 145-160, doi:10.1007/s00382-007-0278-1.

Ling, F., and Zhang, T. (2006) Sensitivity of ground thermal regime and surface energy fluxes to tundra snow density in northern Alaska. *Cold Regions Science and Technology* 44 (2006) 121-130

McGuire, A. D., Christensen, T. R., Hayes, D., Heroult, A., Euskirchen, E., Kimball, J. S., Koven, C., Lafleur, P., Miller, P. A., Oechel, W., Peylin, P., Williams, M., and Yi, Y.: An assessment of the carbon balance of Arctic tundra: comparisons among observations, process models, and atmospheric inversions, *Biogeosciences*, 9, 3185-3204, <https://doi.org/10.5194/bg-9-3185-2012>, 2012.

Mikan, C. J., Schimel, J. P., and Doyle, A. P. 2002. Temperature controls of microbial respiration in arctic tundra soils above and below freezing, *Soil Biol.Biochem.*, 34, 1785–1795, 2002.

Potter, C. S., Davidson, E. A., and Verchot, L. V.: Estimation of global biogeochemical controls and seasonality in soil methane consumption, *Chemosphere*, 32, 2219-2246, 1996.

Riera, J. L., Schindler, J. E., and Kratz, T. K.: Seasonal dynamics of carbon dioxide and methane in two clear-water lakes and two bog lakes in northern Wisconsin, USA, *Can. J. Fish. Aquat. Sci.*, 56, 265-274, 1999.

Sander, R.: Compilation of Henry's Law Constants for inorganic and organic species of potential importance in environmental chemistry, Tech. Rep. Version 3, MPI Mainz, Air Chemistry Department, Max-Planck Institute of Chemistry, 1999.

Schaefer, K. and Jafarov, E. 2016. A parameterization of respiration in frozen soils based on substrate availability *Biogeosciences*, 13, 1991 - 2001, <https://doi.org/10.5194/bg-13-1991-2016>

Schimel, J. P.: Plant transport and methane production as controls on methane flux from arctic wet meadow tundra, *Biogeochem.*, 28, 183-200, 1995.

Smolders, A. J. P., H. B. M. Tomassen, H. W. Pijnappel, L. P. M. Lamers, and J. G. M. Roelofs (2001), Substrate-derived CO<sub>2</sub> is important in the development of *Sphagnum* spp., *New Phytol.*, 152(2), 325- 332.

Spahni, R., Wania, R., Neef, L., van Weele, M., Pison, I., Bousquet, P., Frankenberg, C., Foster, P. N., Joos, F., Prentice, I. C., and van Velthoven, P.: Constraining global methane emissions and uptake by ecosystems, *Biogeosciences*, 8, 1643-1665, <https://doi.org/10.5194/bg-8-1643-2011>, 2011.

Sturm, M., Holmgren, J., König, M., and Morris, K. (1997) The thermal conductivity of seasonal snow. *Journal of Glaciology* 43 (143), 26-41.

Swenson, S.C., Lawrence, D.M., and Lee, H. 2012. Improved Simulation of the Terrestrial Hydrological Cycle in Permafrost Regions by the Community Land Model. *JAMES*, 4, M08002. DOI:10.1029/2012MS000165.

Tang, J., Miller, P. A., Persson, A., Olefeldt, D., Pilesjö, P., Heliasz, M., Jackowicz-Korczynski, M., Yang, Z., Smith, B., Callaghan, T. V., and Christensen, T. R.: Carbon budget estimation of a subarctic catchment using a dynamic ecosystem model at high spatial resolution, *Biogeosciences*, 12, 2791-2808, doi:10.5194/bg-12-2791-2015, 2015.

Wania, R., Ross, I., and Prentice, I. C.: Integrating peatlands and permafrost into a dynamic global vegetation model; 1, Evaluation and sensitivity of physical land surface processes, *Global Biogeochemical Cycles*, 23, doi:10.1029/2008gb003412, 2009a.

Wania, R., Ross, I., and Prentice, I. C.: Integrating peatlands and permafrost into a dynamic global vegetation model; 2, Evaluation and sensitivity of vegetation and carbon cycle processes, *Global Biogeochemical Cycles*, 23, doi:10.1029/2008gb003413, 2009b.

Wania, R., Ross, I., and Prentice, I. C.: Implementation and evaluation of a new methane model within a dynamic global vegetation model: LPJ-WHyMe v1.3.1, *Geosci Model Dev*, 3, 565-584, doi:DOI 10.5194/gmd-3-565-2010, 2010.

Wisser, D., Marchenko, S., Talbot, J., Treat, C., and Frohking, S. (2011) Soil temperature response to 21st century global warming: the role of and some implications for peat carbon in thawing permafrost soils in North America, *Earth Syst. Dynam.*, 2, 121-138

Wolf, A., Callaghan T.V., & Larson K. (2008) Future changes in vegetation and ecosystem function of the Barents Region. *Climatic Change*, 87:51-73 DOI 10.1007/s10584-007-9342-4

Yamamoto, S., Alcauskas, J. B., and Crozier, T. E.: Solubility of methane in distilled water and seawater, *J. Chem. Eng. Data*, 21, 78–80, 1976.

Yurova, A., Wolf, A., Sagerfors, J., & Nilsson, M. (2007) Variations in net ecosystem exchange of carbon dioxide in a boreal mire: Modeling mechanisms linked to water table position, *Journal of Geophysical Research*, 112, art. no. G02025, doi:10.1029/2006JG000342.

Zhang, W., Miller, P.A., Smith, B., Wania, R., Koenigk, T. & Doscher, R., 2013, Tundra shrubification and tree-line advance amplify arctic climate warming: results from an individual-based dynamic vegetation model. *Environmental Research Letters* 8: 034023.